

# UNCLASSIFIED

AD NUMBER
AD063439
NEW LIMITATION CHANGE
TO Approved for public release, distribution unlimited
FROM Distribution authorized to U.S. Gov't. agencies and their contractors; Administrative/Operational Use; Jun 1953. Other requests shall be referred to Director, Wright Air Development Center, Wright-Patterson AFB, OH 45433.
AUTHORITY
AFAL ltr, 17 Aug 1979

THIS PAGE IS UNCLASSIFIED

UNCLASSIFIED

AD

63439

DEFENSE DOCUMENTATION CENTER

FOR

SCIENTIFIC AND TECHNICAL INFORMATION

CAMERON STATION, ALEXANDRIA, VIRGINIA



UNCLASSIFIED

~~SECRET~~  
Bldg. # 45 Area B  
Wright-Patterson, AFB, Ohio 45433

VF

WADC TECHNICAL REPORT 53-142

A00063439

ELECTRONICS

Technical Library

**APPLICATIONS OF THE CORONA DISCHARGE FOR  
MEASUREMENTS OF DENSITY AND VELOCITY TRANSIENTS  
IN AIR FLOW**

**FRANK D. WERNER  
ROBERT L. GERONIME**

**UNIVERSITY OF MINNESOTA**

**JUNE 1953**

**Statement A  
Approved for Public Release**

**WRIGHT AIR DEVELOPMENT CENTER**

## NOTICE

When Government drawings, specifications, or other data are used for any purpose other than in connection with a definitely related Government procurement operation, the United States Government thereby incurs no responsibility nor any obligation whatsoever; and the fact that the Government may have formulated, furnished, or in any way supplied the said drawings, specifications, or other data, is not to be regarded by implication or otherwise as in any manner licensing the holder or any other person or corporation, or conveying any rights or permission to manufacture, use, or sell any patented invention that may in any way be related thereto.



**APPLICATIONS OF THE CORONA DISCHARGE FOR  
MEASUREMENTS OF DENSITY AND VELOCITY TRANSIENTS  
IN AIR FLOW**

*FRANK D. WERNER*

*ROBERT L. GERONIME*

*UNIVERSITY OF MINNESOTA*

**JUNE 1953**

**AERONAUTICAL RESEARCH LABORATORY**

**CONTRACT No. AF 33(038)-15833**

**RDO No. 473-163**

**WRIGHT AIR DEVELOPMENT CENTER  
AIR RESEARCH AND DEVELOPMENT COMMAND  
UNITED STATES AIR FORCE  
WRIGHT-PATTERSON AIR FORCE BASE, OHIO**

## FOREWORD

This report summarizes the work on application of the corona discharge to measurements of density and velocity transients in air flow, which has been carried out at the Rosemount Aeronautical Laboratories of the Department of Aeronautical Engineering, Institute of Technology, University of Minnesota. Thus, this report encompasses our earlier reports on the subject (References 1-4), and much new work in addition. We have selected the most pertinent data from our previous reports and included it in this report so that it is complete in itself. Figure captions in this report are sufficiently detailed to provide a brief outline of much of the work. Since it is expected that this material will be of interest to aerodynamicists who may have had little introduction to corona discharge processes, which are important to a qualitative understanding of our work, we have given a simplified introduction to the corona discharge.

We acknowledge with pleasure the interest and stimulation we have received from Professor John D. Akerman, Head of this Department. Major Julius F. Koetsch, USMC, has received our close co-operation in his Ph.D thesis work which is expected to make use of the corona as an instrument; and in return, he has contributed freely much of his time and effort to some of our problems. Specifically, he carried out the experiments which yielded the data on the current distribution on the plate needles for various air velocities and current. His contributions are gratefully acknowledged. Dr. Loeb's book, "The Fundamental Processes of Electrical Discharge in Gases", has been an especially valuable reference for our brief introduction to the mechanism of corona discharges.

This work was performed under Contract AF 33(038)-15833. The original initiator was Dr. A. M. Kuethe, and this was later carried by Mr. L. S. Wasserman. Mr. L. E. Bollinger followed Mr. Wasserman, and the latter phases of this work has been under the cognizance of Mr. K. E. Kissell. RDO No. 473-163, Glow Discharge for Turbulence Measurements, is the latest project number applicable to this report.

## ABSTRACT

The applicability of the electrical corona discharge from the tip of a fine wire for measurements of density and velocity in air flow has been experimentally investigated in some detail. Density sensitivity of corona discharges for steady state and transient variations is covered in detail. Several velocity sensitive probe types are discussed and comparisons for transverse velocity components between the velocity sensitive corona probe and the hot-wire anemometer are given in a number of oscillograms for turbulence and for a reproducible velocity transient. A corona turbulence measurement at Mach Number 3.1 is described. Background noise, rate of disintegration of the corona wire, and other associated investigations are reported.

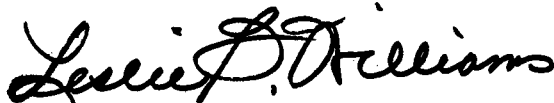
It is concluded that the corona is useful for study at moderate or high turbulence levels for Mach Numbers from 0.1 to at least 3.1, provided the static air density is greater than 0.1 to 0.3 times room density. Conclusions on use for low turbulence levels will depend on background noise measurements with flow; background noise measurements without flow are reported, and if it is assumed that flow causes no effect, turbulence levels may be studied down to a fraction of a percent. Frequency response is determined by the fact that velocity disturbances of dimensions comparable to - or smaller than the probe's electrode spacing will not be faithfully reproduced. At very high velocity, this corresponds to a maximum frequency of 500 kc or more.

It is expected that certain further investigations will show how it will be practical to make simultaneous measurement of density variations and all three components of velocity variations in both compressible and incompressible flow with a single probe. Separation of these variables may be rather difficult in some cases, but is possible in principle.

## PUBLICATION REVIEW

The publication of this report does not constitute approval by the Air Force of the findings or the conclusions contained therein. It is published only for the exchange and stimulation of ideas.

FOR THE COMMANDER:



LESLIE B. WILLIAMS, Colonel, USAF  
Chief, Aeronautical Research Laboratory  
Directorate of Research

# TABLE OF CONTENTS

## Page

LIST OF ILLUSTRATIONS - - - - -	v
LIST OF TABLES - - - - -	viii
INTRODUCTION - - - - -	1
SECTION I - THE MECHANISM OF A CORONA DISCHARGE - - - - -	2
A. Basic Concepts - - - - -	2
B. Negative Corona - - - - -	6
C. Positive Corona - - - - -	9
SECTION II - RELATIONSHIP AMONG THE CORONA VARIABLES: CURRENT, VOLTAGE, DENSITY, SPACING, AND WIRE DIAMETER - - -	11
SECTION III - CORONA BACKGROUND NOISE MEASUREMENTS - - - - -	20
SECTION IV - DENSITY SENSITIVITY - - - - -	25
A. Response of the Corona to Steady-State Density Changes - - - - -	25
B. Frequency Response of the Corona for Periodic Density Variations - - - - -	30
C. Response of the Corona to Transient Density Changes - - - - -	31
SECTION V - VELOCITY SENSITIVITY OF THE CORONA - - - - -	45
A. Ion Trajectories - - - - -	45
B. Model III Corona Probe for Turbulence Measurements - - - - -	54
C. Model IV Corona Probe for Turbulence Measurements - - - - -	60
D. Failure of the Corona Wire Due to Air Loads - - - - -	62
SECTION VI - TURBULENCE MEASUREMENTS - - - - -	63
SECTION VII - INSTRUMENTS - - - - -	76
REFERENCES - - - - -	79
BIBLIOGRAPHY - - - - -	82



# LIST OF ILLUSTRATIONS

<u>Figure</u>	<u>Title</u>	<u>Page</u>
1	Mechanism of the Corona Discharge - - - - -	7
2	Relation Among Variables for Positive Corona at 0.76 mm Spacing - -	14
3	Relation Among Variables for Positive Corona at 1.78 mm Spacing - -	14
4	Relation Among Variables for Positive Corona at 5.08 mm Spacing - -	15
5	Relation Among Variables for Positive Corona at 12.7 mm Spacing - -	15
6	Relation Among Variables for Negative Corona at 0.76 mm Spacing - -	16
7	Relation Among Variables for Negative Corona at 1.78 mm Spacing - -	16
8	Relation Among Variables for Negative Corona at 5.08 mm Spacing - -	17
9	Relation Among Variables for Negative Corona at 12.7 mm Spacing - -	17
10	Effect of Small Radii of Curvature of the Plate - - - - -	19
11	Rate of Disintegration of Corona Wires - - - - -	20
12	Apparatus for Background Noise Measurement - - - - -	21
13	Background Noise of the Corona - - - - -	22
14	Frequency Variation of Trichel Pulses with Corona Current - - - - -	24
15	Variation of Corona Background Noise with Density - - - - -	25
16	Apparatus for Investigation of the Density Sensitivity of the Corona - - - - -	27
17-A	Density Sensitivity of the Positive Corona - - - - -	28
17-B	Density Sensitivity of the Negative Corona - - - - -	30
18	Frequency Response of the Corona - - - - -	31
19	Photograph of the Model V Probe Used in the Shock Tube Work - - - -	32
20	Schematic Diagram of the Setup Used in Shock Tube Investigations of Transient Density Response - - - - -	33
21	Oscillograms of Trichel Pulses as Shock Wave Passed over the Model V Probe - - - - -	33
22	Calibration Curve for the Probe Shown in Figure 19 for Positive Corona - - - - -	34
23	Calibration Curve for the Model V Probe Shown in Figure 19 for Negative Corona - - - - -	35
24	Velocity Calibration of the Model V Probe Used in Shock Tube Work -	37
25	Photograph of Apparatus Used in Shock Tube Work - - - - -	38
26	Time vs. Distance Diagram of the Shock Tube for 12 psi Breaking Pressure - - - - -	39

# LIST OF ILLUSTRATIONS

<u>Figure</u>	<u>Title</u>	<u>Page</u>
27	Time vs. Distance Diagram of the Shock Tube for 6-psi Breaking Pressure - - - - -	40
28	Oscillograms of Positive Corona Current Variations Behind A Shock Wave for 12-psi Breaking Pressure - - - - -	42
29	Oscillograms of Positive Corona Current Variations Behind A Shock Wave for 6-psi Breaking Pressure - - - - -	42
30	Oscillograms of Negative Corona Current Variations Behind A Shock Wave for 12-psi Breaking Pressure - - - - -	43
31	Oscillograms of Negative Corona Current Variations Behind A Shock Wave for 6-psi Breaking Pressure - - - - -	43
32	High Speed Oscillogram of Negative Corona Current Variations Behind A Shock Wave - - - - -	44
33	Probe Used for Velocity Investigations - - - - -	46
34	Current Distribution for Velocity Probe, 10 $\mu$ Amp, Positive Corona	48
35	Current Distribution for Velocity Probe, 15 $\mu$ Amp, Positive Corona	48
36	Current Distribution for Velocity Probe, 20 $\mu$ Amp, Positive Corona	49
37	Current Distribution for Velocity Probe, 10 $\mu$ Amp, Negative Corona	49
38	Current Distribution for Velocity Probe, 15 $\mu$ Amp, Negative Corona	50
39	Current Distribution for Velocity Probe, 20 $\mu$ Amp, Negative Corona	50
40	Ion Trajectories for the Velocity Probe - - - - -	52
41	Experimental Justification of the Ion Trajectory Equation - - - - -	53
42	Model III Probe for Measurement of Turbulence - - - - -	55
43	Electrical Schematic Diagram of Model III Turbulence Probe - - - - -	56
44	Variation of Corona Voltage with Mach Number at Constant Values of Total Current - - - - -	57
45	Electrical Schematic Diagram of Circuit Used with Model III Probe -	58
46	Plot of the Two Sensing Needle Currents vs. Angle of Attack at Various Mach Numbers - - - - -	59
47	Plot of the Two Plate Currents vs. Angle of Attack at Various Mach Numbers with Sensing Needles Left Floating - - - - -	59
48	Model IV Probe Used in Subsonic Turbulence - - - - -	61
49	Electrical Schematic Diagram of Circuit Used with Model IV Probe -	61
50	Transverse Velocity Calibration Curves for Model IV Probe - - - - -	62

# LIST OF ILLUSTRATIONS

<u>Figure</u>	<u>Title</u>	<u>Page</u>
51	Bending Over of Wires Due to the Air Loads - - - - -	-63
52	Preliminary Measurements in Turbulent Air Flow with a Model II Corona Probe - - - - -	-64
53	Comparison of a Large and a Small Corona Probe in the Measurement of Transverse Components of Velocity - - - - -	-66
54	Photograph of Apparatus Used in Hot-Wire and Corona Correlation Tests - - - - -	67
55	Photograph of X-Type Hot-Wire Used in the Turbulence Tests - - - -	69
56	Long-Time Correlation Patterns of Hot-Wire and Corona Signals - - -	69
57	Comparison of Hot-Wire and Corona Observations Behind A Cylinder- -	71
58	Comparison of Hot-Wire and Corona Response to A Transverse Velocity Transient - - - - -	72
59	Oscillogram Illustrating the Directional Sensitivity of Corona - -	73
60	Photograph of Corona Model IV Probe Used in Supersonic Tests - - -	73
61	Oscillograms of Corona Measurements of Turbulence in Supersonic Flow - - - - -	74
62	Schematic Diagram of Special Voltmeter - - - - -	77
63	Schematic Diagram of 10-KV Power Supply - - - - -	77

# LIST OF TABLES

<u>Number</u>	<u>Title</u>	<u>Page</u>
1	Current vs. Voltage for Positive Corona at Various Pressures, for 1.78 mm Spacing and 25.5°C - - - - -	13
2	Data Showing Density Sensitivity of the Positive Corona - - - - -	29
3	Response of Corona to Density Transients in A Shock Tube - - - - -	41

## INTRODUCTION

When there is a sufficiently large potential difference between a pointed electrode and a nearby relatively flat electrode, the air may break down, and a spark may bridge the gap. At a somewhat lower voltage, the point will still have very high electric fields in its immediate vicinity which are higher than the breakdown values for air, however, a spark cannot reach across the gap because far from the point the electric field is too low. The result is that only the air near the point breaks down, and the discharge is called a corona discharge. This discharge is the type of interest and is described in some detail in Section I of the report. This discharge is of special interest because of the following features: (1) The total corona current is sensitive to air density changes and can respond uniformly from zero to several megacycles in some cases. (2) There are no electrical or mechanical resonance effects essential to the discharge in this frequency range. (3) The corona, which is the part sensitive to density changes is very small, of the order of 30 to 40 microns diameter. (4) When the probe is properly designed, the corona can be used in air flow to measure instantaneous velocity variations. (5) The probe may be very well streamlined.

Reference 1 outlines the original exploratory investigation into the possible uses of the corona. The application of this discharge as a microphone useful to 500 kc has been made. Part of Reference 2 discusses the microphone application and other further developments. The application to measurements in air flow is the present purpose. Reference 3 gives the first detailed investigation into the use of the corona in air flow, and Reference 4 continues this investigation.

In regard to measurements in air flow, this report is complete in itself for a general coverage of the most pertinent results of work done up to the present, since it summarizes the pertinent information of References 1-4 in addition to much new work. Unfortunately, since this report includes some of our previous work an inconsistency in units of measurement of wire diameter appears. Thus it is important to recall that 25.4 microns equals one mil (one thousandth of an inch).

SECTION I  
THE MECHANISM OF A CORONA DISCHARGE  
A. Basic Concepts

Basic research into the processes involved in corona discharge is not the aim of this investigation. Rather than this, the aim is to investigate the usefulness of the corona for aerodynamic measurements in moving air. To this end, a knowledge of the basic processes of corona discharge mechanisms is important as a guide to the qualitative understanding of the performance of the corona in the present application, but for quantitative information, because of the great complexity of a detailed analysis of the corona (which has not been completely carried out as yet), we have been forced to rely principally upon an empirical approach. The discussion of the basic corona mechanisms given below is abbreviated and is intended to introduce a reader not acquainted with the processes to the work which is reported. For a more complete discussion of the mechanism of a corona discharge the literature should be consulted, References 5-23 being a recent list. Most of the following discussion follows Loeb's book (Reference 5).

A number of basic and well-known concepts of conduction of electricity in gases and in particular, in air, must be pointed out, as a basis for the following discussion.

1. Ions

In air, positive ions, for our purposes, are considered as individual molecules with an electron removed, rather than a concept once widely entertained in which an ion eventually picked up a permanent aggregate of some ten to thirty molecules. Negative charge carriers are either free electrons or molecules to which an electron has become attached to form a negative ion. Oxygen is the only electron attaching gas considered for our case.  $N_2$ , along with  $H_2$ ,  $CO_2$ ,  $H_2O$ , except by association with other molecules or dissociation, and the inert gases are among those gases which will not form negative ions. Along with  $O_2$  as negative ion forming gases are  $Cl_2$ ,  $SO$ ,  $SO_2$ ,  $NO$ , and others (Reference 24). When  $O_2$  ions encounter such fields\* that  $E\rho_0/760\rho \gg 90$ ,

---

\*In gaseous discharges, the magnitude of the electric field is not so important as is the magnitude of the product of field and mean free path length, since this product defines the energy gained by an ion or electron between collisions. Loeb and others rather consistently write this as  $E/p$  in (volts per cm)/mm of Hg.  $p$  determines the mean free path if --(continued on page 3)

collisions with surrounding molecules have sufficient energy to free the electron (Reference 25).  $E$  is the field strength in volts per cm and the constant 760 is the pressure of a standard atmosphere in mm of Hg.

## 2. Mobility of Ions

When an ion in a gas is in the presence of an electric field, it is subject to the usual electrostatic force laws. In the resulting motion, it frequently collides with neighboring molecules. Therefore, it cannot accelerate indefinitely but quickly reaches an average velocity analogous to the terminal velocity of a particle falling through a viscous medium under the influence of gravity. This average velocity due to the electric field is given by the product of the mobility  $k$  of the gas, and the field strength  $E$ :

$$u = kE \quad (1)$$

where  $k$  has the defining equation:

$$k = K \rho_0 / \rho \quad (2)$$

$K$  in (cm/sec)/(volt/cm), has the value 1.6 for positive ions and 2.2 for negative ions, in pure dry air (Reference 26). Certain gases will associate with the ions in air so as to cause an abrupt change in  $K$ , and when present as impurities, even in very small amounts, chance collisions with ions will happen and alter the above values of  $K$ . Since a molecule in room air has about  $10^9$  collisions per second, the time for this change in  $K$  may be as little as  $10^{-7}$  or  $10^{-8}$  seconds after formation of the ion, depending on the concentration and nature of the impurity.

## 3. Mobility of Electrons

Electrons do not behave quite so simply as ions, but for our purpose, they may be considered to have a mobility of the order of  $10^4$  greater than for the ions (Reference 27).

## 4. Ionization by Electron Collision

When electrons are present in a gas and under the influence of an electric field, they can gain sufficient energy between collisions with molecules that they may dislodge other electrons from the molecules. This is called ionization by collision. When the field strength is high enough (or the density low enough) that  $E\rho_0/760\rho \geq$  about 20 (Reference 28) in air, this process can become active provided free electrons are present. For the present purposes, the

\*(continued from page 2)--temperature is known so  $E/p$  is a satisfactory parameter for experiments performed at a given temperature. In order to remove this unnecessary restriction, we will write  $E\rho_0/760\rho$  rather than  $E/p$ , where  $\rho$  is the density of air and  $\rho_0$  is the air density at  $0^\circ\text{C}$  and 760 mm Hg.

ionization of molecules by collision with either positive or negative ions can be considered negligible.

### 5. Electron Avalanches

It is readily seen that the process of ionization by collisions discussed above will lead to multiplication of the number of ions and electrons rather rapidly, since each new electron released can thereafter help to release more electrons which in turn continue the process. Analysis of this situation for uniform fields shows that the time rate of increase of electrons is an exponential. This situation is expressed by Townsend's equation:

$$i = i_0 e^{\alpha x} \quad (3)$$

where  $i_0$  is the current between infinite parallel plates which would be the result of ionization due to some external source at a distance  $x$  from the anode, if ionization by electron collision were absent;  $i$  is the current in the presence of ionization by collision, and  $e$  is the base for natural logarithms.  $\alpha$  is a constant called the "first Townsend coefficient", which is the number of new electrons released per cm of advance of the initial electron.  $\alpha$  varies through wide limits with field strength and mean free path, i.e., with energy gained by the electrons between collisions, and is best considered as a relation between  $\alpha p_0/760p$  and  $E p_0/760p$  ( $\alpha/p$  and  $x/p$  in Loeb's work).

### 6. Ionization by Photons

In addition to the ionization by electron collision which is discussed above, one other source of ionization is of fundamental importance. When the ionization by collision processes are taking place at the higher values of  $E p_0/760p$ , it frequently happens that collisions give much more energy than necessary to ionize the molecule. This leaves the ion excited and it returns to normal by emitting a photon, some of which may be very energetic. Occasionally one of these photons encounters a molecule and may be strong enough to cause ionization.

### 7. Ionization by External Causes

The ionization discussed above in items 4 and 6 are caused by the gaseous conduction processes themselves. Ions may also be formed in the gas by the well-known processes which depend upon external agents, such as photoelectric ionization due to X-rays, ultraviolet light,  $\gamma$  radiations, etc., and by  $\alpha$  and  $\beta$  particles passing through the gas.



## 8. Emission of Electrons from the Cathode

The usual electron emission processes are: thermionic emission, high-field emission, photoelectric emission, and secondary emission due to bombardment by positive ions. At very high currents for fine negative points, we have observed the platinum point to glow with a bright yellow color, and under these conditions, thermionic emission may be effective; but for most cases, thermionic emission is not important. With the finest wires, perhaps the 1 and 3.5-micron sizes, the electric field near the tip of the negative wire may be high enough for appreciable high-field emission. This requires fields of  $10^6$  to  $10^7$  volts per cm at the tip of the wire (Reference 36). For negative points, the emission of electrons by bombardment from positive ions is the most important process to be considered. When  $E_{p_0}/760p$  has a value of the order of 2000 at the wire surface, positive ions strike the cathode with some 20 electron volts energy, and begin to be effective in causing the emission of electrons (Reference 29). The remaining type of emission to be considered is the photoelectric emission. Since the tip of a fine wire cathode has a very small area, the probability of photons striking here is greatly reduced, and therefore, photoelectric emission effects for pointed cathodes are negligible. In the case of positive points, the cathode is a relative large area. In this case, emission either from photons emitted by the corona processes or from externally formed photons may be important at the cathode.

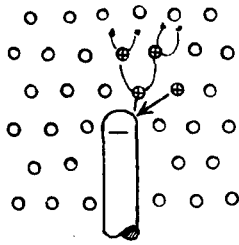
## 9. Space Charges

Space charges play a very important part in corona discharges. In the discussion of electron avalanches of item 5 above, electrons rush through a field of molecules, generating many more electrons. Since electrons have of the order of  $10^4$  greater mobility than the positive ions which are formed by the avalanche, they quickly disappear from the scene and leave a cloud of slowly moving positive ions. These contribute a net charge to the volume they collectively occupy which is known as the space charge. This must be treated with full respect as an electrical charge and as such may greatly modify the electric field in the vicinity. The electrons themselves also constitute a space charge, but it moves away so rapidly, that for many purposes its effects are less important. If the electrons later encounter a field low enough so that they can attach themselves to the  $O_2$  molecules, slow-moving ions result and again may contribute important space charge effects.

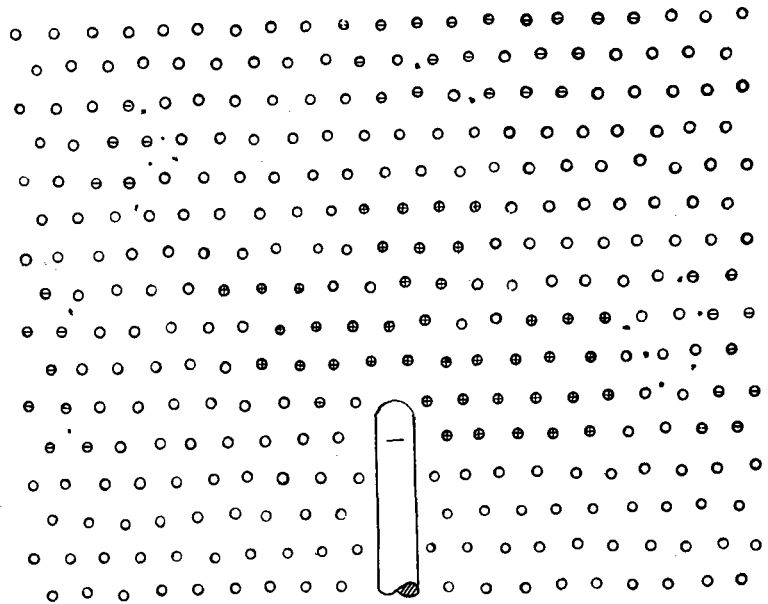
With the above outline of the basic processes of interest, we can proceed with a discussion of the coronas. Two cases must be discussed separately, negative points and positive points. The negative corona will be discussed first. For simplicity, the electrodes considered will be a point (or the tip of a fine wire) and a plane some distance away. This electrode model will serve as a basis for qualitative understanding in the case of practical electrode types, provided the electrode opposite the point (hereafter called the "plate") has not any area with a radius of curvature less than about 100 times the radius of curvature of the point. Even a larger radius of curvature of the plate must be used for relatively high corona currents.

### B. Negative Corona

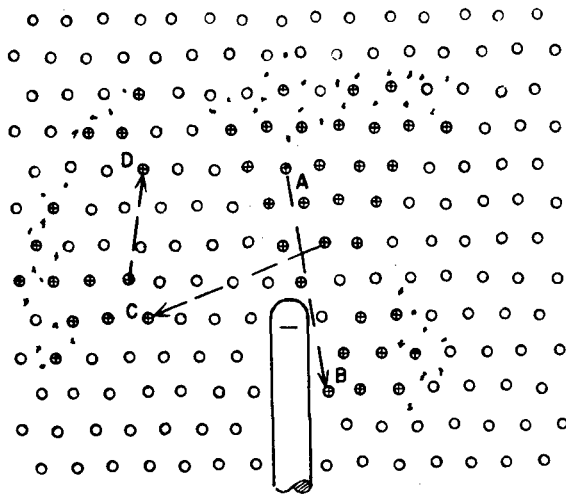
In the gap between the negative point and the plate, ions will occasionally be formed from external causes. When a low voltage is applied between the point and plane, these ions are attracted to the appropriate electrodes and constitute a feeble current. The electric field near the point is very much higher than any other region in the gap. The positive ions from these occasional ionizing events move to the point, and as the voltage is raised, this high field eventually becomes high enough to cause an occasional positive ion to liberate an electron from the point by bombardment. This electron rushes outward through the high-field region and forms an electron avalanche. Figure 1 at (a) depicts the release of an electron by bombardment from a positive ion and the beginning of an avalanche. At (b) in Figure 1, this initial avalanche is shown at a very short time later. Also shown at (b) are the effects of photoionization in initiating neighboring avalanches. In (b) at C, a photon has started a new avalanche, which in turn has provided the photon which started a third avalanche at D. The initial avalanche has also accounted for the initiation of an avalanche at B. Many of the photons which are emitted, do not happen to ionize molecules in the high-field region where the electrons liberated can form avalanches. Figure 1 at (c) shows the corona at a slightly later time. The positive ions have started to move toward the cathode, but the most important new effect is indicated farther out from the point near the edge of the sketch. The field here is so low that electrons no longer have



(a) Initiation of an avalanche by positive ion bombardment of the cathode.



(c) A later stage of the avalanches of (b), in which the fields at the outer ends of the avalanches are too low for further ionization but the fields are low enough for negative ion formation. More avalanches which would have formed are not shown.



(b) Development of the initial avalanche and initiation of others by photoionization from the first.

Figure 1. Schematic illustration of the formation of a Trichel pulse in negative corona, for a small diameter cathode. The dots represent electrons, the circles are molecules, ions are + or - signs in the molecule, and photon paths are indicated by the dotted lines, (Reference 4).

the ability to ionize by collision, for two reasons: (1) the field normally decreases rapidly as a function of distance from the point, and (2) the space charge produced by the positive ions near the point is of opposite sign from

the charge induced on the point by the applied voltage, and therefore, the electrons which are repelled from the point also are attracted by this positive space charge, i.e., the space charge has lowered the electric field in the vicinity of the electrons. The electrons begin to attach themselves to the  $O_2$  molecules to form negative ions and these drift to the plate while the positive ions are swept to the point. The space charge produced by the  $O_2$  ions also helps reduce the field below the level required for ionization by collision. Figure 1 at (c) shows only the avalanches which were started in Figure 1 at (b). Actually, the processes of (b) continue to form avalanches, and the result is that (c) actually would show a much greater number and perhaps more uniform distribution of ions. An avalanche may form in the order of  $10^{-9}$  seconds, and the entire pulse in  $10^{-7}$  or  $10^{-8}$  seconds (Reference 30). In this latter situation, the space charges prevent the formation of any further avalanches of significance and nothing further happens until most of the positive charges have been swept to the point. One or more of the last few positive ions arriving at the point is likely to cause the emission of a secondary electron which can start the whole cycle over, as outlined above.

It is clear from the above description of the negative corona that the negative corona current will come in the form of pulses. This pulse is called a "Trichel" pulse. Raising the voltage causes these pulses to repeat more rapidly because with higher voltages, a new pulse can start somewhat before the positive ion space charge has completely drifted away. These pulses form quite regularly and for fine points, we have observed frequencies up to more than 5 mc. Frequencies as low as 5 kc have been observed (Reference 31). At very low currents, the pulses become nonperiodic. For a particular spacing, when the voltage becomes too high, the corona may give way to a spark which bridges the gap.

The size of the corona is small compared with the gap between electrodes.

The glow of the corona close to the wire originates in the emission of photons of various wave lengths corresponding to a contribution to the molecule by the colliding electron of more than the energy of ionization. The extra energy excites the molecules and they quickly return to the normal state by emission of light. Outside this region is a dark region where the field is too low for further ionization by electron collisions. This dark region is difficult if not impossible to observe because of the spherical geometry involved. It is probably very small for our cases. Beyond this, electrons

which attach to  $O_2$  molecules give up small amounts of energy and a relatively pale glow results. Except when the voltage is near the value for a spark, the remainder of the gap is quite dark for negative corona. Even a two-hour exposure on presensitized EK Linagraph Ortho film with an f/1.5 glass lens fails to detect any light in the gap.

### C. Positive Corona

The positive point corona has nearly all the basic processes of gaseous conduction which appear in the negative corona, and although there is a similarity in the relations among current, voltage, spacing, and density, for positive and negative coronas, the basic processes cooperate in a rather different way. Positive corona is characterized by two types of pulses, the "burst" and the "streamer" pulses. These pulses are not regular as in the case of Trichel pulses for the negative point. There are several distinct regimes for the positive corona.

As the potential across the gap is increased from low values, a small current can be detected, resulting from the small amount of ionization normally present in the air. With an external ionizing agent, this current can be increased. As the potential is further increased so that  $E_p/760p$  is equal to or greater than 90 at a distance of at least a few mean free paths away from the point, a new regime is encountered. The negative ion approaching the point sheds its electron, and the electron is capable of ionizing any further molecules with which it collides in traveling to the point. This regime is called "the field-intensified ionization discharge" or "Townsend discharge". The current increases by several orders of magnitude as the potential is increased and larger (burst) pulses appear. This regime is called the "Geiger counter" or "intermittent burst pulse" regime. In this regime both burst and streamer pulses are possible, as further discussed in a later paragraph. External ionization is still required to initiate the pulses. As the potential is increased further, the pulses become more numerous until the burst pulses become continuous. This point is called the onset potential for continuous burst pulse corona. After this point, external ionization is not needed because the pulses are able to initiate succeeding pulses. Further increase in potential leads only to increased size and frequency of the pulses.

The only type of pulse in this regime until the corona approaches a spark discharge is the burst pulse. Just before the spark breaks down the gap, the streamer pulses are again present. In this case the streamer pulses are larger and are more commonly called pre-breakdown streamers. These are the distinct regimes of the positive corona.

It is in the intermittent corona regime, where there are two types of pulses, that the streamer pulses are found. Once the burst pulses become continuous, the streamers disappear. The streamer pulses serve to initiate the burst pulses in this regime under favorable conditions in the following manner. The initiating negative ion sheds its electron some distance from the point and a rather large avalanche is created. The electrons are rapidly drawn into the point leaving the positive ions behind. At the outer tip of this avalanche, the field is much increased because the positive ion space charge adds to the static field. The new field is much like the field from a new positive wire with its tip at the outer tip of the avalanche. As the field was greater than that for the Townsend discharge, some of the molecules of the first avalanche received enough energy to become excited and therefore they emitted photons. Some of these photons are able to produce photoelectrons farther out in the gap. These electrons are now able to cause avalanches which descend on the outer tip of the first avalanche. Thus the process can continue because the positive ions left by the second avalanche will still further increase the field near its outer tip. As the avalanches build farther out into the gap, the static electric field for the point-to-plane becomes so low that even with the increase of the field due to the space charge, the field is too small to continue creating avalanches. The pulse can no longer propagate. Then the positive ions in the gap start drifting toward the plate. The time for this streamer pulse to form is very short, i.e., about  $10^{-8}$  seconds (Reference 32). It propagates outward from the point at about the velocity of electron travel.

While the streamer propagates itself outward into the gap, some of the photons may start avalanches near the tip of the wire as well as near the tip of the streamer. If the static field is not too low, these can form small avalanches as the electrons descend on the wire. These small avalanches are unlikely to propagate far out into the gap as did the original streamer because the positive space charge of the streamer is so located with respect to these latter avalanches as to somewhat reduce the point-to-plane static field. Thus these small avalanches propagate only a small distance and

encounter too low a field for further activity; hence they are sometimes referred to as "incipient streamers". These avalanches may continue for a short time after the initiating streamer has become inactive. These avalanches constitute the "burst" or "incipient streamer" pulse.

When the static point-to-plane field is raised still more, these burst pulses may continue indefinitely, providing their own initiating ionization. The space charge, which they leave, drifts outward continuously and never allows the presence of the high field necessary for the streamer to form. This is the "continuous burst pulse regime". At least one streamer is always present to initiate it, but once formed, streamers are not observed. Only when the static point-to-plane field is so high that spark crossing the gap is imminent, do the streamers again find the field high enough to put in another appearance.

The ion motions outlined above can be visualized better, perhaps in view of the processes outlined for the negative corona and partly illustrated in Figure 1.

## SECTION II

### RELATIONSHIP AMONG THE CORONA VARIABLES:

#### CURRENT, VOLTAGE, DENSITY, SPACING, AND WIRE DIAMETER

There is no convenient theory to predict the relationship among the various variables which are involved in the corona discharge, but nevertheless it is very important to have available a convenient and at least approximate relationship, if the corona is to be useful as a measuring device. Two of the more important variables (current, voltage, density, and spacing) may be considered as parameters. One of the remaining two may be considered the independent variable and its value can then be determined by observation of the fourth variable which is treated as the independent variable. The application of the corona discharge to use as a microphone is an example in which the corona was operated at constant voltage and spacing, with density as the independent variable, and current as the dependent variable. Figures 2 through 9 give experimental data for both positive and negative points, for

densities from about 0.1 to 5 times the density at standard conditions,  $\rho_0$ , currents from 1 to 30 microamperes, spacings from 0.76 to 12.7 mm, and voltages from 600 to 10,000 volts. Spacing is the parameter which varies from each figure to the next; density is the parameter from one curve to another on a particular figure, current is the ordinate, and voltage is the abscissa.

The data were taken in the following manner: A point-to-plane type of corona probe was mounted in a cylindrical steel chamber 6 inches in diameter and 10 inches high. A steady flow of dried high-pressure air was passed very slowly through a dust filter of oily glass wool and then through the test chamber. By having a needle valve at the input and exit of the test chamber and a vacuum pump on the exit side, all the pressures in the above range could be obtained. A small flow of air is required in this experiment to keep the composition of the air a constant. This point will be covered more completely under the heading of "Density Sensitivity".

In taking the data, the following technique was used: The voltmeter and ammeter were placed close together under a flood light. The two meter faces were then photographed with a motion picture camera. When the pressure in the test chamber was at the correct value, the corona voltage was slowly increased and a complete set of data of current vs. voltage was then obtained. Each run was taken in less than 15 seconds so that needle disintegration and collection of dust was not a problem. The curves of Figures 2 through 9 were then plotted from the rolls of film. The data shown in Figure 3 is typical and has been tabulated as shown in Table 1. The data in Figures 2 through 9 are for point-to-plane geometry only. For geometry which does not depart greatly from point-to-plane, this information is still of value as a first approximation. It is conceivable that the corona could be used as a density, spacing, voltage, or current meter, although it is of special interest for density since, in most cases, spacing, voltage, and current are readily measured by simpler devices.

The data are in a form which is inconvenient for analytical treatment of the performance of the corona. For this reason, considerable attention was given to the problem of fitting an empirical expression to the data. As a first attempt, a dimensional analysis (Reference 37) was attempted, making use of 12 "variables", only five of which are actually subject to change. The variables were: current, voltage, spacing, wire diameter, molecular mean free path, charge of an electron, work function of the cathode, energy to remove an electron from a molecule, energy to remove an electron from a



TABLE 1

Current vs. Voltage for Positive Corona at Various Pressures, for 1.78 mm Spacing and 25.5°C. The numbers in the body of the table are corona voltage in volts.

Wire Dia. Microns	I, $\mu$ Amp	Pressure, mm Hg					
		70	150	400	700	2280	
9	1	950	1100	1400	1530	2350	2900
9	3	1010	1200	1630	1840	2930	3680
9	5	1070	1280	1780	2090	3380	4300
9	10	1170	1420	2080	2480	4200	5350
9	15	1220	1500	2350	2850	4880	6250
9	20	1290	1600	2500	3030	5400	6830
9	25	1320	1700	2680	3250	5800	7400
9	30	1360	1770	2770	3450	6200	7900
3	1	975	1125	1300	1460		
3	2	1010	1170	1450	1650		
3	3	1030	1215	1540	1800		
3	4	1040	1260	1650	1950		
3	6	1070	1340	1820	2250		
3	8	1150	1410	1980	2450		
3	10	1160	1480	2100	2650		
1.5	0.5	900	1010	1190	1300		
1.5	1.0	925	1050	1280	1450		
1.5	1.5	950	1075	1360	1525		
1.5	2.0	970	1090	1425	1650		

a negative ion, mean free path of an electron, mass of a molecule, and mass of an electron. The fundamental units were taken as mass, length, time, and charge. A variety of dimensionless parameters could be formed, and the most convenient of these sets of parameters were chosen. This set of dimensionless parameters contained all five of the variables of interest in four of the parameters, and the other four parameters contained only combinations of "variables" which were actually not subject to change. This would have reduced the original number of variables to be considered from five to four, but the data failed to correlate when plotted as relations among these dimensionless variables. It was found necessary to introduce another length to the list of twelve variables in order to provide a hope for correlation of the data, but this resulted in five parameters involving the five variables of interest, which nearly eliminated the value of the dimensionless analysis, and the procedure was abandoned.

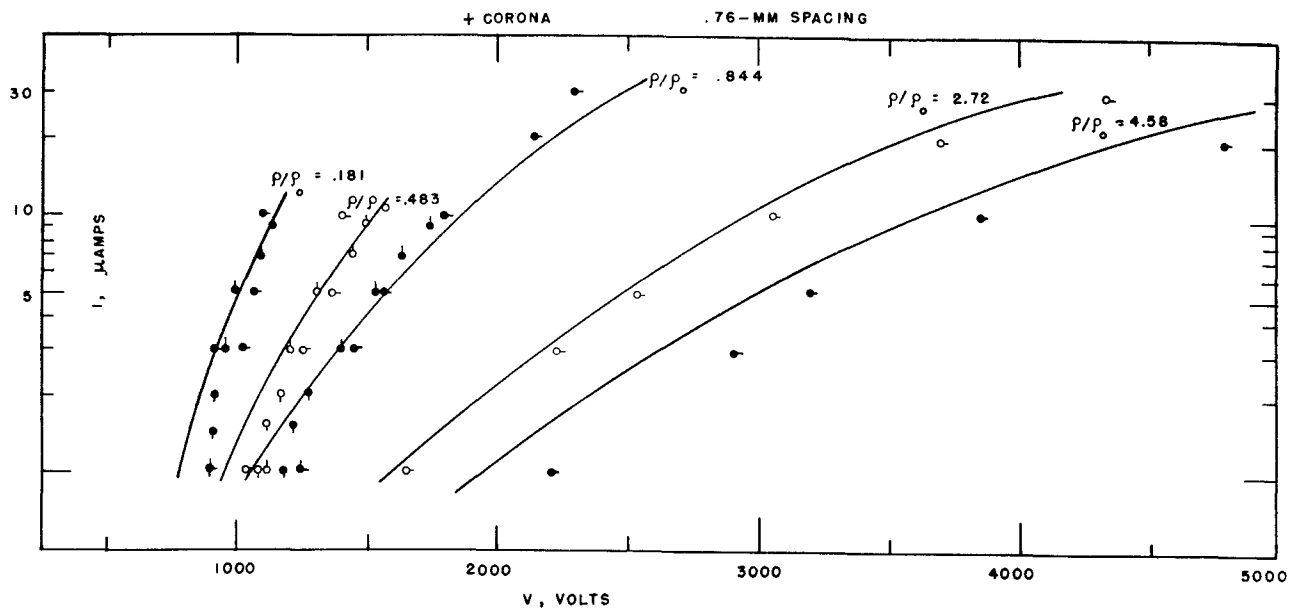


Figure 2. Data for positive corona at various densities and at 0.76 mm spacing. The solid lines are from the empirical relation among voltage, current, density, and spacing, (Reference 4). Indices to the right, top, and bottom are for wire diameters of 9, 3, and 1.5 microns, respectively, (approximately 0.36, 0.12, and 0.06 mils, respectively). Black and white circles are merely to identify points with the respective groups.

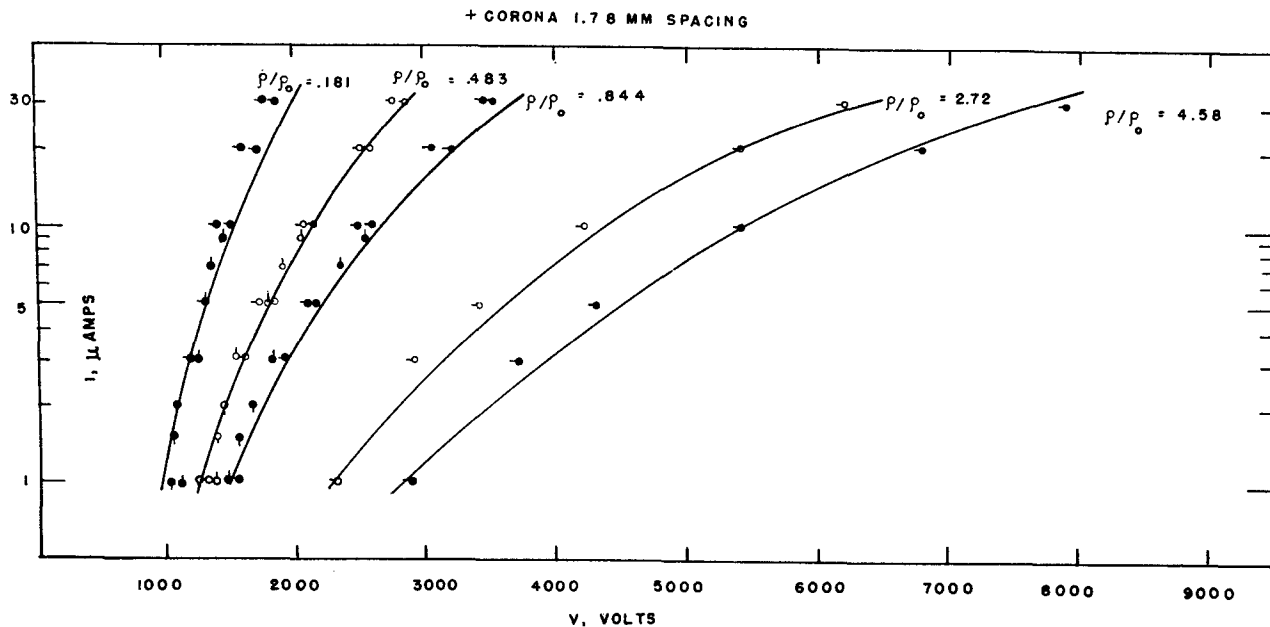


Figure 3. Data for positive corona at various densities and at 1.78 mm spacing. The solid lines are from the empirical relation among voltage, current, density, and spacing, (Reference 4). Indices to the left, top, and bottom are for wire diameters of 9, 3, and 1.5 microns, respectively, (approximately 0.36, 0.12, and 0.06 mils, respectively).

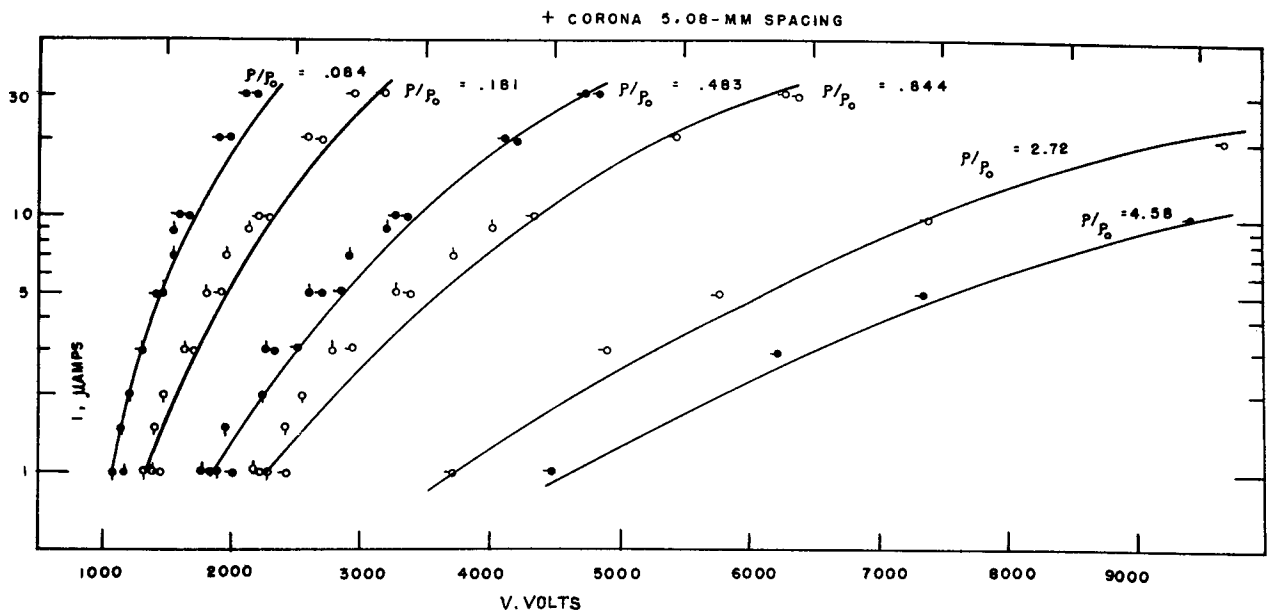


Figure 4. Data for positive corona at various densities and at 5.08 mm spacing. The solid lines are from the empirical relation among voltage, current, density, and spacing, (Reference 4). Indices to the left, top, and bottom are for wire diameters of 9, 3, and 1.5 microns, respectively, (approximately 0.36, 0.12, and 0.06 mils, respectively).

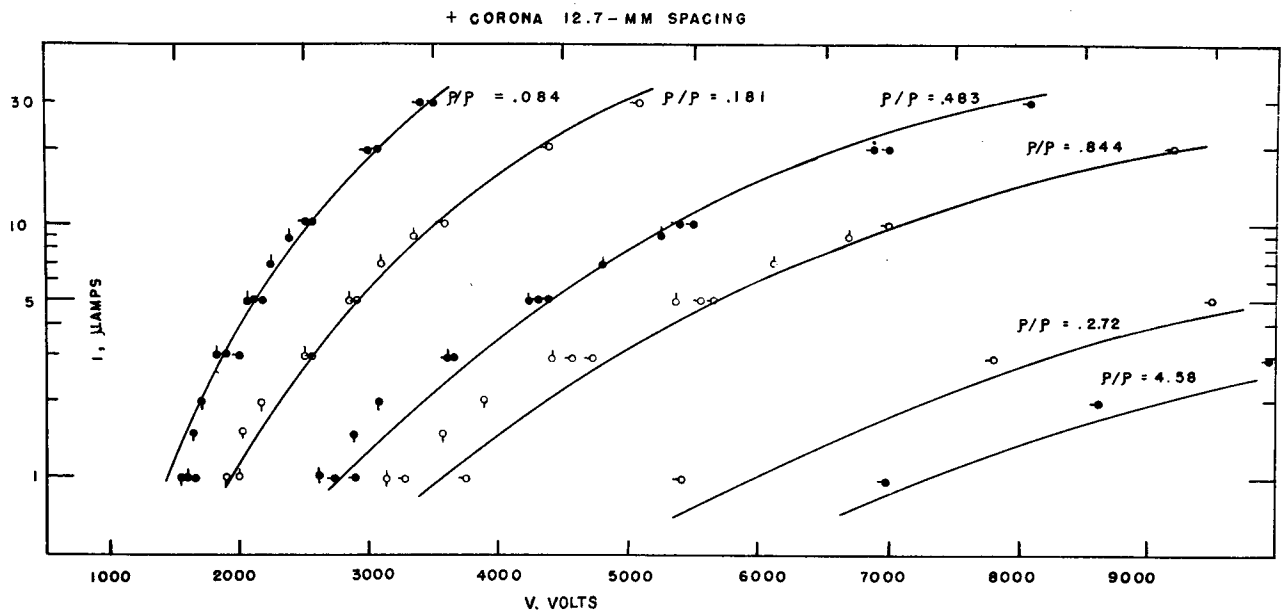


Figure 5. Data for positive corona at various densities and at 12.7 mm spacing. The solid lines are from the empirical relation among voltage, current, density, and spacing, (Reference 4). Indices to the left, top, and bottom are for wire diameters of 9, 3, and 1.5 microns, respectively, (approximately 0.36, 0.12, and 0.06 mils, respectively).

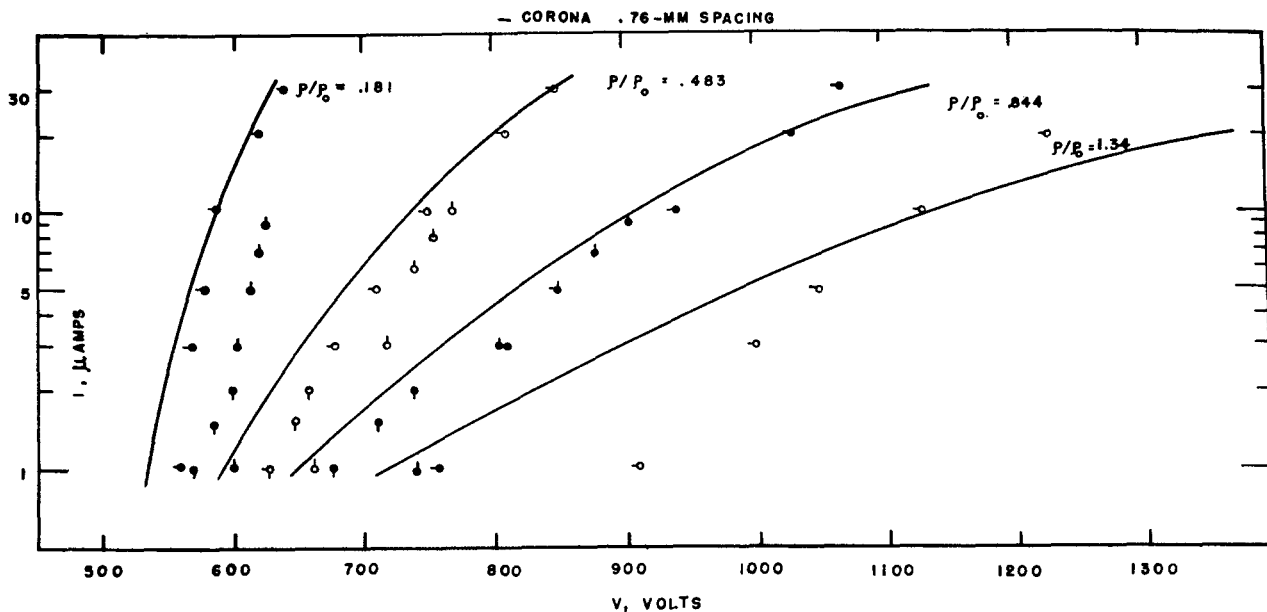


Figure 6. Data for negative corona at various densities and at 0.76 mm spacing. The solid lines are from the empirical relation among voltage, current, density, and spacing, (Reference 4). Indices to the left, top, and bottom are for wire diameters of 9, 3, and 1.5 microns, respectively, (approximately 0.36, 0.12, and 0.06 mils, respectively).

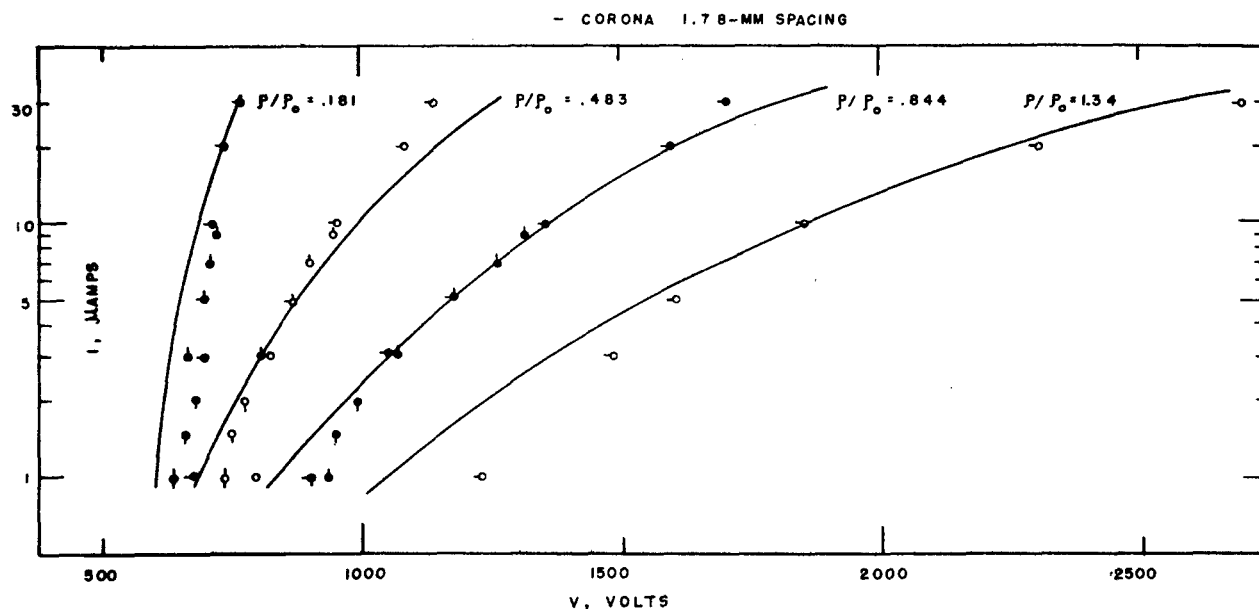


Figure 7. Data for negative corona at various densities and at 1.78 mm spacing. The solid lines are from the empirical relation among voltage, current, density, and spacing, (Reference 4). Indices to the left, top, and bottom are for wire diameters of 9, 3, and 1.5 microns, respectively, (approximately 0.36, 0.12, and 0.06 mils, respectively).

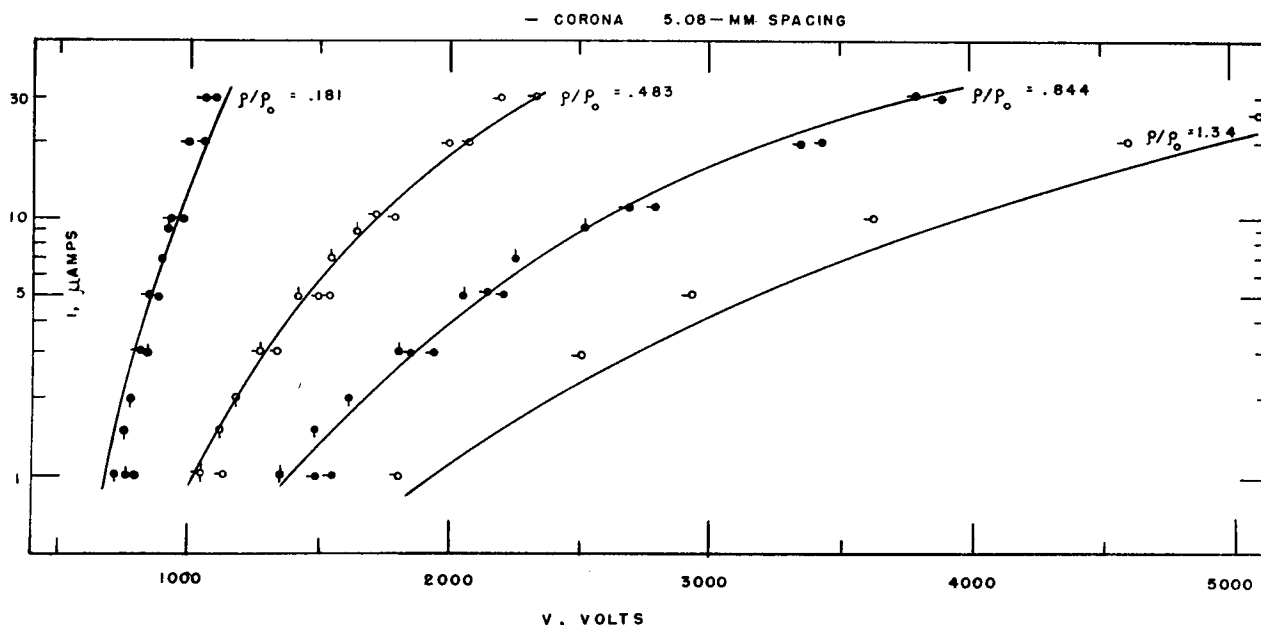


Figure 8. Data for negative corona at various densities and at 5.08 mm spacing. The solid lines are from the empirical relation among voltage, current, density, and spacing, (Reference 4). Indices to the left, top, and bottom are for wire diameters of 9, 3, and 1.5 microns, respectively, (approximately 0.36, 0.12, and 0.06 mils, respectively).

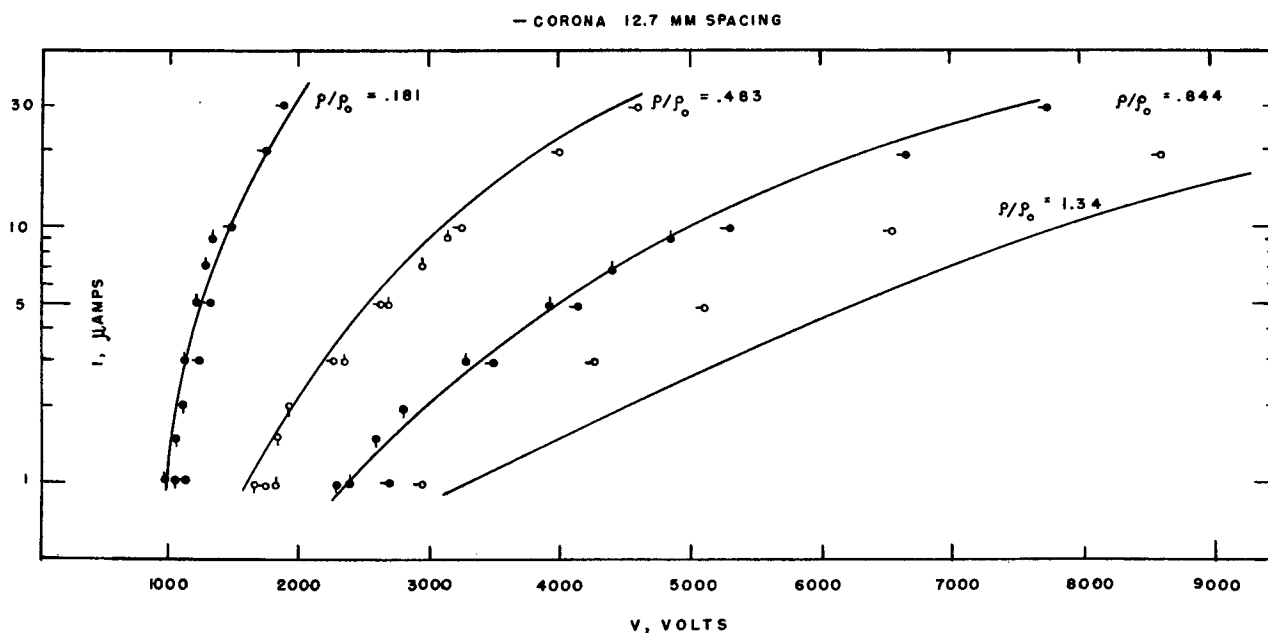


Figure 9. Data for negative corona at various densities and at 12.7 mm spacing. The solid lines are from the empirical relation among voltage, current, density, and spacing, (Reference 4). Indices to the left, top, and bottom are for wire diameters of 9, 3, and 1.5 microns, respectively, (approximately 0.36, 0.12, and 0.06 mils, respectively).

After some effort, equation (5) for positive corona and equation (6) for negative corona were arrived at empirically by assuming that they have the form:

$$I = C(\rho/\rho_0)^a (s)^b (V - V_0)^c \quad (4)$$

where  $V$  is voltage in volts,  $I$  is current in microamperes,  $s$  is the spacing in millimeters,  $\rho$  is the density of the air, and  $\rho_0$  is the density of air at  $0^\circ\text{C}$  and 760 mm of Hg. By plotting density against voltage at various currents with the spacing held constant and extrapolating to zero density, it was noted that when  $\rho$  was zero,  $V$  was approximately 500 volts.  $V_0$  was therefore assumed to be 500 volts.  $a$ ,  $b$ , and  $c$  were determined by making similar plots on log graph paper. The constant  $C$  was chosen such that the sum of squares of the observed current minus the predicted current was a minimum.

A least squares equation is of little value unless one has some idea of the variability of the observed current from the predicted current. The standard error of estimate,  $S_e$ , is the root mean square of these differences. If the observations come from normal populations with homogenous variances, i.e., the variance is independent of the particular value which is picked, 68% of the values will lie within  $S_e$ , 95% within  $2S_e$  of the predicted value, etc. The empirical expressions, together with  $S_e$ , were found to be:

$$I = 1.91 (\rho/\rho_0)^{-3/2} s^{-5/3} (V/1000 - .5)^3, S_e = 1.84 \mu \text{ amp (+ corona)} \quad (5)$$

$$I = 37 (\rho/\rho_0)^{-8/3} s^{-7/3} (V/1000 - .5)^{8/3}, S_e = 5.50 \mu \text{ amp (- corona)} \quad (6)$$

These equations are plotted as the solid lines in Figures 2 through 9. A close examination of the data for various wire sizes will confirm our conclusion that to a fair approximation, wire diameter is of no importance in the relationship. This is found not to be true at relatively high density and low current, and probably results from the fact that the radius of the small wire is negligible compared to the length of the avalanches which make up the pulses only if the current is high and the density of the air is low. In the case of low density and high current, it is presumed that the change in length of the avalanche which results from the use of a small wire is insignificant, and wire diameter is unimportant under these circumstances.

A standard error of estimate of 5.5 for negative corona seems so high as to impair the usefulness of the equation, however, it should be noted that in a large part of the region under consideration, a very small change in voltage causes a relatively large change in current.

Figure 10 was taken from Reference 1. It gives some interesting data on the effect of cylinder radius for a point to cylinder discharge. The cylinder axis was perpendicular to the axis of the point and the nearest point on the cylinder was at a distance of 3 mm from the corona. The data serve as a basis for estimating how far from flat plate geometry one can deviate without significant change. At the smaller plate radii, a second corona at the cylinder surface became evident and accounts for the peculiar shape of the curves in this region. It is to be noted that for small currents, plate radius has a somewhat smaller effect at very small plate radii.

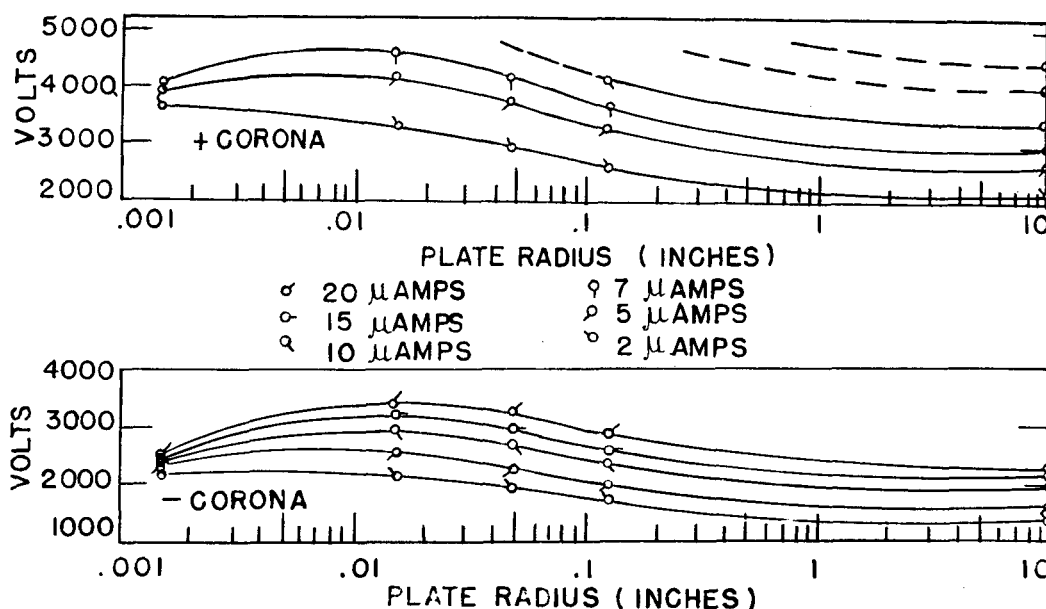


Figure 10. Effect of variation of plate radius on the + and - corona from the tip of a 25-micron (1 mil) wire. The plate was in the form of a long cylinder whose axis was perpendicular to the axis of the wire. The nearest surface of the cylinder was 3 mm from the corona. Tests were in room air. (Reference 1.)

Figure 11 was taken from Reference 3. It shows the rate at which a platinum wire tip disintegrates for negative coronas under the influence of positive ion bombardment. This process is commonly called sputtering. The current density is referred to the cross sectional area of the wire. An analytical expression for the line is:

$$\delta = 3.37 \cdot 10^{-4} \cdot i^{1.42} \quad (7)$$

where  $i$  is the current density referred to the wire cross section in amperes per square centimeter, and  $\delta$  is in cm per hour. The presence of dust will

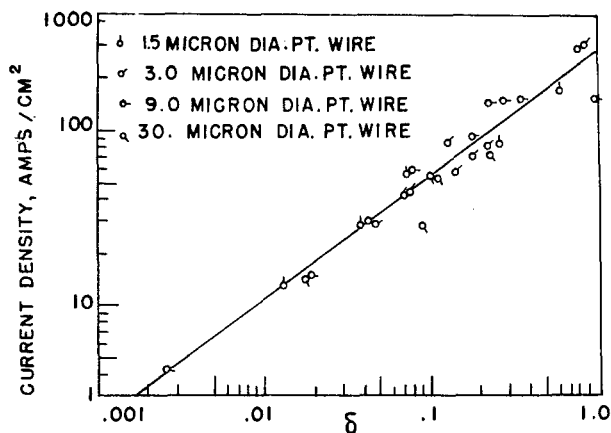


Figure 11. Rate of disintegration of negative wire tips. Current density is referred to the cross sectional area of the wire. Positive wire disintegration is less than one-thousandth that for the negative wire.  $\delta$  is wire disintegration in cm/hour.

greatly reduce the rate of disintegration. These data provide information on the useful time available for a negative corona wire of a given length and current density.

For the positive corona, tests were also performed to measure the rate of disintegration of the needle. The results show that if there is positive corona disintegration, it is less than one one-thousandth that of the negative corona.

### SECTION III

#### CORONA BACKGROUND NOISE MEASUREMENTS

Measurements of the corona background noise for negative corona have been reported in Reference 3. In recent studies interest has been revived for positive coronas. Therefore tests were performed to measure the background noise of positive corona, and the negative corona data were also repeated.

The circuit used is shown in Figure 12-A. A point-to-plane type of corona was used. The spacing was 4.05 mm and the plate diameter 25.4 mm. The probe was placed in a glass chamber which was provided with a very low velocity flow of dust-free air. The signal was developed in a 470-K ohm load resistor and fed into a broad-band (0.5 to 50 kc) amplifier. The output of the amplifier was fed into a Hewlett-Packard Model 300-A Wave Analyzer. The pass band of the wave analyzer was carefully measured and a plot of the pass band is shown on Figure 12-B. The background noise of the corona gave a constant output voltage as the analyzer frequency was varied from 100 cps to 16 kc. Thus the corona noise in this range is "white" noise, since the noise voltage is dependent on the bandwidth and not the center frequency of the pass band. White



noise voltage is proportional to the square root of the bandwidth (Reference 38). Various bandwidths were used on the wave analyzer, and it was found that the corona voltage was proportional to the square root of the bandwidth as this reference predicts.

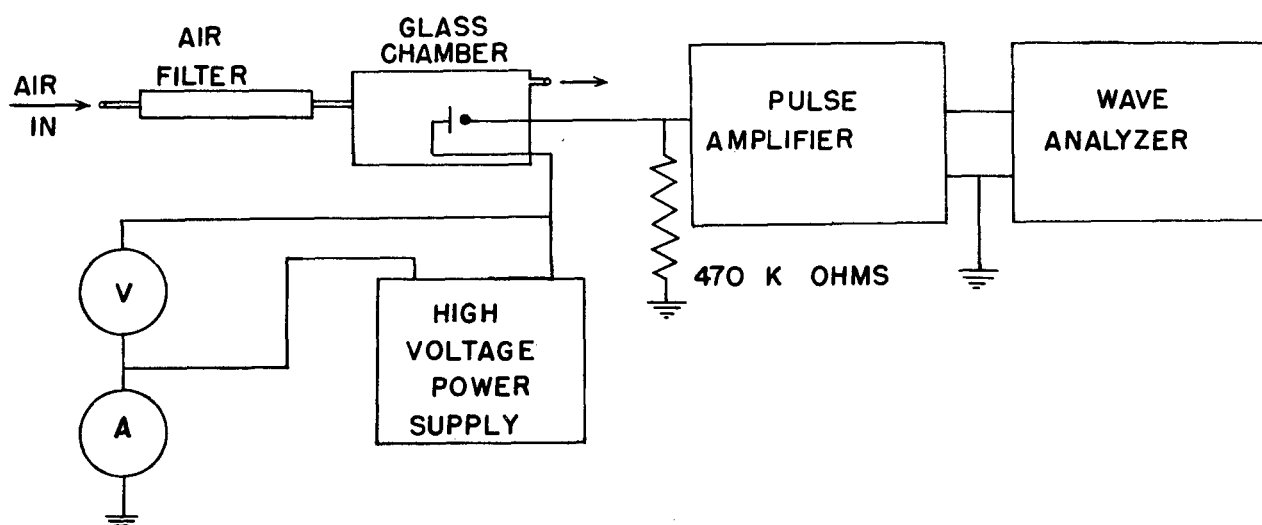


Figure 12-A. Schematic diagram of apparatus for background noise measurement. (Reference 4.)

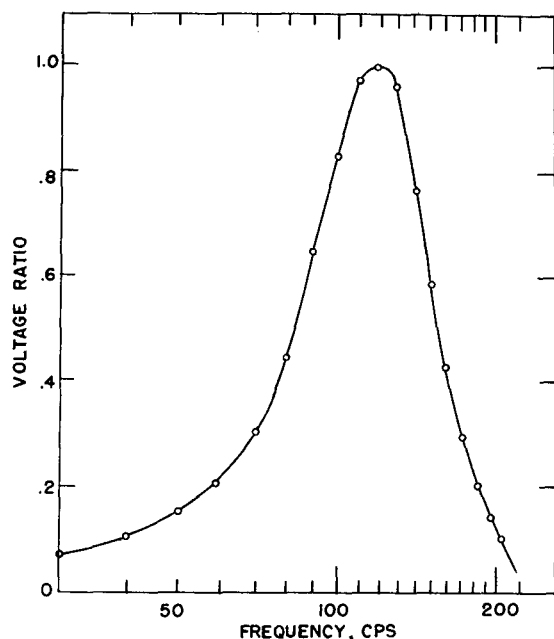


Figure 12-B. Pass band characteristic of the wave analyzer. (Reference 4.)

The data were computed in the following manner: The corona DC current was set at various values, and the output voltage of the wave analyzer was recorded. From this output voltage, the peak values of corona AC current in the 470-K load resistor, per unit bandwidth, were computed from the square-root-of-the-bandwidth law and from a knowledge of the voltage gain involved. If a change in density is to be detected by the corona, it must produce a change in current approximately equal to the noise level; and if it is to be

measured, the change of current must be much larger than the noise level. Thus we have presented the background noise data as shown in Figure 13 in

terms of the intensity of sound which gives a density change that is equal to the noise level of the background noise for 1-cps bandwidth.  $\nu$  is defined as  $20 \log I/I_0$  where  $I$  is the intensity of the sound and  $I_0$  is the reference level intensity of  $10^{-16}$  watt/cm<sup>2</sup>. The  $\rho_a/\bar{\rho}$  scale is defined similarly as the amplitude of the oscillating density variations divided by the average density of the gas which would cause a signal equal to the background noise for 1-cps bandwidth.

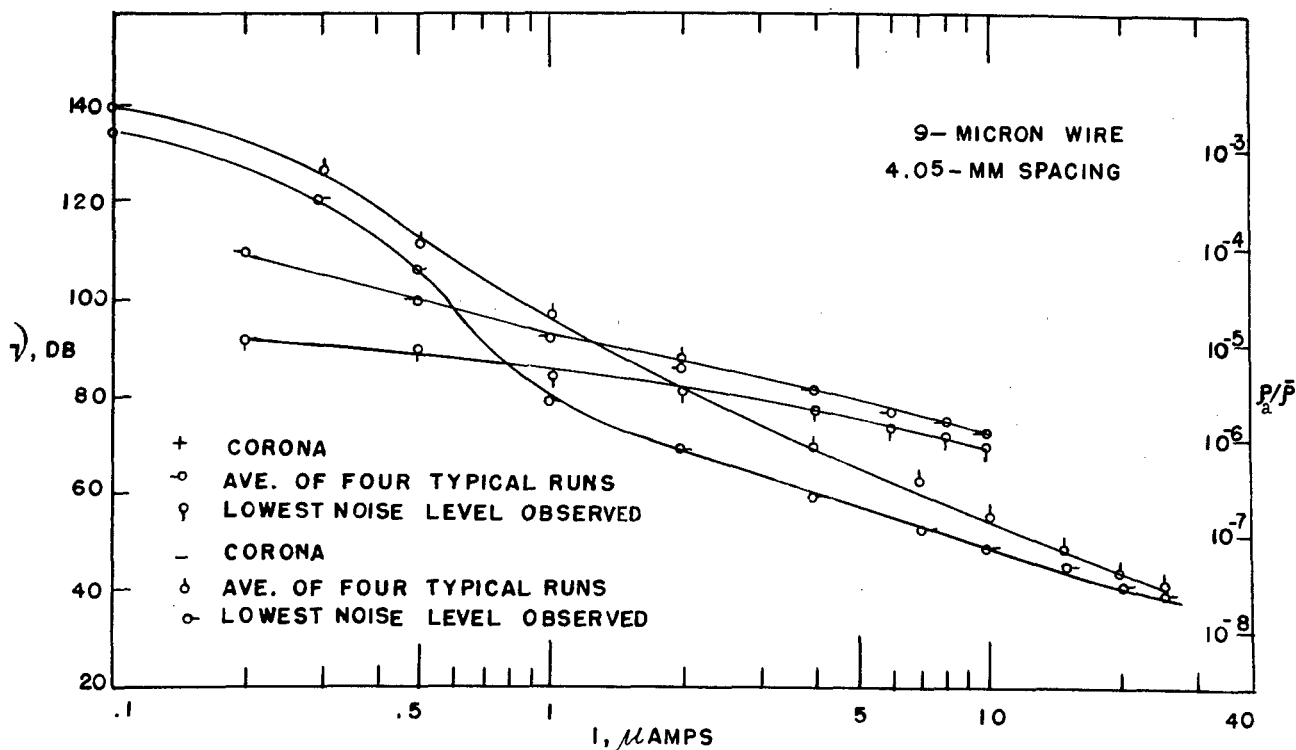


Figure 13. Background noise of the corona.  $\rho_a/\bar{\rho}$  gives the peak value of a harmonically varying density that would give the same average voltage for a 1-cps bandwidth as the corona background noise.  $\bar{\rho}$  is the density at 24°C, 740 mm Hg,  $\nu$  is the corresponding sound level in decibels to  $10^{-16}$  watts per sq. cm. (Reference 4).

The data shown in Figure 13 are for both positive and negative corona. The negative background noise data were compared with the data that were given in Reference 3 after the data were put into terms of a density sensitive corona. The previous data taken with different equipment and for the same conditions were about 10% higher than the average of the present data. Better filtering of the air may account for this as small particles of dust on the needle make the corona pulses more erratic and increase the noise voltage.

The higher noise curves in Figure 13 were the average of four runs which were typical of runs with clean wires. The lower curves were the lowest noise levels we have observed. In this latter case, great care was used to keep dust from the wire, and the wire was well rounded on the tip.

For positive corona, the corona pulses were observed with a Tektronix 513-D oscilloscope as the noise data were recorded. There was no apparent change in the shape or regularity of the pulses which caused the change in noise voltage. In negative corona, the situation is quite different. It was clear that more regular and constant amplitude Trichel pulses accompanied reductions in noise voltage. The Trichel pulses were regular in our most quiet runs, even at small currents. As soon as they became erratic, the noise voltage increased. It appears that the noise voltage could be greatly reduced if the Trichel pulses could be spaced regularly. Thus if a triggering voltage spike were superimposed on the DC voltage from the power supply at a frequency somewhat higher than the normal frequency of the Trichel pulses, this voltage pulse would trigger the Trichel pulses at a regular rate making the height and the frequency of the pulses to be more nearly constant as the conditions for each pulse would become the same. For ideal triggering, the corona would be quiet in all regions of frequency below the frequency of the pulses, i.e., no sub-harmonics of the Trichel pulse frequency would be generated.

In observing the Trichel pulses on the Tektronix 513-D oscilloscope, the frequency was noted and compared with Loeb's data (Reference 35). Our corona wires were evidently much smaller than Loeb's point with the result that the frequency was much higher. The plot of frequency versus corona current is shown in Figure 14. It was noted that spacing had little or no effect on the frequency which confirms Loeb's findings. Also the pressure was varied 200 mm of Hg above and below atmospheric pressure at constant temperature with less than 10% change in frequency for a given current. The plot for 9-micron wire is for a clean needle. When a particle of dust settles on the needle near the corona, the frequency may change by as much as 50%. The frequency was relatively unstable with the 3-micron wire. The Trichel pulses were irregular at very low currents, and they lost their usual character again at high currents. When Trichel pulses were present, they were at a higher frequency for the same current for the 3-micron than for the 9-micron needles. If dust settled on the needle, the pulses appeared at a lower frequency, typical of larger wire sizes. Several tests were made with 1.5-micron wire but no typical Trichel

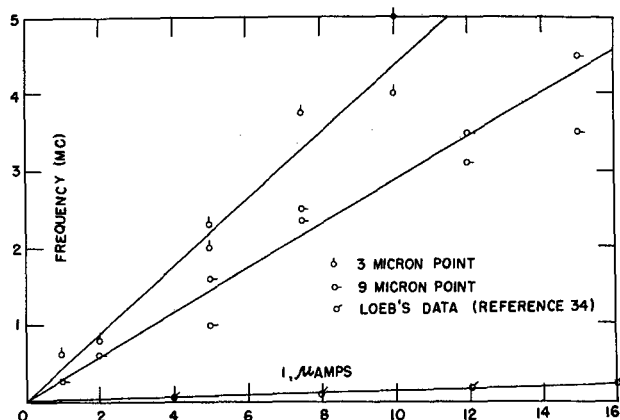


Figure 14. Frequency of Trichel pulses for negative corona at the tip of a fine wire. The effect of current and diameter of wire on the frequency is shown. The frequency of these pulses is subject to random changes of considerable magnitude. (Reference 4.)

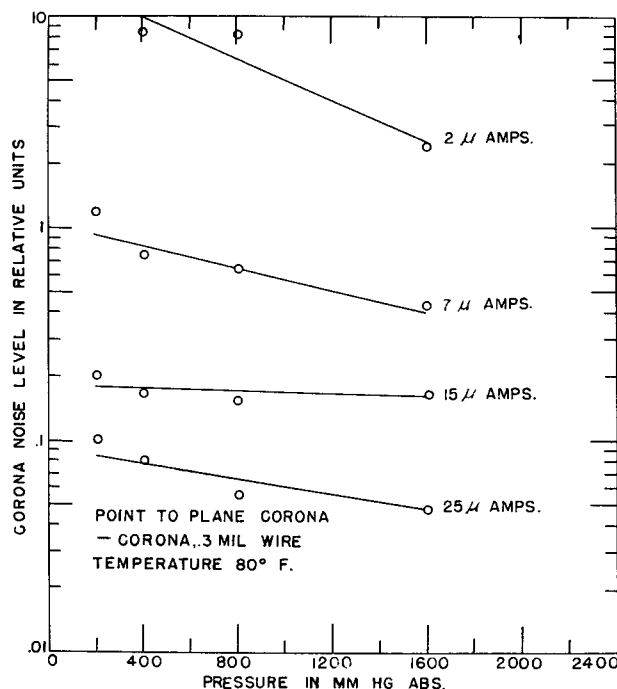
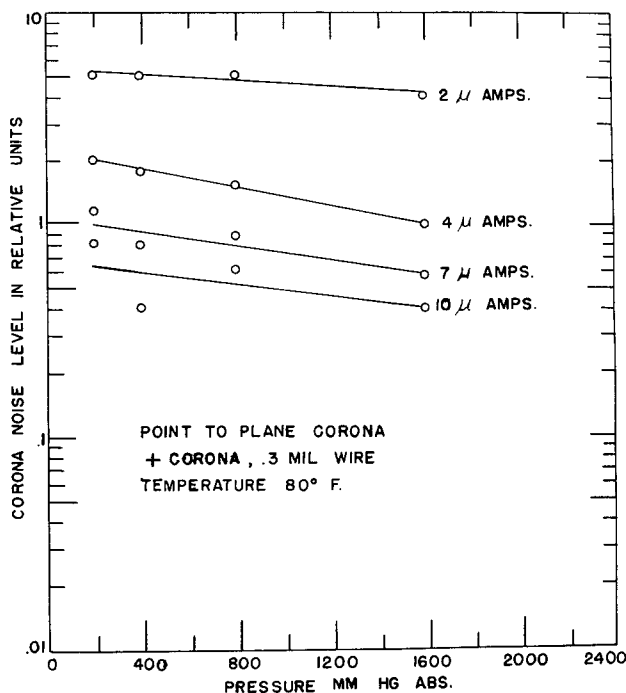
pulses were observed. The pulses which are present for 1.5-micron wire have a distinctly lower peak current, are about twice as long in time duration as the Trichel pulses, and the current does not go to approximately zero between pulses. We suggest as an explanation that high field emission of electrons begins to be a significant part of the total current, leaving a tendency toward the Trichel pulse mechanism, but reducing the importance of the role of these pulses in the mechanism of the discharge.

The effect of density on the background noise of the corona has been investigated. The experiment was performed in the following manner: A point-to-plane type of corona probe with 200 mils spacing was mounted in a 6-inch diameter, 10-inch high steel container. Clean, dry, high pressure air was admitted into the chamber by an input valve. An exit valve on the chamber was connected to a vacuum pump. By controlling the two valves, the various pressures were obtained. A resistor was placed in series with the corona. The corona noise generated in the resistor was amplified and fed into the wave analyzer described above.

The data are shown in Figures 15-A and B. The data are plotted in arbitrary units. The actual noise level per unit bandwidth can be obtained by comparison with Figure 13. These data show that density has little effect. However, the acoustic signal which generates current changes equal to the noise level of the corona varies with average density. The oscillating density amplitude is given in Reference 43 by:

$$J = (K_1 \rho_a \gamma)^2 / (2 \bar{\rho} v)$$

where  $K_1$  is a constant dependent on the units,  $\bar{\rho}$  is the average density,  $v$  is the velocity of propagation of the sound waves in the medium,  $\rho_a$  is the amplitude of the oscillating density variations,  $\gamma$  is the ratio of specific heats, and  $J$  is the sound intensity.



Figures 15-A and B. The variation of corona background noise with density for positive and negative corona. (Reference 4.)

From this equation and from  $\partial I / \partial \rho$  calculated from either Equation (5) or (6), it can be shown that for a given current and spacing the minimum sound intensity  $J$  which the corona can resolve varies with the 3.8 power of the average density, assuming the effect of density on background noise is negligible, per Figure 15. Stated in other terms, the minimum density variation which can be resolved can similarly be shown to be proportional to the first power of density.

#### SECTION IV DENSITY SENSITIVITY

##### A. Response of the Corona to Steady-State Density Changes

Density sensitivity was assumed and discussed in the foregoing, but it merits further consideration. In earlier corona studies made at this laboratory, it was assumed that the temperature within the corona was very high. This appeared to be valid and seemed to be supported by experimental evidence (Reference 1). If this were true, the corona would not appear to be sensitive to small changes of ambient temperature. This would make it insensitive to

density and essentially a pressure-sensitive device. The tests (Reference 1) were performed in a closed vessel, giving time for nitrogen oxides and ozone to accumulate and change the composition of the air being measured. In more recent studies a continuous-flow method was used which supplied air of constant composition. In these studies a temperature effect was noted. From plots of temperature and pressure data, the corona was found to essentially density sensitive.

In these more recent studies, the density was varied from one-tenth to almost three times the density at standard conditions. A sketch of the experiment is shown in Figure 16. A point-to-plane type of corona electrode was used. The spacing was 5.1 mm and the diameter of the plate was 38.1 mm. The corona probe was mounted in one end of a 36-inch length of 3-inch diameter, insulated pipe. A 500-watt conical heater was mounted at the other end. An inlet valve admitted high-pressure, dust-free air into the chamber which then passed over the heater. It passed slowly down the chamber over the corona and out through an exit valve. A thermocouple was mounted near the corona to measure the temperature of the gas. Tests were made which showed that the gas temperature was uniform in the vicinity of the corona. For low pressures a mercury manometer was used and for the higher pressures, a specially calibrated, Bourdon type gage was used. With this arrangement, any temperature and pressure within the range of the investigation could be provided. We were also able to regulate the amount of air that flowed through the chamber by the adjustment of the inlet and exit valves. Regulation of the air flow is important, for if the flow is insufficient, there is a composition change of the air due to ozone and nitric oxides created by the corona (Reference 33), which will change the data appreciably if present even for small amounts. The check consisted of increasing the low velocity at the corona. When this caused no change in the current-voltage relationship, gas composition changes due to stagnant air were considered to be non-existent. The highest velocity involved was very low and always much smaller than the smallest velocity of interest for the velocity-sensitive corona discussed later in this report.

The voltmeter and ammeter were placed close together and the data recorded by photographing these meters simultaneously with a motion picture camera as described in Section III. The voltage was increased slowly and continuously

so that a current range from 0 to 40  $\mu$  amp was covered. It was important that the voltage be increased slowly enough so that the two meters were able to follow the changes. Thus the runs were about 10 to 15 seconds in length. This rapid data recording was advantageous since there was less chance for the air to suffer composition change, the disintegration rate of wire tips was negligible, and the chance of collecting small particles of dust was greatly reduced.

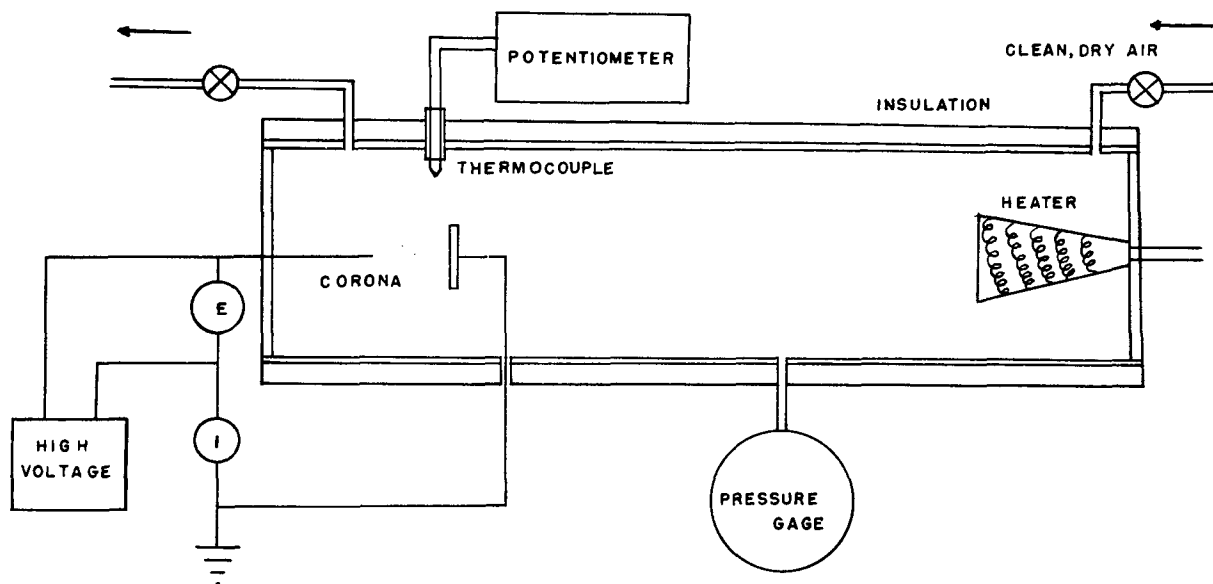


Figure 16. Apparatus for investigation of the density sensitivity of the corona. The air supply was a 200-psi oil lubricated compressor whose output was filtered and dried in a "Lectrodryer" which lowered the dew point to about  $-30^{\circ}\text{F}$ . The air was stored in a large tank. (Reference 4.)

The sets of data were taken in three steps. First, the temperature was held constant at room temperature and the pressure was increased in steps of about 5 inches of Hg per step from 2.5 inches of Hg to 90 inches of Hg. Then the pressure was held constant at 90 inches of Hg and the temperature was increased in steps of  $20^{\circ}\text{C}$  to a final temperature of  $170^{\circ}\text{C}$ . The last step was to hold the temperature constant at  $170^{\circ}\text{C}$  and reduce the pressure in steps of about 7 inches of Hg. The last few runs in this step were difficult to obtain as the vacuum pump used was not large enough to maintain the desired air velocity. This was also a factor for some of the scatter in the low density region.

The data were plotted and are shown in Figure 17. The graphs are density vs. voltage at constant values of current. The point of interest is that the corona is independent of temperature and pressure separately and depends

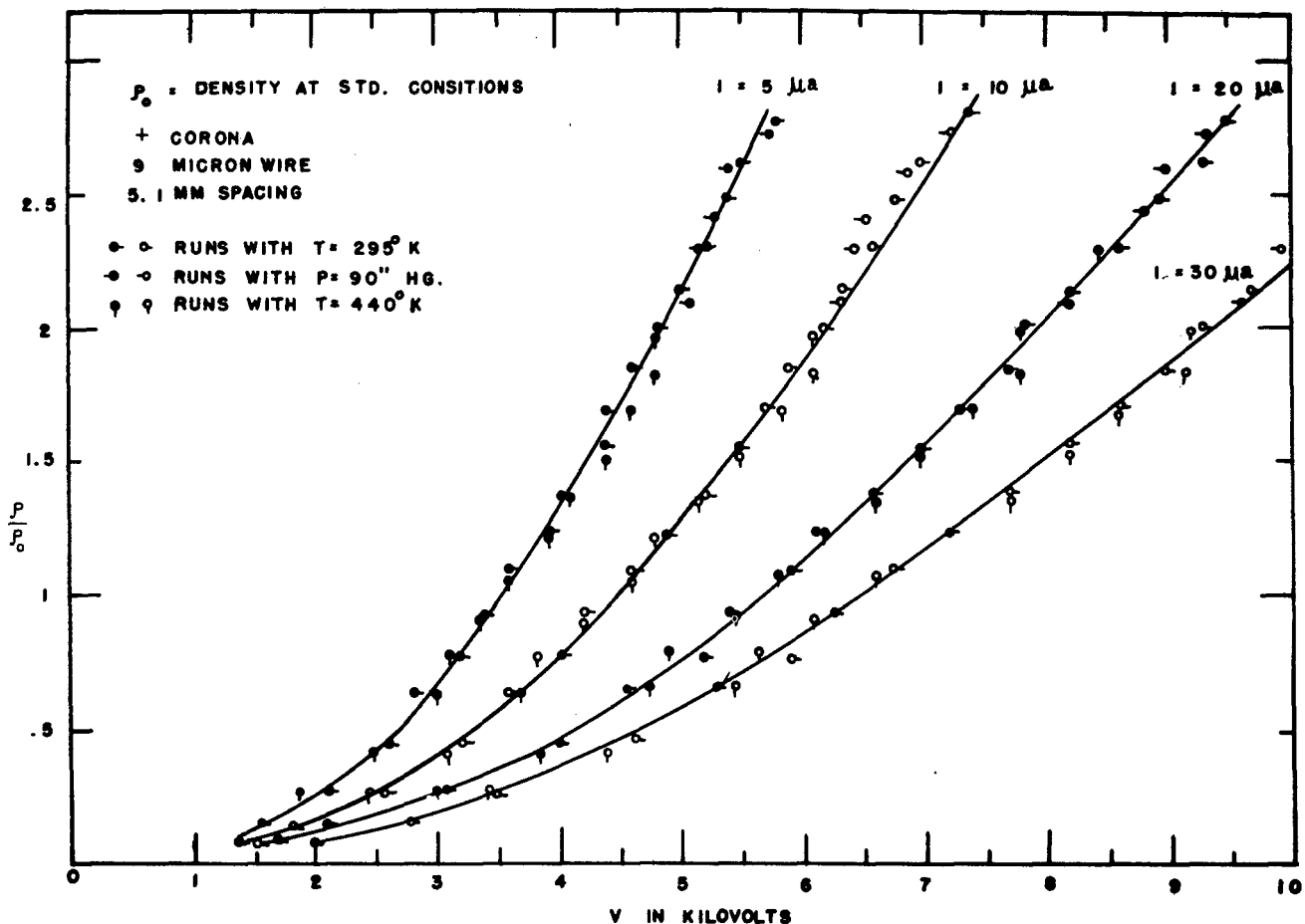


Figure 17-A. Data for positive corona which show that the corona is sensitive to density, but not pressure or temperature separately. (Reference 4.)

primarily on the density of the gas. The data shown in Figure 17-A are typical and have been tabulated as shown in Table 2.

There is some scatter of the data, but it appears to be random, and we believe it results primarily from experimental errors. The spacing and wire size were held constant but the wire points were replaced periodically. We used a dust filter consisting of 1-1/4-inch pipe, 14 inches long, which was filled with spun glass wool moistened with vacuum pump oil, but the corona point still collected very fine particles of dust after a number of runs. This could be a source of the scattering (Reference 34).



TABLE 2

Data Showing Density Sensitivity of the Positive Corona. The numbers in the four columns to the right are corona voltage in volts.

Run #	T, °C	P, In. Hg	$\rho/\rho_0$	Current, $\mu$ Amp			
				5	10	20	30
1	291	3.3	0.104	1350	1500	1680	1970
2	291	5.1	0.160	1550	1750	2120	2800
3	291	9.0	0.282	2120	2500	3100	3500
4	291	15.0	0.470	2600	3200	3950	4620
5	291	20.0	0.628	2900	3550	4640	5450
6	291	25	0.782	3200	4020	5200	5900
7	291	30	0.941	3420	4200	5400	6270
8	294	35	1.078	3600	4600	5900	6730
9	294	40	1.238	3900	4930	6100	7200
10	294	45	1.392	4000	5200	6600	7700
11	294	50	1.548	4400	5500	7050	8200
12	294	55	1.691	4400	5700	7300	8600
13	294	60	1.860	4600	5900	7700	9000
14	294	65	2.01	4800	6200	7850	9300
15	294	70	2.16	5000	6350	8200	9700
16	295	75	2.32	5240	6600	8580	10000
17	295	80	2.46	5400	6800	8950	
18	295	85	2.62	5500	7000	9300	
19	295	90	2.76	5800	7400	9500	
20	301	90	2.72	5750	7350	9400	
21	314.9	89.6	2.58	5400	6900	9000	
22	335	89.6	2.43	5300	6500	8700	
23	354	89.6	2.30	5170	6400	8400	9900
24	386	89.1	2.10	5200	6400	7200	9600
25	416	89.6	1.97	4800	6000	7800	9200
26	439	88.0	1.82	4950	6200	7800	9150
27	439	80.4	1.66	4600	5900	6400	8600
28	439	73.4	1.52	4400	5500	7000	8200
29	439	65.1	1.35	4100	5180	6600	7700
30	439	59.1	1.22	3900	4800	6200	7200
31	439	51.1	1.06	3600	4600	5800	6570
32	439	44.1	0.940	3330	4200	5400	6110
33	439	37.1	0.770	3100	3800	4800	5600
34	394	27.0	0.624	3000	3700	4750	5450
35	375	19.1	0.464	2500	3100	3840	4400
36	439	14.1	0.291	1900	2400	3000	3450

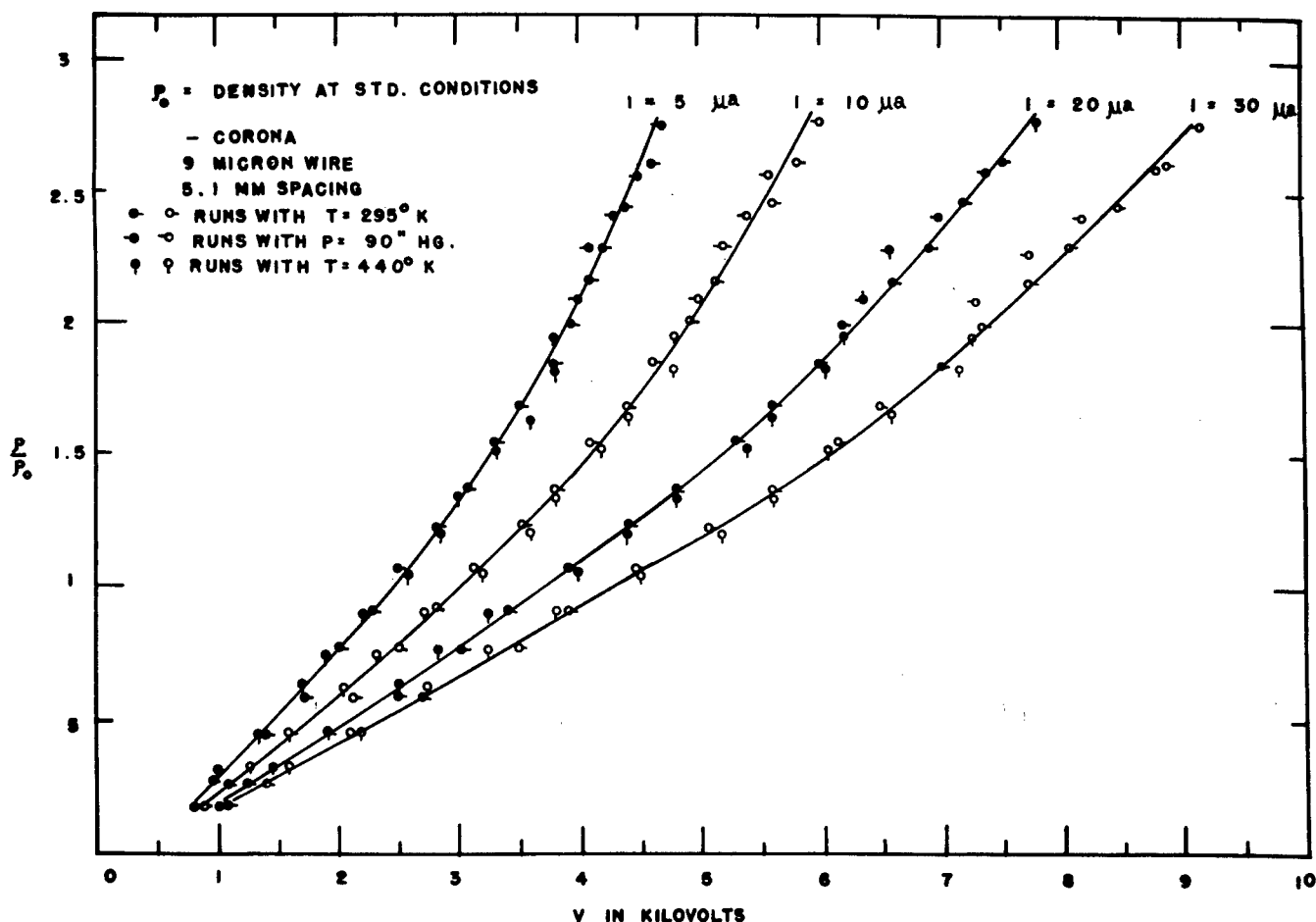


Figure 17-B. Data for negative corona which show that the corona is sensitive to density, but not pressure or temperature separately. (Reference 4).

#### B. Frequency Response of the Corona for Periodic Density Variations

In previous work (Reference 2), an investigation was carried on to measure the frequency response of the corona to changes in density. This discussion is repeated here for completeness of this report.

Density variations were generated as a sound (or ultrasound) field. The density variations up to 5 kc were measured by means of a General Radio Type 759-B Sound Level Meter, under approximately free field conditions. The sound level meter was replaced with the corona discharge, and the current variations were observed. The response of the corona, as plotted in Figure 18, is proportional to the ratio of the corona current variations to air density variations. For the higher frequencies, several quartz crystals were driven at

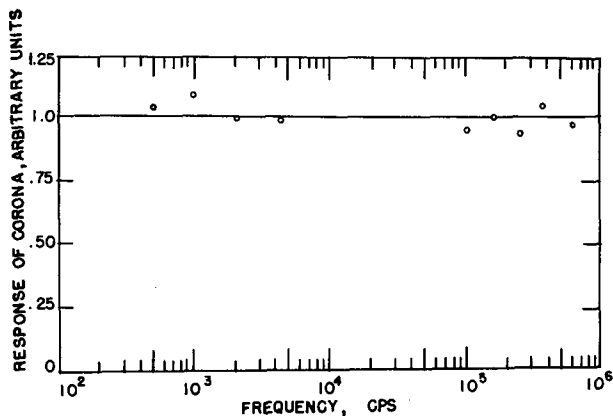


Figure 18. Effect of frequency of density changes on response of a corona, for a negative 9-micron wire tip, at a current of 3  $\mu$  amp. (Reference 2.)

lower frequencies, the detector was a Hewlett-Packard Model 200-A Wave Analyzer; and at the higher frequencies, a communications receiver with a crystal filter was used.

The data show no significant trend since the experimental error was considerable, but nevertheless, it confirms approximately the basic ideas of high frequency response for the corona. This was a very difficult method from which only approximate results could be obtained, and therefore, a new method was devised.

#### C. Response of the Corona to Transient Density Changes

The new method was the use of a shock tube to provide an instantaneous change in density. Thus one is able to find the rise time and ultimately the frequency response of the corona. There are two ways of observing the information which will result from such an experiment. The first method is to observe the individual pulses as the shock wave passes over the corona probe with an amplifier which is approximately flat to several megacycles. This method works very well for negative coronas as the Trichel pulse frequency is a fairly regular phenomena. Since the positive corona pulses are random, information obtained by this method is hard to interpret. The second method is to observe the average DC corona current, i.e., use of an amplifier which

their resonant frequencies to generate approximately plane parallel sound waves. The sound level was measured by observation of the reflection pressure on a sound reflecting plate which was at least eight wave lengths in diameter. The corona was inserted in the same sound field, and again the ratio of corona current changes to air density changes was plotted. In all cases, a narrow band detector was used to measure the corona current variation. At the

is flat to only 0.5 mc or less and with a sharp cutoff, so that individual pulses are not resolved. Either positive or negative corona can be used with this second method. These experiments demonstrate the frequency response of the corona and also the application of the corona as a useful tool for measuring density transients. For these experiments, a ring type probe (called Model V), shown in Figure 19, was used. The probe was constructed with a thin cylindrical plate 1/2-inch in diameter and 1/4-inch in length. The center needle was a 0.3-mil platinum wire soldered to a common sewing needle. The 513-D Tektronix oscilloscope was used to photograph these transients.

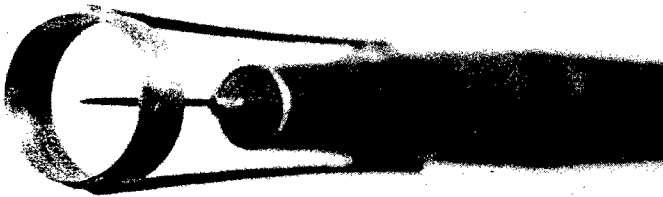


Figure 19. The Model V probe which was used in the shock tube work to investigate the frequency response of corona discharge to density transients. The diameter of the plate was 1/2 inch and length 1/4 inch. The corona needle was a .3-mil platinum wire rounded on the tip.

For the first method, the frequency response of the Tektronix oscilloscope was intentionally reduced so that the writing rates would be low enough for good photography.

The experimental setup which was used is shown in Figure 20. The data are shown in Figures 21-A, B, and C for negative corona. The sweep

speed for pictures A and B was

40  $\mu$  sec/div and for C the sweep speed was 10  $\mu$  sec/div. The pressure on the high-pressure side of the diaphragm was 6 psi above atmospheric while the low-pressure chamber was at atmospheric pressure. The average DC current for A was 5  $\mu$  amp, for B 10  $\mu$  amp, and for C 15  $\mu$  amp. Thus the frequency of the pulses for these currents before the shock wave passed over the corona probe was approximately 250, 400, and 800 kc, respectively. As can be seen, the frequency of the Trichel pulses dropped abruptly as the shock wave passed over the probe, and the amplitude of the pulses increased. As the density behind the shock wave increased, the average DC corona current decreased, which caused the drop in the lower base line of the pulses. It is important to note that the corona responds within one pulse. These oscillograms show that the corona has a very high frequency response for density changes, and that the region which is sensitive to density is very small, and presumably confined to the corona itself (of the order of 1 or 2 mils diameter). For most applications, currents of about 35  $\mu$  amp would be used with this probe. Unfortunately, the

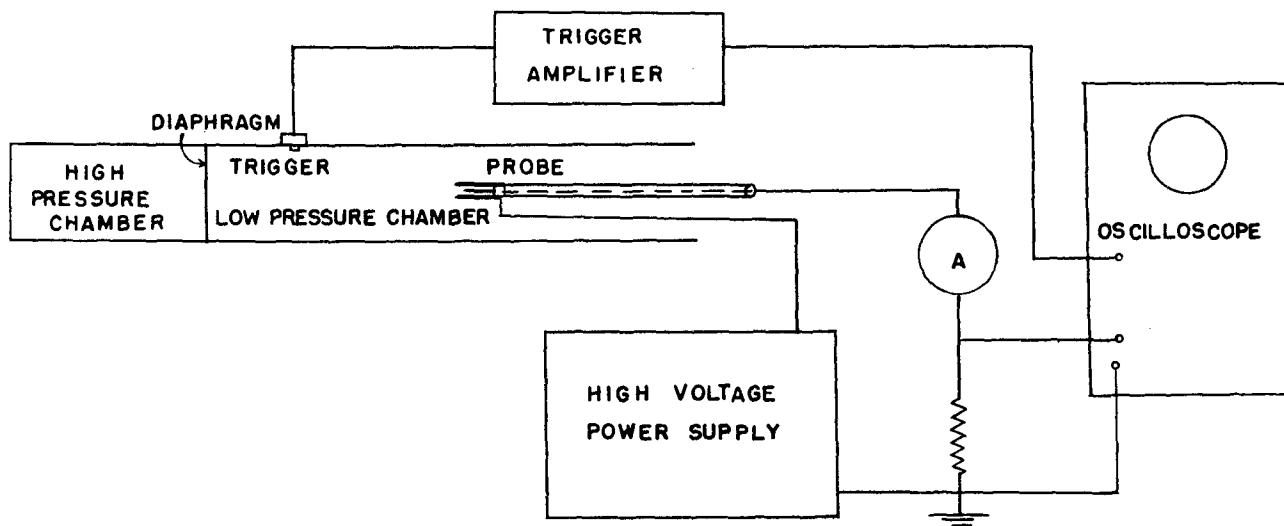


Figure 20. Schematic diagram of the setup used in shock tube investigations of the transient density response.

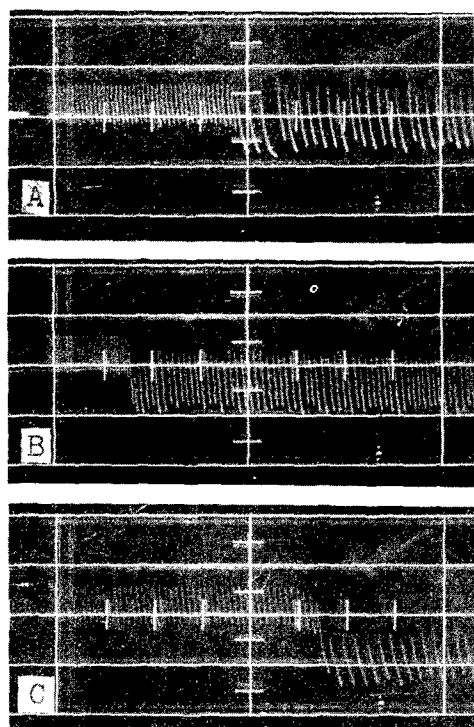


Figure 21. Wave forms obtained as the shock wave passed over the corona probe. All variables were held constant except corona current and sweep speed. In A the current was  $5 \mu$  amp, sweep speed  $40 \mu$  sec/div. In B current was  $10 \mu$  amp, sweep speed  $40 \mu$  sec/div. In C the current was  $15 \mu$  amp, and sweep speed was  $10 \mu$  sec/div.

pulse rate would be several megacycles and the writing rate would be too high for good photography for this current. Transients which were visually observed under these conditions showed the same trends established by Figure 21. We conclude that the corona could be used with a high frequency amplifier having a very sharp high frequency cutoff, in which case, the frequency response is limited only by the Trichel pulse rate which may be several megacycles (see Figure 15).

Positive corona does not have the regular pulses, so that the above remarks do not apply directly for positive corona. However, visual observation of oscilloscope traces showed that the positive corona was also able to follow extremely rapid density transients.

In the second method, which filters out the individual pulses, it was possible

to make calculations of the amplitude of the density change. As will be seen, the frequency response for this second method is determined by the amplifier characteristics and not by the corona. The absence of any variations in the corona response at intermediate or low frequency is confirmed by these experiments.

For quantitative density observations with the corona, it was necessary to calibrate the Model V probe over the range of densities involved. The density calibration was performed in the following manner: The Model V probe was mounted in a cylindrical container 10 inches high and 6 inches in diameter. As usual, a constant flow of air was passed through the container to flush out the ozone and nitrogen oxides created by the corona discharge, and the velocity was very small so that there would be no velocity effect. The temperature was held constant and the pressure inside the chamber was varied in steps of 2 inches of Hg in a range of 10 inches above to 16 inches below atmospheric pressure. The current ranged from 3  $\mu$  amp to 20  $\mu$  amp for the positive corona and 5  $\mu$  amp to 60  $\mu$  amp for the negative corona with a center needle of 1 mil diameter. The graphs in Figures 22 and 23 show this density calibration.

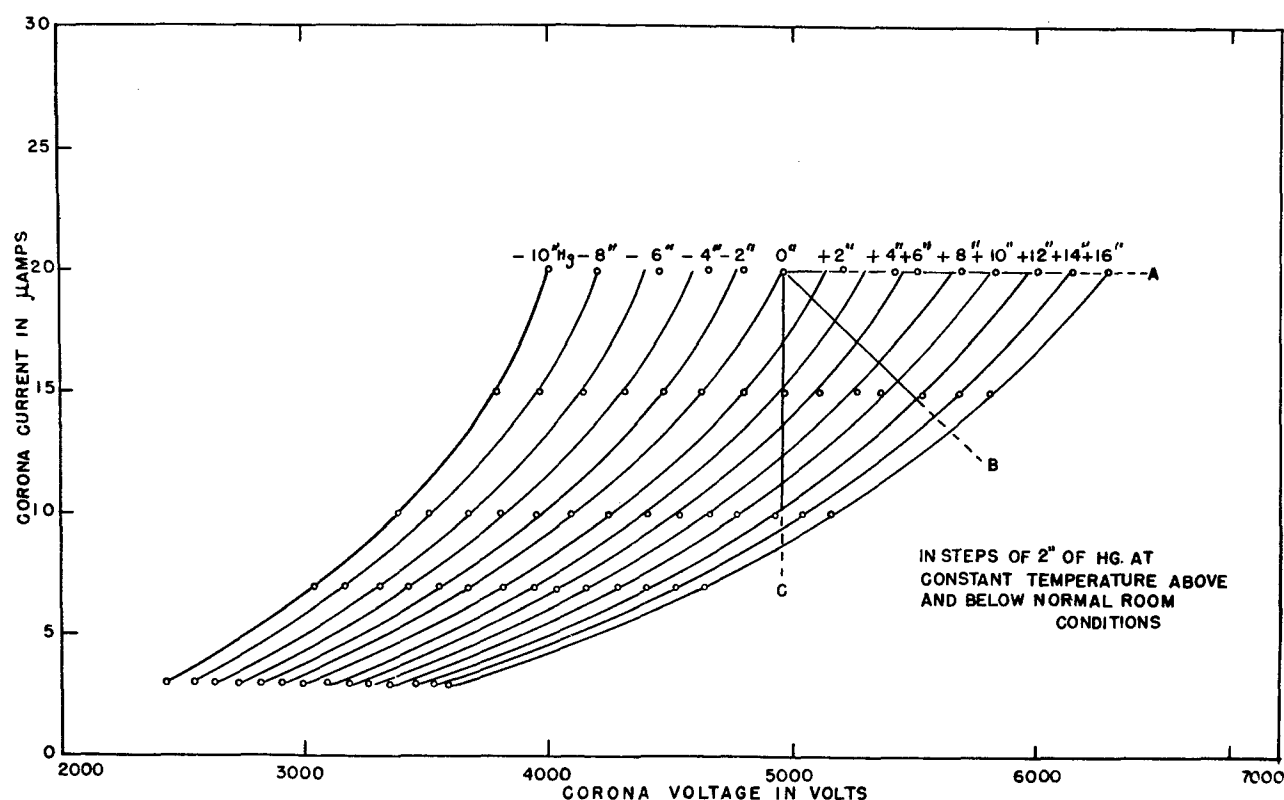


Figure 22. Positive corona calibration curve for Model V probe shown in Figure 19.

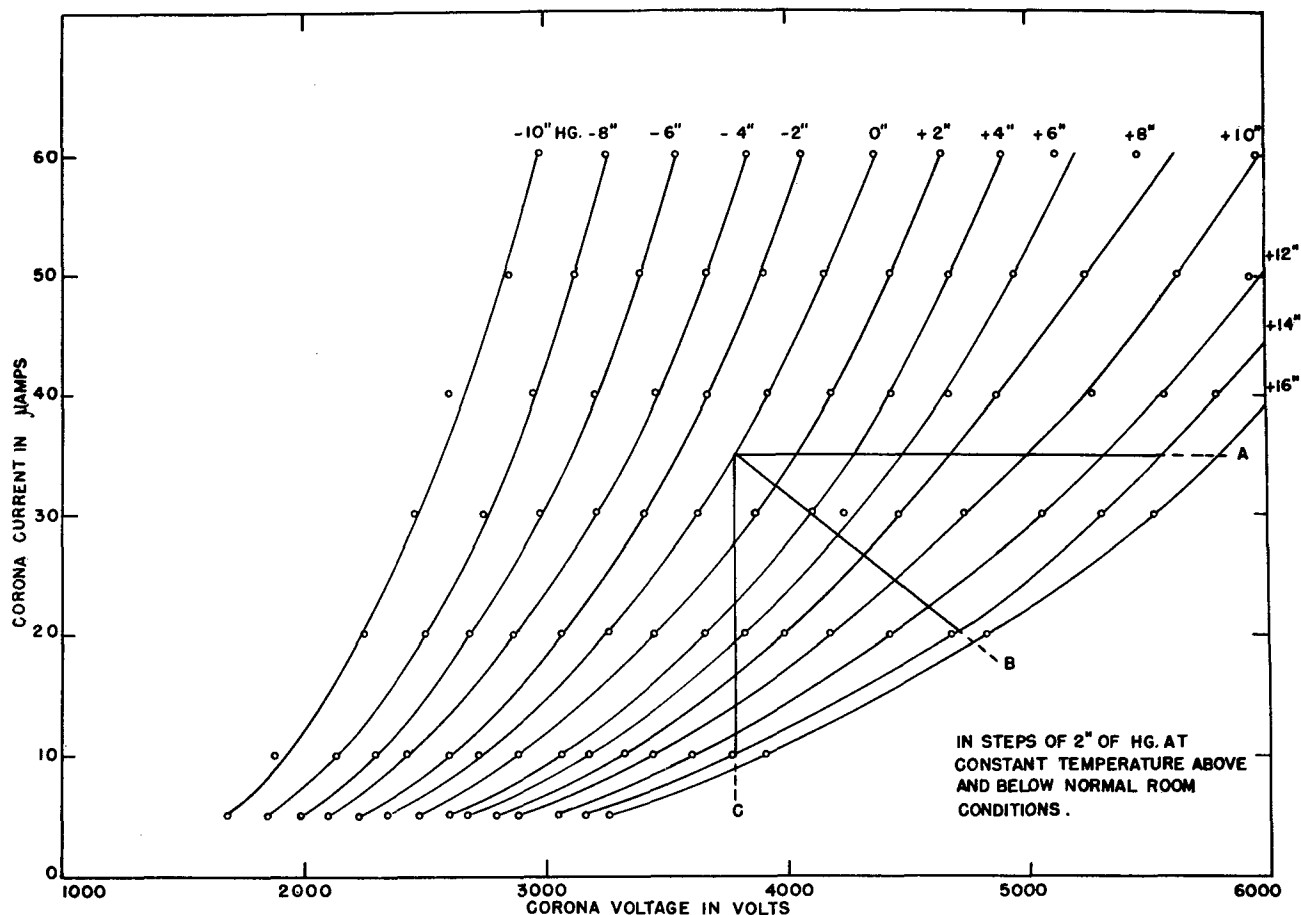


Figure 23. Negative corona calibration curve for Model V probe shown in Figure 19.

For this work, rather large density changes were caused by the shock tube so that the corona response was nonlinear, and this problem was considered in some detail. On Figures 22 and 23 are drawn the three possible methods for operating the corona. A is the load line for constant current operation, B is the load line for intermediate operation, and C is the load line for constant voltage operation. Calculation of the total distortion for these three types with a signal varying from 0 to +14 inches Hg at constant temperature gave the following values for the positive and negative corona: For type A the total distortion is 3%, for type B the total distortion is 5%, and for type C the total distortion is 22%. In order to realize the more linear operation, we considered the design of a suitable constant current power supply. We found that the impedance of the power supply could not be made high enough compared with the corona impedance to appear as a constant current power supply to the corona at the high frequencies. The corona can be considered as a very high

impedance triode vacuum tube. Its plate impedance is  $\left(\frac{\partial E_p}{\partial I_p}\right)$ . This plate impedance is of the order of 15 to 100 megohms. If the corona probe is considered as a triode vacuum tube, changing density would be analogous to changing grid voltage. We will arbitrarily define our fictitious triode as having a 1-volt grid voltage signal if it is acted upon by a changing density equal to 1 inch of Hg pressure change at constant temperature. With this definition, it is found that transconductance will be as follows:  $gm = \left(\frac{\partial I_p}{\partial E_g}\right) E_p$ . Also the  $\mu$  of our triode can be defined as  $\mu = \left(\frac{\partial E_p}{\partial E_g}\right) I_p$ . Upon calculating these values, it is found that the transconductance of the corona is in the range of 0.5 to 5 micromhos. The  $\mu$  of the corona is in the range of 40 to 200. As can be seen electrically, this would be a very strange triode. The plate resistance is extremely high so that any capacitance from plate to cathode greatly attenuates the higher frequency input signals. This is the case whenever one tries to operate the corona at constant current with several  $\mu$ fd of cathode-to-plate capacitance. This would give a high frequency half-power point of the order of 400 cycles. Things can be improved somewhat but the most optimistic outlook would be only several thousand cycles. Even if a higher frequency response were obtainable by this method, the problem of obtaining a signal would still be present. Whatever type of sensing device is used, an input impedance comparable to the impedance of the corona would be required. We conceived several types, but as the frequency response when operating at constant current was so poor, these devices were not tried.

For the same reason, a load line solution is not possible. If a large load resistor were used to operate the corona in a more linear range, the same problem is encountered. The cathode to plate capacitance is effectively across this resistor. As the frequency under measurement increases, the corona no longer follows this curve but one which is more nearly vertical. Then we would have the corona operating at constant current only for low frequency and at constant voltage for high frequency. The impedance of the grid-to-plate capacitance is comparable to the load resistor. The data would be difficult to interpret in this case.

The more desirable way to operate the corona is at constant voltage. If large density changes are to be measured, the distortion will be bad. The only solution to the problem is to make use of an accurate calibration curve to determine the density change for a given current change, except for small changes. At present, it seems possible to construct an amplifier which is



nonlinear in such a manner as to exactly compensate the nonlinearity in the corona, as is done in hot-wire work (Reference 39) to compensate for dependence of the hot-wire response on time. An amplifier was built at our laboratory to obtain such a nonlinearity. It was felt that it was possible to make this amplifier accurate to at least 5 percent but the time required was not warranted.

For these experiments, a value of  $35 \mu$  amp was chosen for the negative corona, and a value of  $20 \mu$  amp was chosen for the positive corona. These values of the corona current were for room density conditions (i.e., before the shock wave passed over the probe). The velocity behind a shock wave is fairly large and can be easily calculated, and therefore it was desirable that the probes should be calibrated for these velocities so that the velocity effect could be allowed for in the response. The velocity calibration was obtained by mounting the Model V probe in a small 3-inch subsonic wind tunnel. At zero velocity and room density, the current was adjusted to  $20 \mu$  amp for the positive corona and  $35 \mu$  amp for the negative corona. The corona voltage was held constant and the current variation was observed over a range of Mach numbers from 0 to 0.4. The results are shown in Figure 24. Since the static density

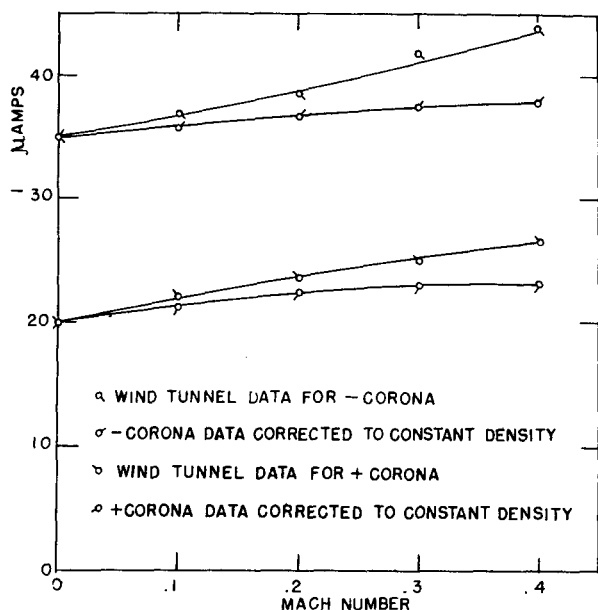


Figure 24. Velocity calibration curves for Model V probe for both positive and negative corona.

of the wind tunnel changed slightly for this range of Mach numbers, the data was corrected for this density change, according to the density calibration for this probe in still air.

With the calibration completed, the probe was mounted in the shock tube as shown in Figure 25. The schematic setup of the experiment is shown in Figure 20. The only major difference in the setup of this method as compared to the first method is the frequency response of the amplifier. This point will be discussed more completely at a later

point. In order to study the transient response of the corona to large density changes, we used two different breaking pressures to generate the shock waves. In the first test, we had a pressure of 12 psi above atmospheric pressure in

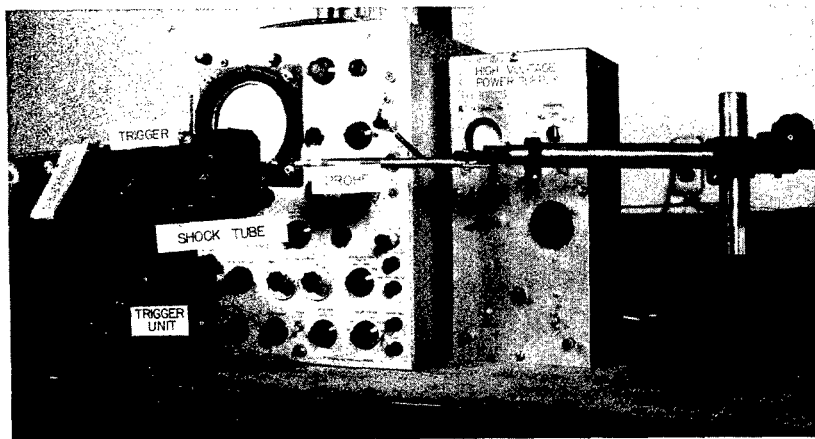


Figure 25. Photograph of the apparatus used in shock tube investigations of the transient density response.

the pressure chamber and atmospheric pressure in the low pressure side of the shock tube. In the second test, we had 6 psi above atmospheric pressure in the high pressure chamber and atmospheric pressure in the low pressure chamber. The corona probe was mounted at various positions in the shock tube. The points were

arbitrarily chosen as 2, 10, 18, and 26 inches from the open end of the 36-inch shock tube. By placing the probe in these positions, we were able to study the various transient density conditions, showing the shock wave, the rarefaction from the open end of the tunnel, and the temperature discontinuity. The position of these three density transients as a function of time and the values of the density changes can be predicted analytically, and these calculations are given in Figures 26 and 27. The interpretation of the symbols used in Figures 26 and 27 is as follows:  $P$  is pressure,  $\rho$  is density,  $A$  is velocity of sound,  $u$  is particle velocity,  $M$  is Mach number, and  $T$  is temperature. The subscript  $o$  denotes the conditions in the high pressure side of the shock tube before the diaphragm is broken,  $1$  denotes the conditions in the low pressure side of the tube before the diaphragm is broken,  $2$  denotes the conditions in the region behind the shock wave,  $22$  denotes the conditions in the region behind the temperature discontinuity, and  $M_s$  denotes the Mach number of the shock wave. A small trigger was mounted in the wall of the shock tube in front of the probe to trigger the oscilloscope trace just before the shock wave passed over the corona probe.

The data of these experiments are shown in Figures 28, 29, 30, and 31. The sweep speed was chosen as 1 millisecond per division to enable us to see all the pertinent facts in a single trace. The amplitude sensitivity was  $10 \mu$  amp per division for the negative corona and  $5 \mu$  amp per division for the positive corona. Each of the Figures 28 to 31 has four separate photographs showing the density transient as the Model V probe was moved from 2 inches from

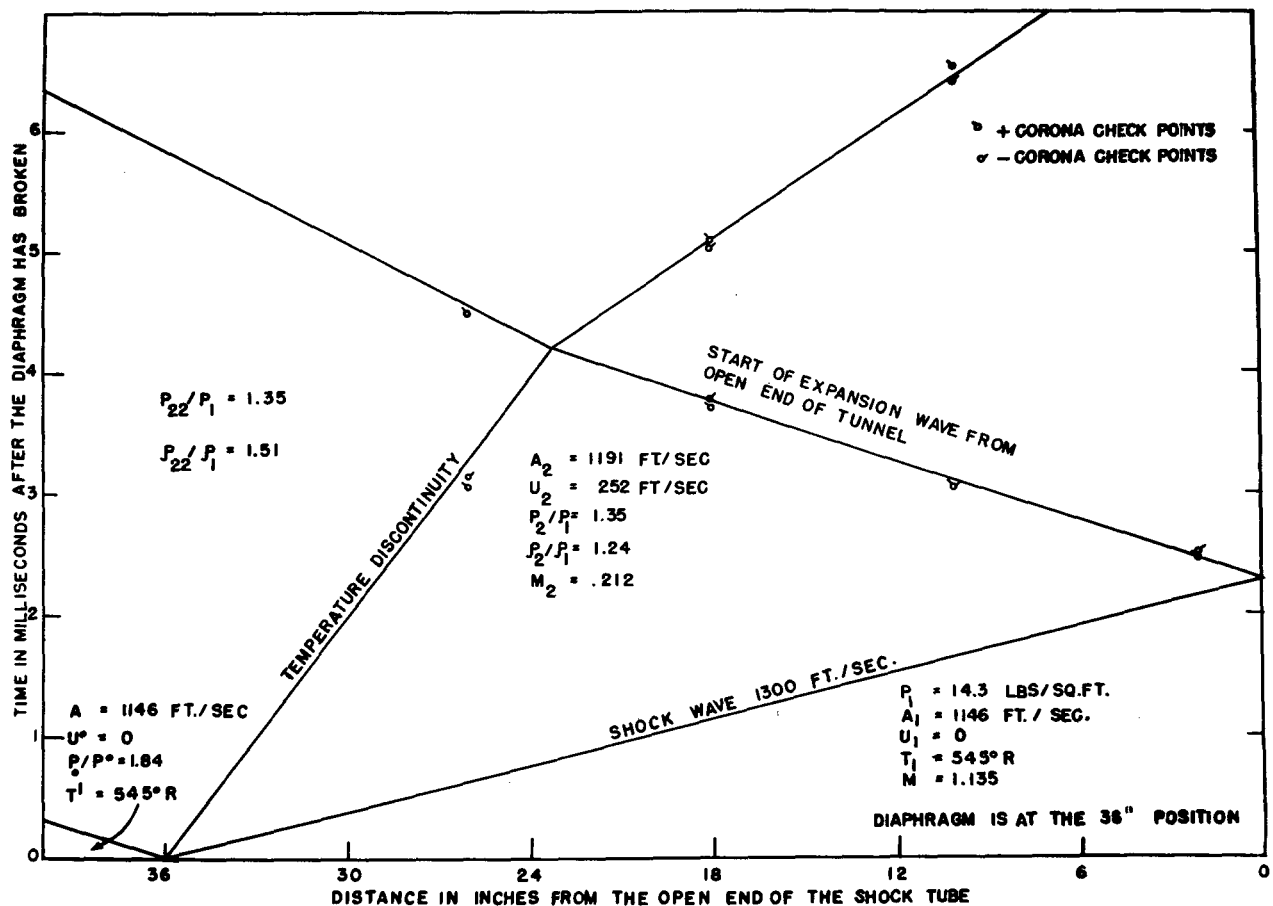


Figure 26. Diagram showing position vs. time for the shock wave, temperature discontinuity, and secondary density disturbances for 12-psi breaking pressure, a 72-inch, high-pressure chamber, and 36-inch shock-tube length. The points are measurements by means of the corona, taken from Figures 28 and 30. Flow conditions are stated for each region. See text for definition of symbols.

the open end of the shock tube to 26 inches from the open end. Figures 28 and 30 show the case with a breaking pressure of 12 psi for positive and negative corona, respectively. Figures 29 and 31 show the case with a breaking pressure of 6 psi for positive and negative corona, respectively. By observing the pictures, one notes the excellent correlation between plus and minus corona. There is also the expected systematic change as one goes from a position of 2 inches from the open end of the shock tube to a position 26 inches in the open end. The times at which the various density transients reach the Model V probe is recorded by their positions on the oscillograms, and it is found that these times agree with the theoretical values within experimental accuracy as shown by the points which are plotted in Figures 26 and 27.

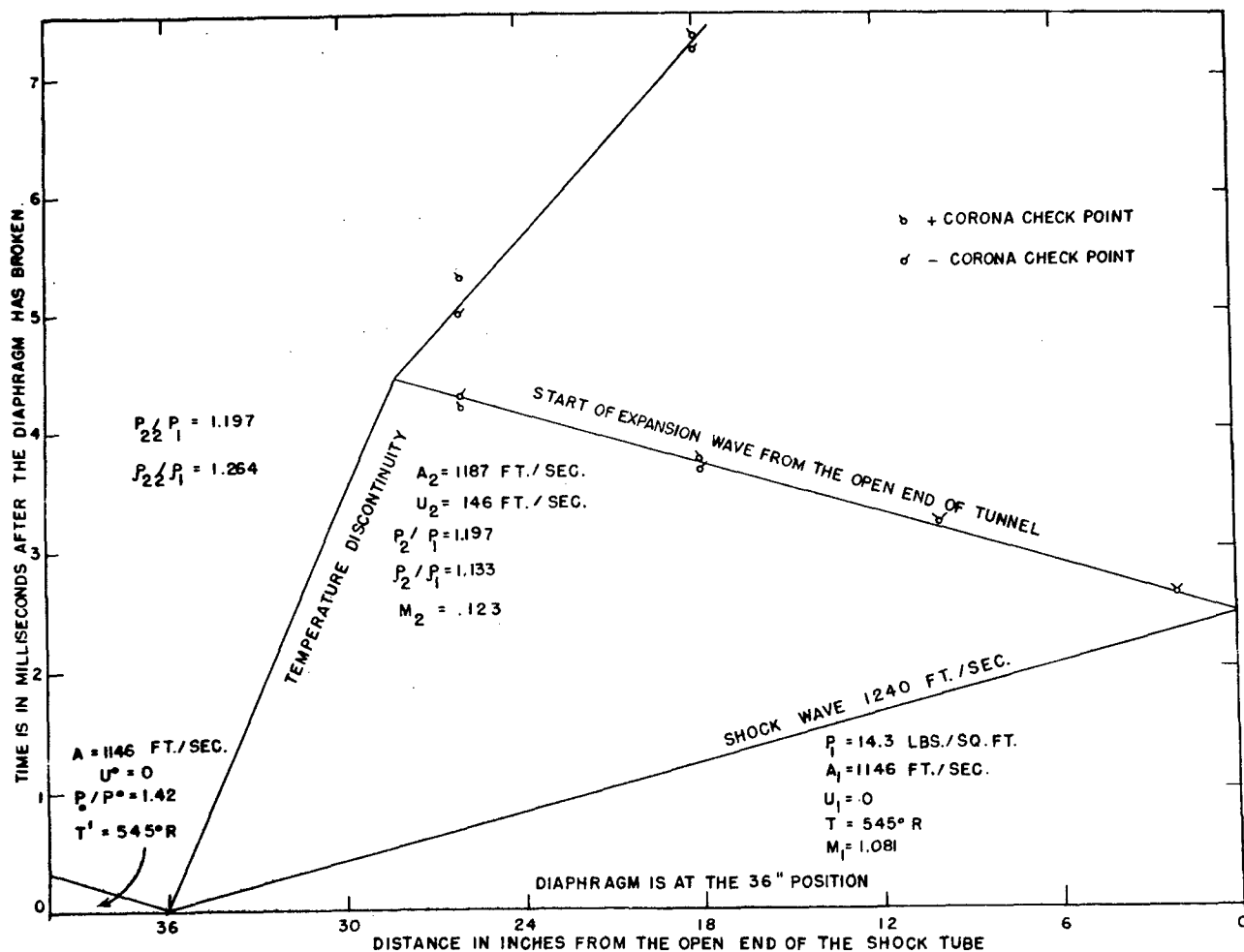


Figure 27. Diagram showing position vs. time for the shock wave, temperature discontinuity, and secondary density disturbances for 6-psi breaking pressure, a 72-inch high-pressure chamber, and 36-inch shock-tube length. The points are measurements by means of the corona taken from Figures 29 and 31. Flow conditions are stated for each region. See text for definition of symbols.

By using the static calibration curves and the velocity sensitivity curves for the Model V probe, and noting the change in corona current from the photographs of Figures 28 through 31, one is able to calculate the density in the various regions of the oscillogram. One finds that the results agree very closely with those given by shock tube theory (Figures 26 and 27). These results along with the velocity corrections are given in tabulated form in Table 3. Thus one is able to measure density changes in such a case to an accuracy of a few percent.

TABLE 3

Response of Corona to Density Transients in a Shock Tube. Line A is the value of the corona current obtained from the calibration curves Figures 22 and 23, knowing the theoretical value of density at these points. Line B is corona current before correction for the velocity effect as measured from the oscillograms of Figures 28 through 31. The values of current before the shock was 35  $\mu$  amp for negative corona and 20  $\mu$  amp for positive corona. Line C is the velocity effect as determined from the velocity in this region and the velocity calibration curve in Figure 24. Line D is the corrected experimental corona current as compared to Line A, the calculated value. No value is given for the current behind the cold front in the 6-pound case as the rarefaction from the open end of the tunnel occurred first.

### 12-Pound Breaking Pressure

#### Positive Corona

I (behind shock)	I (behind cold front)
A. 13.2 $\mu$ Amp	9.6 $\mu$ Amp
B. 15.6 $\mu$ Amp	12.7 $\mu$ Amp
C. 2.7 $\mu$ Amp	2.7 $\mu$ Amp
D. 12.9 $\mu$ Amp	10.0 $\mu$ Amp

#### Negative Corona

A. 18.0 $\mu$ Amp	10.4 $\mu$ Amp
B. 20.2 $\mu$ Amp	13.0 $\mu$ Amp
C. 2.0 $\mu$ Amp	2.0 $\mu$ Amp
D. 18.2 $\mu$ Amp	11.0 $\mu$ Amp

### 6-Pound Breaking Pressure

#### Positive Corona

I (behind shock)
A. 15.60 $\mu$ Amp
B. 16.75 $\mu$ Amp
C. 1.50 $\mu$ Amp
D. 15.25 $\mu$ Amp

#### Negative Corona

A. 23.6 $\mu$ Amp
B. 24.0 $\mu$ Amp
C. 0.7 $\mu$ Amp
D. 23.3 $\mu$ Amp

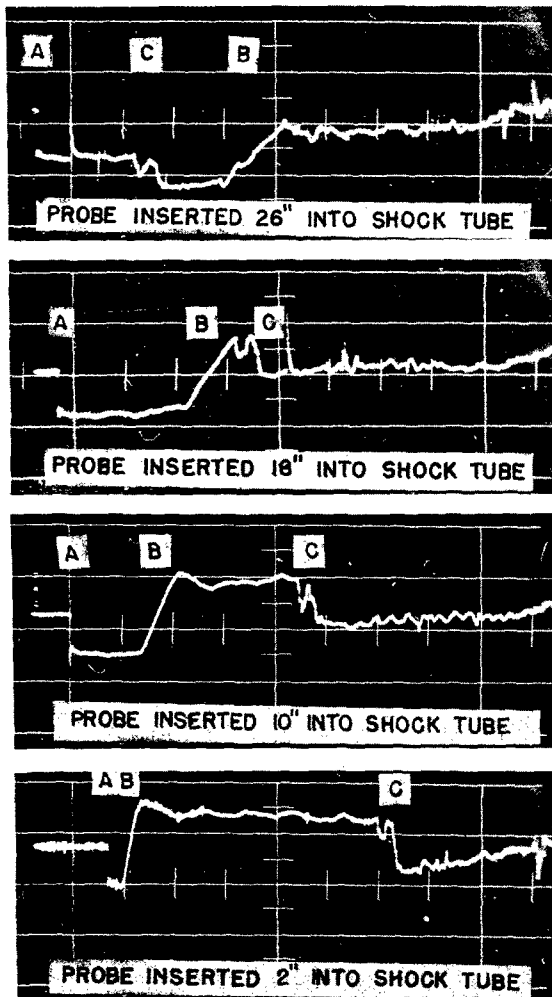


Figure 28. The changes in the relation between density and time as the probe is inserted into the shock tube. Initial conditions were 12#/sq. in. breaking pressure, 20  $\mu$  amp positive corona current, oscilloscope sensitivity 5  $\mu$  amp/div, and oscilloscope sweep-speed 1 millisc/div. The variable is probe location. In the above pictures A is the shock wave, B is the rarefaction from the open end of the tunnel, and C is the temperature discontinuity.

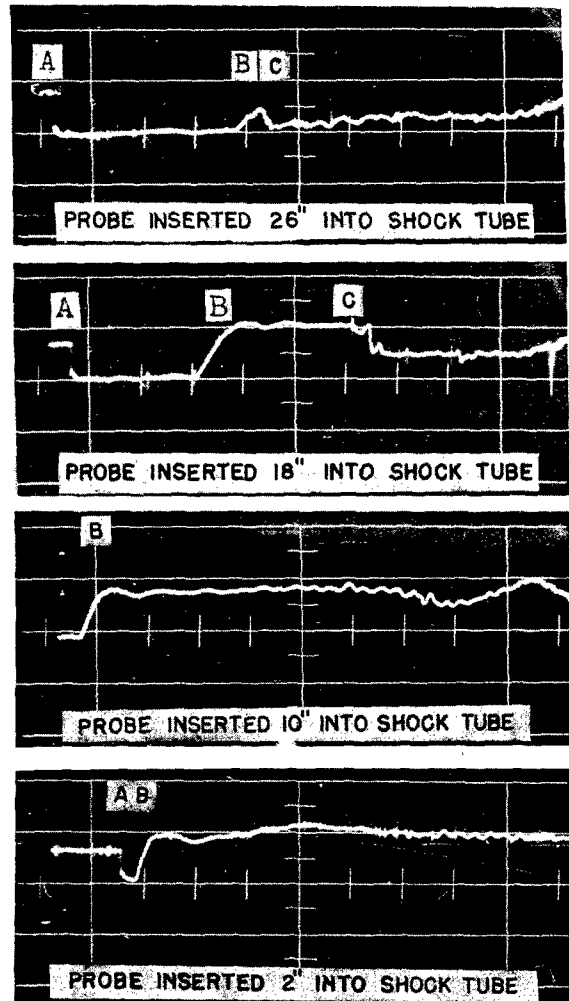


Figure 29. The changes in the relation between density and time as the probe is inserted into the shock tube. Initial conditions were 6#/sq. in. breaking pressure, 20  $\mu$  amp positive corona current, oscilloscope sensitivity 5  $\mu$  amp/div, and oscilloscope sweep-speed 1 millisc/div. The variable is probe location. In the above pictures A is the shock wave, B is the rarefaction from the open end of the tunnel, and C is the temperature discontinuity.

As the corona current consists of many short duration pulses, a high-frequency, broad-cutoff amplifier would give many sharper peaks due to the pulses. Thus in order to obtain a flat DC level with low corona noise, the amplifier must have a sharp cutoff. Therefore, the amplifier used in obtaining Figures

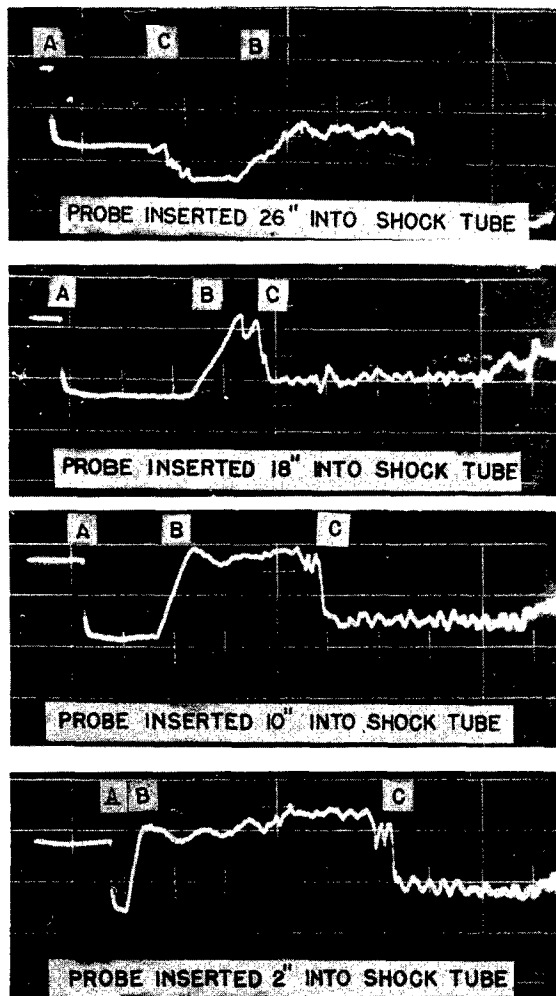


Figure 30. The changes in the relation between density and time as the probe is inserted into the shock tube. Initial conditions were 12#/sq. in. breaking pressure, 30  $\mu$  amp negative corona current, oscilloscope sensitivity 5  $\mu$  amp/div, and oscilloscope sweep-speed 1 millisec/div. The variable is probe location. In the above pictures A is the shock wave, B is the rarefaction from the open end of the tunnel, and C is the temperature discontinuity.

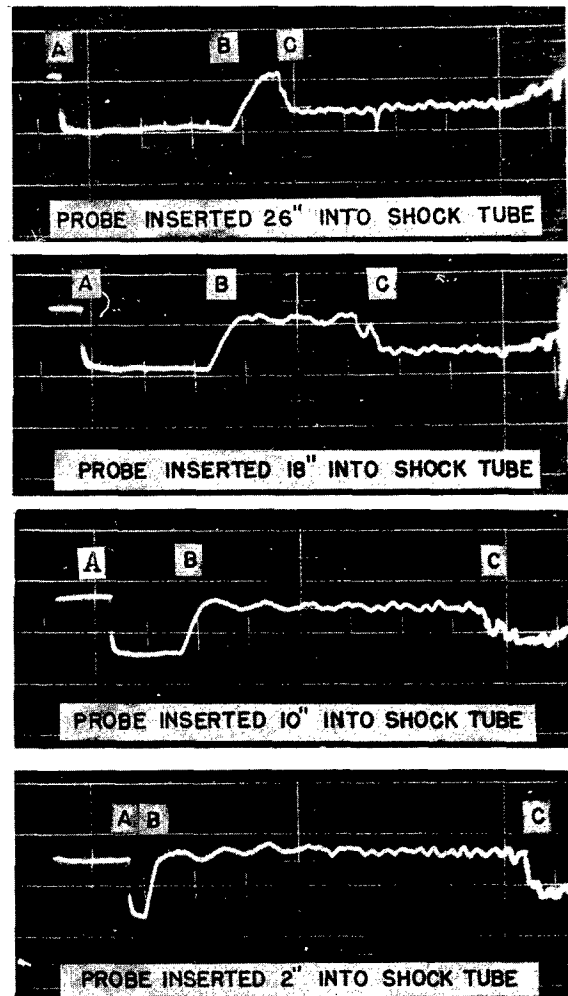


Figure 31. The changes in the relation between density and time as the probe is inserted into the shock tube. Initial conditions were 6#/sq. in. breaking pressure, 35  $\mu$  amp negative corona current, oscilloscope sensitivity 5  $\mu$  amp/div, and oscilloscope sweep-speed 1 millisec/div. The variable is probe location. In the above pictures A is the shock wave, B is the rarefaction from the open end of the tunnel, and C is the temperature discontinuity.

28 through 31 was only 100 kc, as no sharp-cutoff, higher-frequency amplifier was available. Frequencies as high as 500 kc have been used successfully in some applications here at the laboratory. Figure 32 shows the shock wave passing over the corona for which case the oscilloscope sweep-speed has been greatly

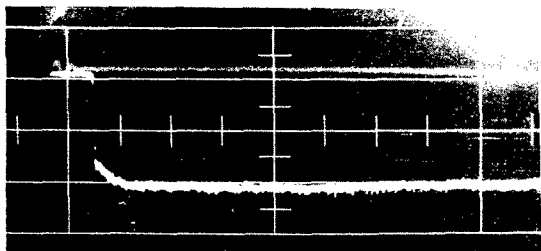


Figure 32. An oscillogram with an increased sweep speed to show in detail the shock wave as it passes over the corona probe. Sweep speed is 50  $\mu$ -sec/div.

increased. The sweep speed of this picture is 50  $\mu$ -seconds per division. The small trail-off immediately following the shock wave cannot be attributed to a corresponding density change in the shock wave, and is probably caused by the 100-kc upper frequency response of the amplifier.

Since the density behind the shock wave remains a constant for 3 or more

milliseconds in the cases shown and the corona pictures showed a flat response for this entire region, the frequency response must be flat as low as at least 300 cycles per second. Furthermore, it is known that the corona measures steady-state densities as shown by the static calibration curves. Thus, it can be assumed that the corona has a uniform response for density changes from DC to a frequency of the order of 1 to 5 mc, as determined by the frequency of the corona pulses and the type of amplifier available.

Several authors (References 1 and 40) have discussed the sensitivity of the corona as being primarily pressure-sensitive. As discussed earlier in this section, we have more recently shown that the corona is sensitive to density changes rather than pressure. This agrees with Weimer's recent investigations (Reference 45). By observing the upper oscillogram of Figures 28 and 30, it is found that the corona measured the density change behind the temperature discontinuity. The pressure and air velocity on both sides of the temperature discontinuity are the same. The only change is in temperature, which causes a change in density. This change in density, when referred to the corona calibration curve, predicts, within experimental error, the observed current change for the corona. As the initial calibration was made at constant temperature and the temperature discontinuity observation was taken at constant pressure, the only variable common to both observations is the density. Thus we have another excellent confirmation of our previous results (Reference 4).

In concluding this section, the important results obtained in the shock tube work should be emphasized. It was found that the corona response is flat from DC response to an upper limit which may be as high as about 5 mc. The corona follows the step function change in density within one pulse as shown in Figure 21 and Reference 41. It is clear that an amplifier with a sharp



cutoff at a frequency somewhat below the Trichel pulse rate could be used for the negative corona, and would result in a limiting frequency for the corona which approaches the Trichel pulse-rate. The whole experiment demonstrates the successful operation of a corona discharge in measuring the rapidly fluctuating density phenomena, and the problems which must be considered in applying the corona.

## SECTION V

### VELOCITY SENSITIVITY OF THE CORONA

#### A. Ion Trajectories

Figure 33 illustrates a type of corona probe which is generally well suited to insertion in an air flow, and this simple model serves well to explain the effect of velocity on the discharge, and also was the probe type used for the more recent fundamental experimental investigations into the velocity effect. The probe consists of a Lucite rod  $5/8$ -inch in diameter with a chisel-shaped wedge machined on its end. Mounted in the leading edge of this chisel are three sewing needles, as shown in the end view in Figure 33. The Lucite rod is short, and the end opposite the chisel is fixed into the end of a  $1/2$ -inch OD brass tube. Electrical connections to the three needles are brought out through this hollow brass tube. For some purposes, the two outer needles are connected together and may be connected to the circuit via the brass tube. For the present, the insulating ring which separates the fore portion of the lower needle from the rear portion may be neglected so that the needle is one piece.

If, in the absence of air flow, the center needle is negative with respect to the outer needles, the fine wire at its tip will have the typical negative corona with Trichel pulses. Electrons leaving the high field near the wire will attach to  $O_2$  when the field is sufficiently low, and therefore, drift nearly all the way across the gap to the other electrode as negative ions. For the positive point, positive ions drift across the gap after each burst pulse. Neglecting space charges and centrifugal forces (which is relatively safe out in the gap), the ions would be expected to move to the outer electrode, called the "plate", along electric lines of force, with a velocity  $kE$ , where  $k$  is the

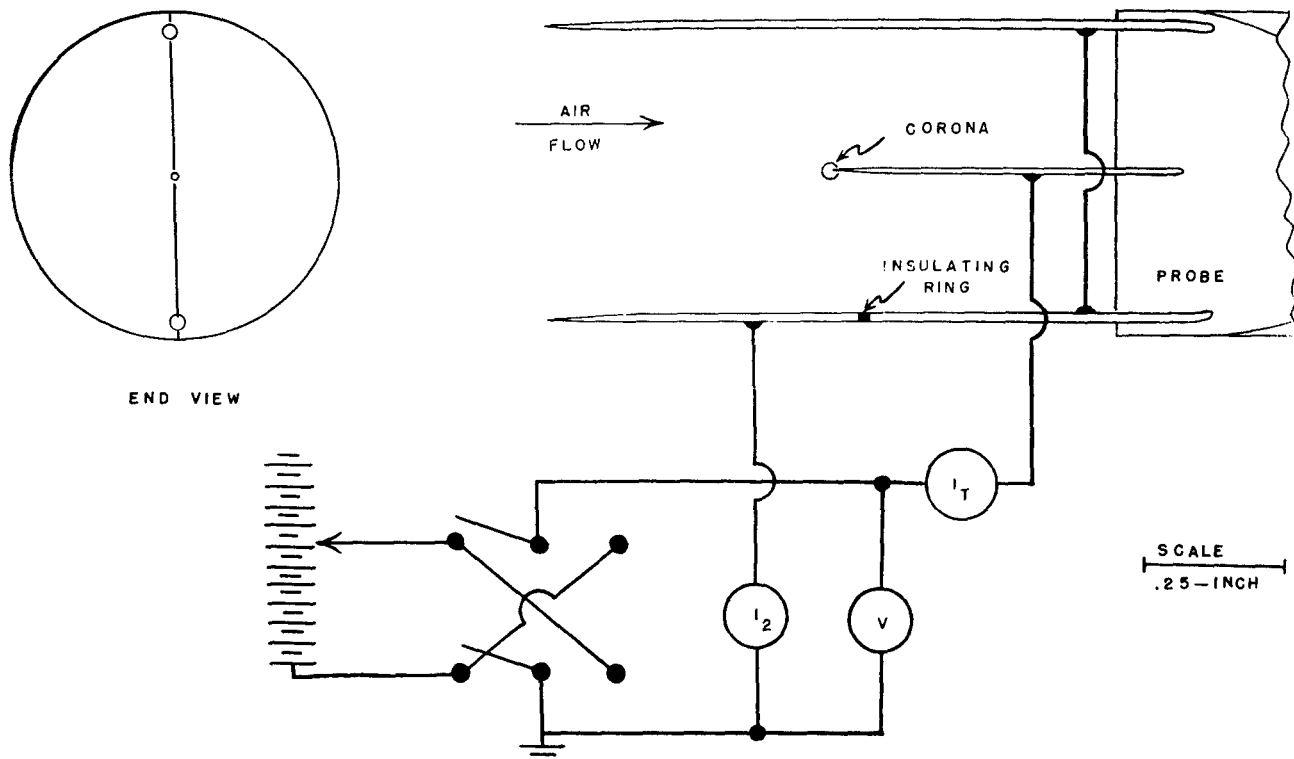


Figure 33. Probe showing the electrode arrangement used for the fundamental velocity investigations, drawn to the indicated scale. The forward portion of the lower plate electrode was electrically insulated from the rear half, and this electrode was movable in a direction parallel to its axis. The heavy lines are a schematic of the electrical circuit. Actually, all the leads to the electrodes are within the probe, the rear part of the lower plate being hollow to accommodate the lead to the insulated fore portion. (Reference 4.)

mobility of the ion and  $E$  is the electric field strength. When the air velocity has a value  $u_x$  parallel to the needles, the ions would have the motion which is determined by the ion velocity produced by the electric field and the velocity  $u_x$ , and it would be possible to determine the trajectory of the ion graphically if the electric field is known. To investigate this approach to predicting the ion motions, a large model of the electrodes was made and the electric field was plotted in an electrolytic tank. The model was 20 times the size of the probe, and tap water was used in a metal tank 2 x 3 x 5 feet, with the model submerged to approximately the center. An insulated exploring electrode was used with only its tip bare in the usual AC type of circuit. When the resulting data was examined, it was found to predict that all ions from the corona in Figure 33 would have trajectories such that all ions should arrive on the plate electrodes more than 1/4-inch ahead of the corona, in the

absence of the air flow. In order to verify this theory for the trajectories, the insulating ring shown on the lower plate needle of Figure 33 was provided. The fore portion of the needle was insulated from the rear portion by the insulating ring, and the electrical connection to the fore portion was taken out through the center of the rear part of this needle which was in the form of a hollow tube. The circuit shown was used so that the division of current between the fore and rear portions of the lower needle could be observed. The difference in potential between the fore and rear portions caused by the current  $I_2$  flowing through the microammeter was negligible. By removing small lengths of material from the rear end of the front portion and pushing out the rear portion of the needle from the Lucite chisel enough to compensate, it was possible to retain the electrode geometry and obtain data on the distribution of current on the plate electrodes. It was immediately apparent that the peak of this current distribution curve was opposite the corona, and not at a point  $1/4$  inch or more forward. This invalidated the idea of predicting the trajectories from the static field.

It was not surprising that the static field does not predict the ion trajectories because it was known that the space charges near the corona are great, since they play such a fundamental role in the mechanism of the discharge. After some further measurements on the current distribution at various currents and with air flow at various subsonic Mach numbers, as described below, we were able to conclude that the ion trajectories are essentially the same as would result if the three needles were infinite in extent, with an ion source at a point on the center needle, and with the air blowing parallel to the conductors. Using infinite needles as a model for the electrodes, the predicted point at which the ions reach the plate agreed well with the experimental measurements of the peak in the current distribution on the plate, as discussed further below. Our qualitative explanation of this is that the mutual repulsion of ions in the space charge is very great near the corona, and that the space charge caused by those ions in the forward portion of the corona is such as to urge a major part of the ions which are situated farther back more or less straight across the gap toward the plate in the absence of flow. The presence of flow merely gives a downwind motion in addition to this. When the ions arrive at the plate, the current distribution is not highly peaked up, because of the diffusion apart of the ions, caused by their repulsion during the journey.

In taking the data referred to above with air flow, it was noted almost immediately that the length of the lower, divided exploring needle was not important, provided it reached at least one-half inch forward from the corona. Varying this length made an insignificant effect on the distribution of current between the two needles, as well as on the distribution of current on the divided needle itself. Having satisfied ourselves of this fact experimentally, the taking of current distribution was made much easier since a long fore portion could be used on the divided lower needle of Figure 33. A sliding mount for this needle made it convenient to slide this needle fore and aft for the exploration.

Figures 34 through 39 give the results of these current distribution investigations for both positive and negative points, at currents of 10, 15, and 20  $\mu$  amp, and for Mach numbers from 0 to at least 0.708. The data are in terms of fraction of the total current to the lower needle per inch of needle.

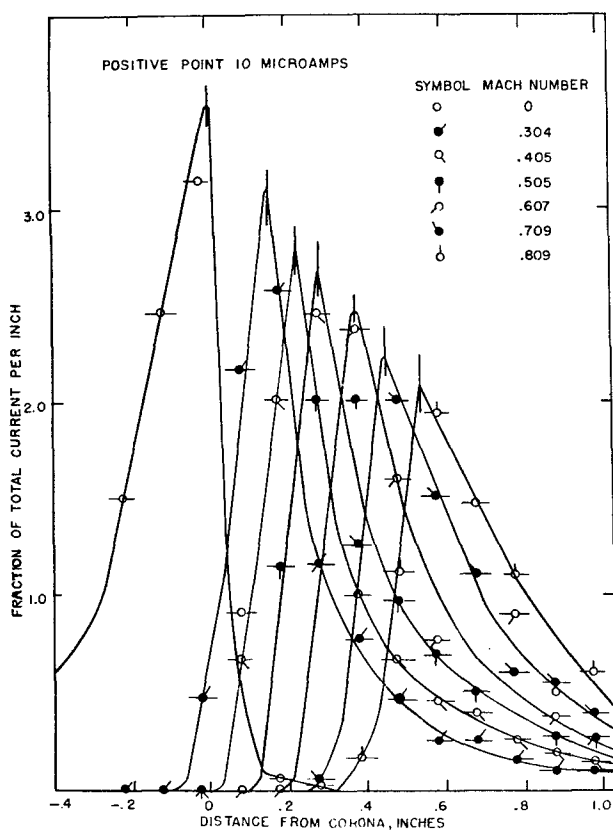


Figure 34. Current distribution on the "plate" needles for various Mach numbers for 10  $\mu$  amp current from a positive point. The origin is at the point on the plate which is directly opposite the corona. The abscissa scale is in tenths of an inch. (Reference 4.)

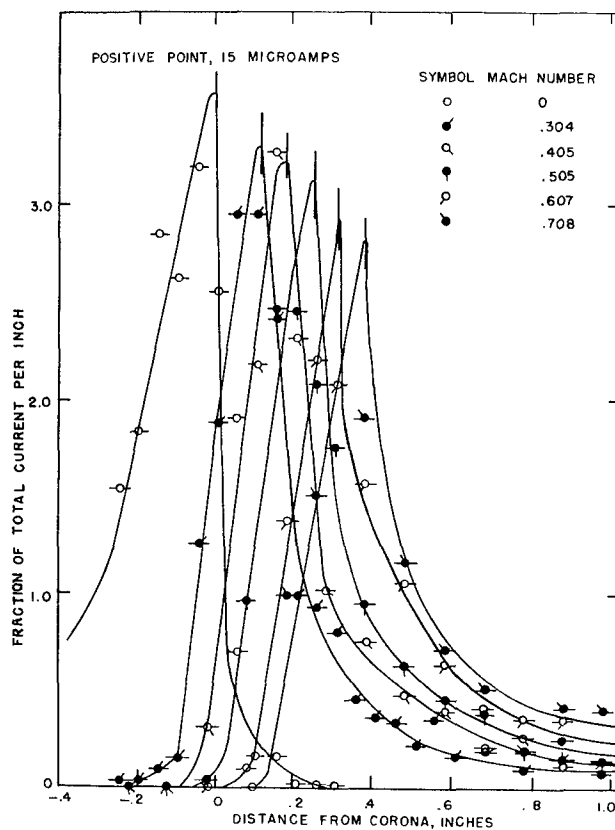


Figure 35. Current distribution on the "plate" needles for various Mach numbers for 15  $\mu$  amp current from a positive point. The origin is at the point on the plate which is directly opposite the corona. The abscissa scale is in tenths of an inch. (Reference 4.)

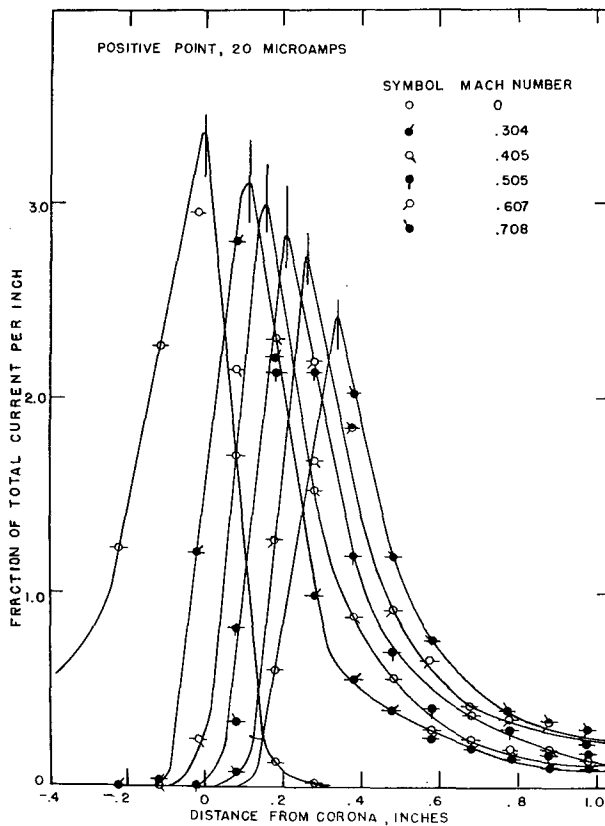


Figure 36. Current distribution on the "plate" needles for various Mach numbers for 20  $\mu$  amp current from a positive point. The origin is at the point on the plate which is directly opposite the corona. The abscissa scale is in tenths of an inch. (Reference 4.)

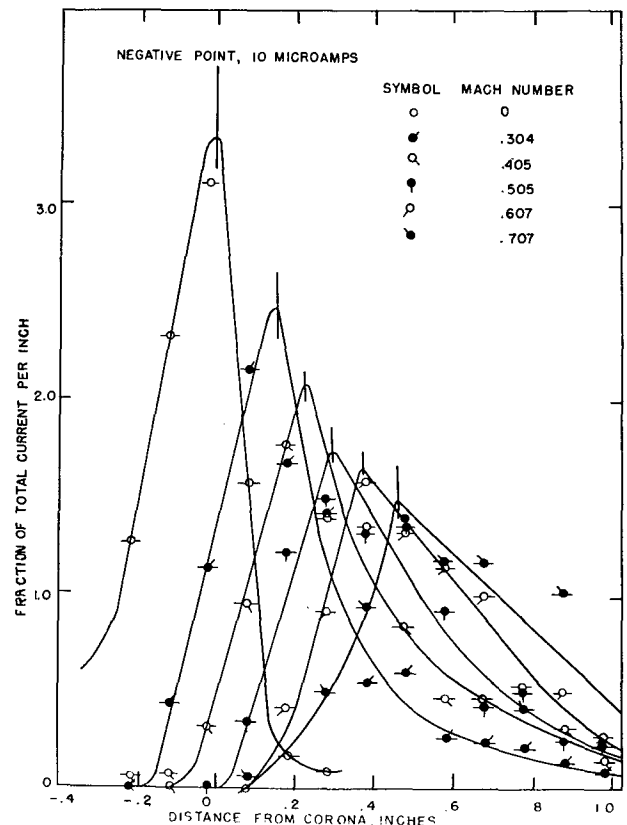


Figure 37. Current distribution on the "plate" needles for various Mach numbers for 10  $\mu$  amp current from a negative point. The origin is at the point on the plate which is directly opposite the corona. The abscissa scale is in tenths of an inch. (Reference 4.)

Throughout the experiment the upper and lower needles had very nearly the same total currents. The data were obtained by moving the exploring electrode 0.1 inch between readings, so the resolution of shape of these curves is not all that might be desired, but nevertheless, it is practical to fair in curves as shown and estimate the location of the peak of current. It is important to note the regular downstream shift of the peaks of these current distributions as the velocity increases.

It is not difficult to calculate analytically the trajectory of an ion, if the simplified electrode model of three parallel, co-planar, infinite wires is used instead of the actual electrodes of Figure 33. The two outer wires are of radius  $a_2$ , voltage zero, and are spaced  $2S$  apart; and the inner wire is of radius  $a_1$ , is at a voltage  $V$ , and is located midway between the other two wires.

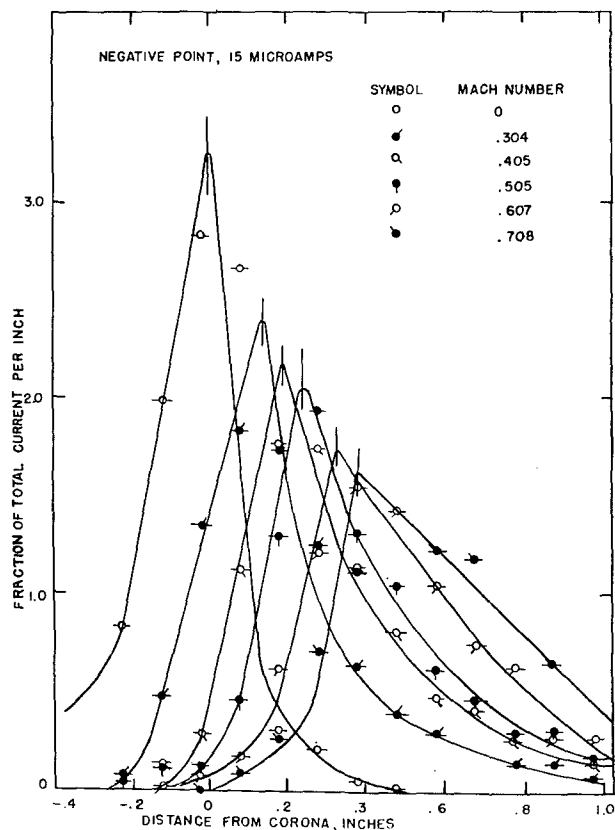


Figure 38. Current distribution on the "plate" needles for various Mach numbers for 15  $\mu$  amp current from a negative point. The origin is at the point on the plate which is directly opposite the corona. The abscissa scale is in tenths of an inch. (Reference 4.)

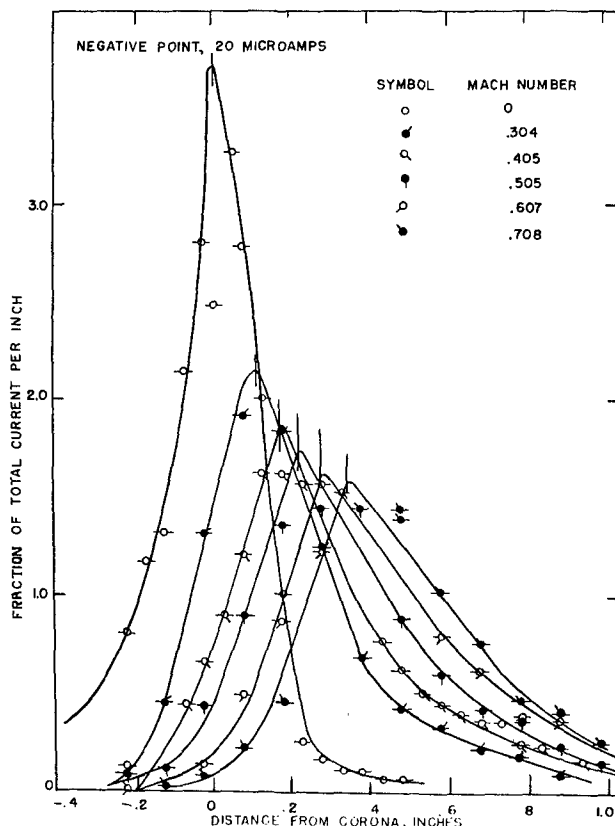


Figure 39. Current distribution on the "plate" needles for various Mach numbers for 20  $\mu$  amp current from a negative point. The origin is at the point on the plate which is directly opposite the corona. The abscissa scale is in tenths of an inch. (Reference 4.)

The highest concentration of ions will be in the plane of the three wires, so in view of the approximate nature of the analysis, only the motion of ions in this plane is considered. The electric field  $E$  in this plane of symmetry is found to be:

$$E = [-B/S] \left[ Y/(1 - Y^2) + Y^{-1} \right] \quad (8)$$

where

$$Y = y/S, \quad (9)$$

$$B = -2V/\log A, \text{ and} \quad (10)$$

$$A = (2a_2S - a_2^2) (S^2 - a_1^2)^{-1} a_1^2 (S - a_2)^{-2}. \quad (11)$$

$E$  is the electric field strength,  $V$  is the voltage difference between the wires,  $S$  is the center-to-center distance from the center wire to either of the outer wires,  $y$  is the distance from the center of the center wire to the point of

interest, and  $a_1$  and  $a_2$  are the radii of the center and outer wires, respectively. If there is a velocity  $u_x$  parallel to the wires and a velocity  $u_y$  perpendicular to the wires, but in the plane of the wires, we have two parametric differential equations of the ion trajectory. The first is:

$$dx/dt = u_x \quad (12)$$

The velocity in the y direction is  $u_y$  plus the velocity resulting from the electric field. Therefore, the other parametric equation is:

$$dy/dt = u_y + [k B/S] [Y/(1 - Y^2) + Y^{-1}] \quad (13)$$

If there is a question as to the sign of the second term on the right side of equation (13), note that for a positive point with a positive ion in the gap  $\log A$  is negative, since  $A$  is always less than 1, and therefore, this term gives a positive component of velocity which is physically correct. Thus a + sign is associated with  $k$  for positive ions. When negative ions are present in the gap,  $V$  will also change sign so this term is always positive. When equation (12) is integrated with  $x$  and  $t$  going from 0 to  $x$  and 0 to  $t$ , respectively, we have

$$X = tu_x/S, \quad (14)$$

where

$$X = x/S \quad (15)$$

To integrate equation (13), it is written in the form:

$$kBS^{-2}dt = dY (Y - Y^3) \left[ 1 + 4D_y (Y - Y^3) \right]^{-1} \quad (16)$$

where

$$D_y = u_y S/4hB \quad (17)$$

We have found no way to integrate the rhs\* of equation (16) in closed form.

---

\*rhs. means right hand side.

When there is no angle of attack,  $D_y$  is zero. In this case, equation (16)

reduces to:

$$X = D_x(2Y^2 - Y^4) \quad (18)$$

which is readily found directly from equation (14) and (16), since equation (16) is easily integrated in this case.

Equation (18) is plotted in Figure 40. This ordinate is  $Y$  and the abscissa is  $X$ . The lower graph shows the trajectories to a distance downstream which is twenty times the distance between wires, and the upper graph is a ten times enlargement of the first part of the lower graph. The corona is depicted at the origin, and the outline of the needle used for the data of Figures 34 through 39 is sketched approximately to scale in heavy lines. The inner half of the

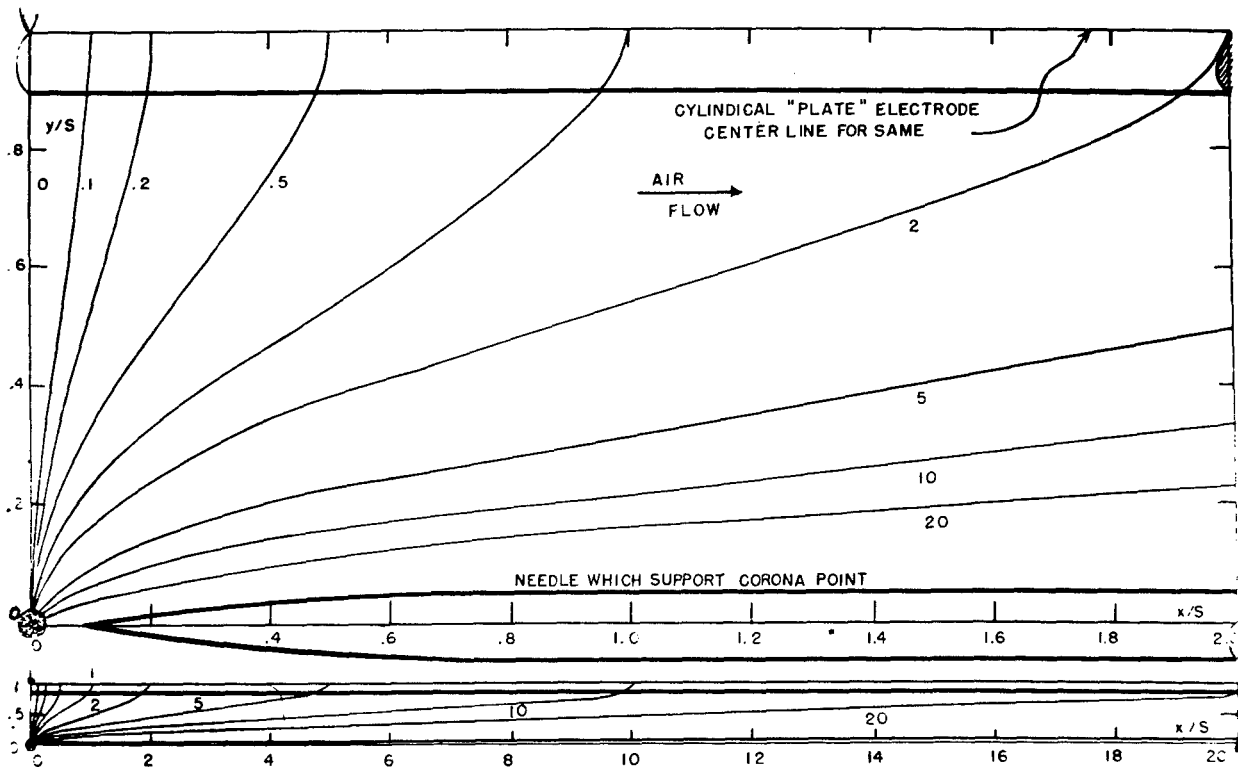


Figure 40. Ion trajectories. The upper graph is ten times the scale of the lower. The heavy lines show the parts of the probe. The parameter is the quantity  $D_x$  from the semi-empirical trajectory equation. The dotted lines show the effect of an angle of attack such that  $u_y/u_x = \pm 0.1$ . The corona is at the origin as illustrated. (Reference 4.)



outer wire is also shown approximately to scale in heavy lines at the top of the graphs.

For the probe used for the data of Figures 34 through 39 on the current distribution on the plates,  $a_1$  was 0.016 inch,  $a_2$  was 0.031 inch, and  $S$  was 0.281 inch so that the value for  $\log A$  was -4.75. At the surface of the plates i.e., the outer wires,  $y$  has the value 0.25 inch so that along this plate equation (18) reduces to

$$X = 0.95D_x \quad (19)$$

This result is plotted as a  $45^\circ$  line in Figure 41. For the data of Figures 34 through 39,  $0.95D_x$  was calculated from the experimental data on  $V$ , stagnation temperature  $T_o$ , stagnation pressure  $p_o$ , and static pressure  $p$ , and using equation (2) to determine  $k$  from the value of  $\rho$  which was computed from the

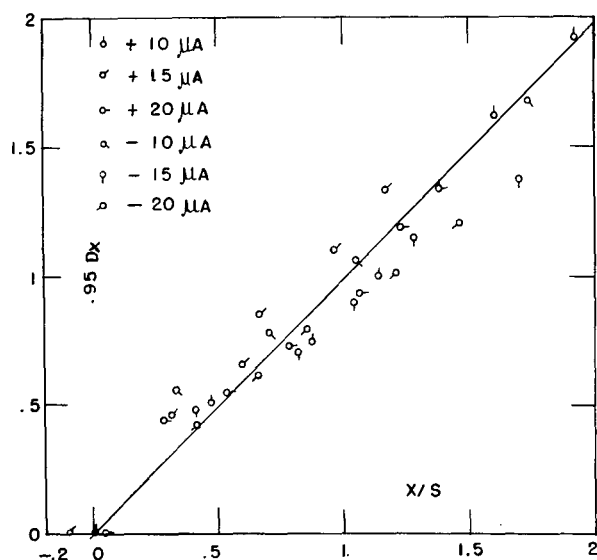


Figure 41. Experimental justification of the ion trajectory equation. The  $45^\circ$  line is the point of termination of the trajectories as predicted by the semi-empirical trajectory equation. The experimental points are the estimated location of the peaks of the current distributions on the plate. (Reference 4.)

observed data by means of the isentropic channel flow equations.  $X$  was taken as the value of the peak of the faired-in current distribution curves (Figures 34 through 39). These experimental data on  $X$  vs.  $0.95D_x$  are also plotted in Figure 41. The agreement between the predicted point of arrival of the ions on the plate, and the experimental data on the location of the current peaks is thus seen to be fair. It is within the experimental errors of measurement, since 0.1-inch steps were used in measuring the current distribution. This agreement is the

more remarkable since it depends upon our fortunate choice of an analytical model of electrodes which provide a static electrical field that seems to give nearly the same trajectory as the true electrical field which varies with time and the space coordinates in a very complex manner. This result is very encouraging since it makes possible an approximate way to predict the performance of a probe when used in flowing air. As work evolves, it will be worthwhile to examine the accuracy of this semi-empirical ion trajectory theory in more detail.

### B. Model III Corona Probe for Turbulence Measurements

Based on this design information, we have designed the probe, called Model III, which is shown in Figure 42, for measurements of turbulence in air flow, to succeed the Model II probe type which was used for some preliminary turbulence measurements discussed in Section VI. The chisel-shaped support G for the corona point H and the two exploring or "sensing" points F is of 1/16-OD, 0.011-inch ID, pyrex, capillary tubing, and has a platinum coating fired to the outer corners to which the fine-wire sensing points can be soldered. This chisel has also been made of nylon rod, with the sensing wires cemented to its sides. This is supported by the larger cone C which, in turn, mounts on a hollow brass tube E. This tube acts as a support for the two outer plate electrodes D, as an electrical conductor to them, and as an electrical shield for the inner leads from which the signal will be observed.

Figure 43 is a schematic diagram of the electrical circuit planned for use with the Model III probe of Figure 42. The Model III probe itself is shown schematically at the right. The two outer wires, i.e., the plate electrodes, are connected together and go to one side of the voltage supply, which is indicated by the battery. This side of the circuit is ordinarily to be at ground potential. The sensing electrodes connect through the resistors  $R_y$ , which develop the signal for the cross component of velocity, to the resistor  $R_x$ , which develops the signal for the longitudinal component of velocity, and thence through the microammeter  $I_3$  and to the voltage supply. In use, the voltage  $V$ , indicated by the tap on the right hand side of the battery, is raised until the desired total current, as read by the microammeter  $I_t$ , is reached (in the vicinity of 10 to 20 microamperes). The voltage  $V_3$  is then adjusted until  $I_3$

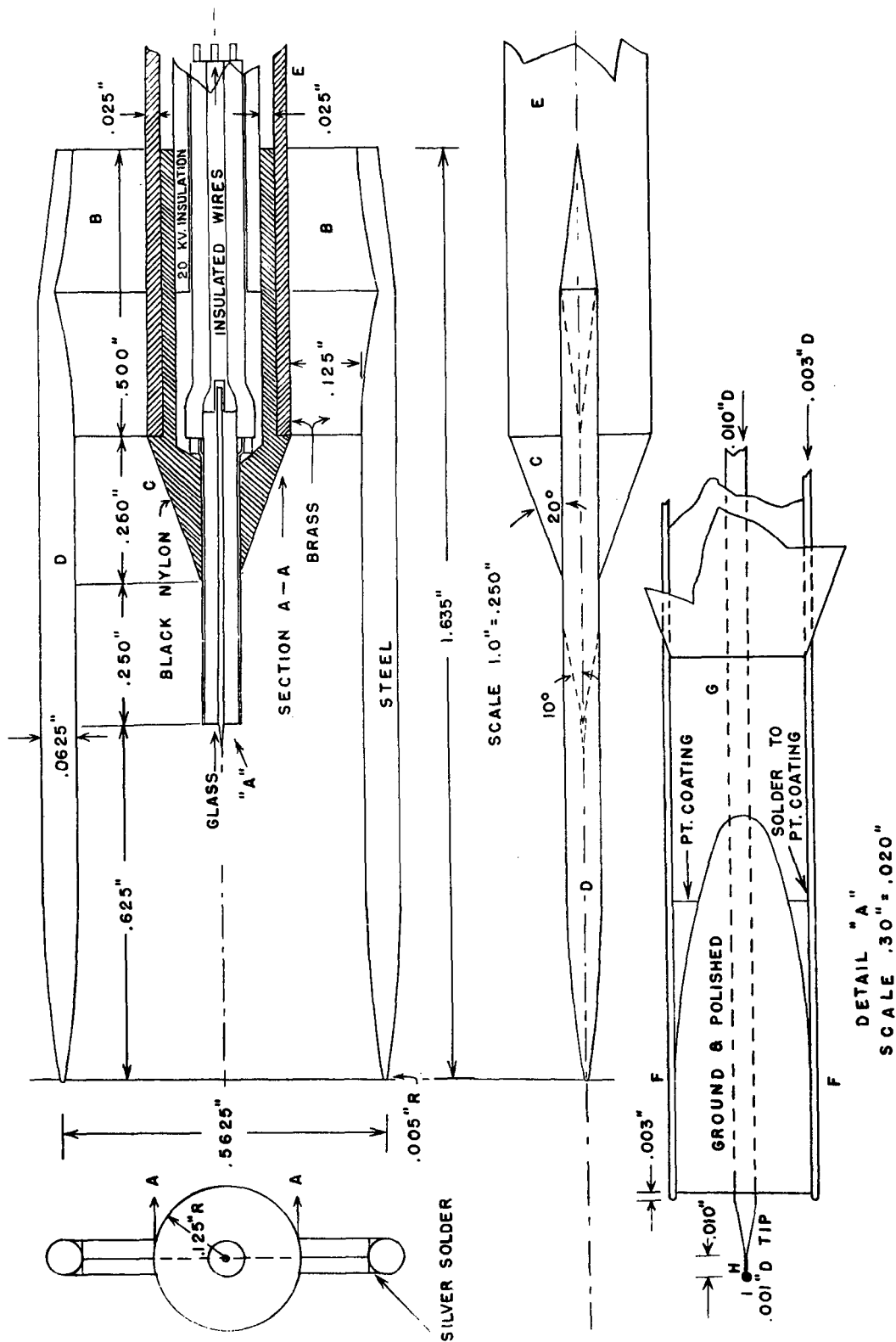


Figure 42. Model III corona probe for measurement of turbulence. D are the outer "plate" electrodes, H is the corona electrode, and F are the sensing electrodes. I is the corona. The lower view is an enlarged drawing of the sensing electrode arrangement. (Reference 4.)

is about one-tenth or two-tenths of  $I_t$ . In practice, it is necessary to adjust  $V$  and  $V_3$  simultaneously. The center wire  $G$  in Figure 42 is movable in a direction parallel to the air flow and can be set near the position which causes the expected ion trajectory as determined from Figure 40 to pass near or slightly ahead of the sensing electrodes. When  $V_3$  is adjusted, it provides control over the electric field strength near the tips of the sensing electrodes, and this distorts the ion trajectories somewhat from the normal position. The actual ion motion is that of a cloud of ions which centers on or near the predicted trajectory and diffuses into a larger and larger cloud as it leaves the corona.

Now it is clear from the data of Figure 40 that variations in  $u_x$  will change  $D_x$  in the same proportion and cause a corresponding change in  $I_3$  so that  $I_3$  is a measure of variations in  $u_x$ , other things being constant. The sensitivity of  $I_3$  to changes in  $u_x$  can be computed when analytical information on the distribution of ions in the ion cloud, which constitutes the actual space current, is known. It seems likely that some useful analytical information in this respect can be evolved.

When there is a change in the cross component of turbulence  $u_y$ , the dashed curves in Figure 40 apply. The important point here is that when  $u_y$  shifts the trajectory, say, toward the plate on one side of the corona, the effect will be to shift away from the plate on the opposite side. Thus,  $I_4$  and  $I_5$ , while nominally equal when  $u_y$  is zero, will differ, and a voltage at  $u_y$  in Figure 43 will be developed which will be a measure of the cross component. It is necessary to make one of the two resistances  $R_y$  slightly adjustable, so that if there are slight differences in the average value of  $I_4$  and  $I_5$ , the effect can be balanced out. This is the same as saying that the separation of  $u_x$  and  $u_y$  signals can be accomplished by adjustment of this resistor.

The situation is not quite so simple as outlined above. It was implicitly assumed above that velocity has no direct effect on the total current. This is approximately true at low velocity but velocity becomes important independently at higher velocity, as shown in Figure 44. In each case in this figure, the

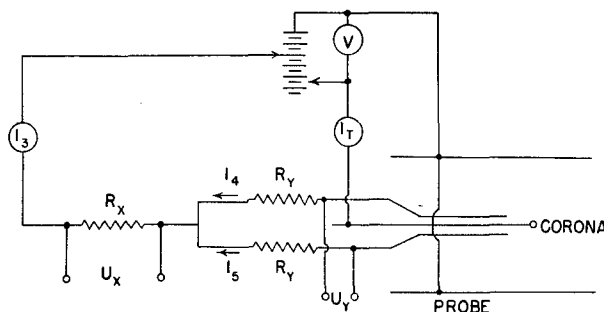


Figure 43. Electrical schematic diagram of Model III turbulence probe. (Reference 4.)

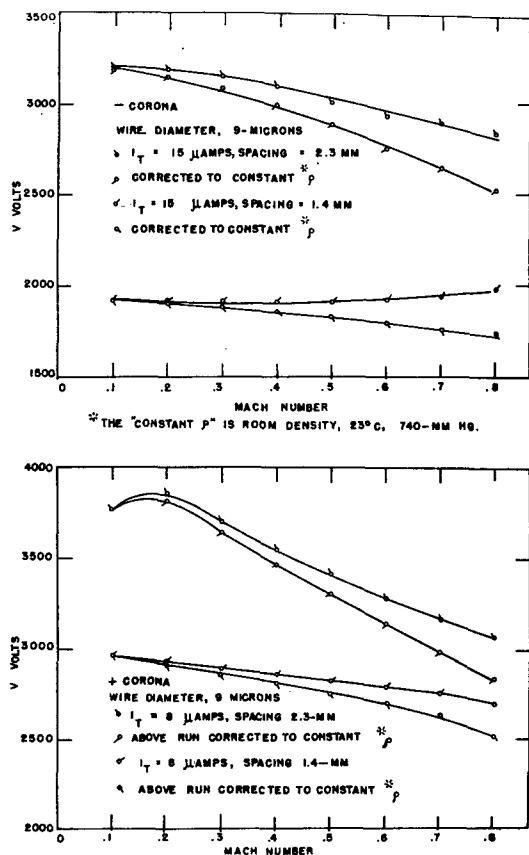


Figure 44. Variation of corona voltage with Mach number at constant values of total current for + and - corona. (Reference 4.)

and frequency response to the order of 100 kc or more, with no necessity for frequency compensation. It is entirely conceivable that a more advanced form of the Model III probe could have another set of outer needles D and of sensing electrodes F in a plane parallel to the flow but perpendicular to the plane of the electrodes of the Model III probe, so that all three components of turbulence could be measured. It should also be pointed out in connection with the possibilities of measuring turbulence in compressible, and even in supersonic flow, that for low turbulence levels, an observer moving with the flow would observe turbulence as an incompressible flow phenomenon superimposed upon the main flow. Such an instrument as the hot-wire anemometer necessarily is concerned in part with stagnation conditions, but the corona probe, depending as it does on ion motions in air which is almost completely undisturbed by the presence of the probe itself, may be expected to observe low-level turbulence in compressible flow as a constant-density phenomenon.

lower of the pairs of curves is of special interest because it indicates the effect of velocity on the total current  $I_t$  for constant density. This data was taken with the Model II probe shown in the upper rhs. of Figure 52 in a 1/2-inch diameter free jet. The static density varied with Mach number. To correct for this, the probe was calibrated in still air over a small density range near the values realized in the jet. The data as taken were corrected accordingly to 23°C, 749 mm Hg, resulting in the lower set of curves.

As a result of these investigations, it appeared reasonable to hope that in a compressible flow, a single such installation will be able to simultaneously provide measurements of density, longitudinal velocity variations, and one of the cross components of velocity variations, with negligible cross coupling among the terms,

For investigations with the Model III probe, the probe was connected as shown in Figure 45. Two power supplies were used so that the sensing needles could be operated at any potential from the center needle potential to plate needle potential. The spacing  $B$  was chosen at 35 mils. By use of the curves on Figure 40,  $A$  was chosen for a Mach number of approximately 0.3. The sensing

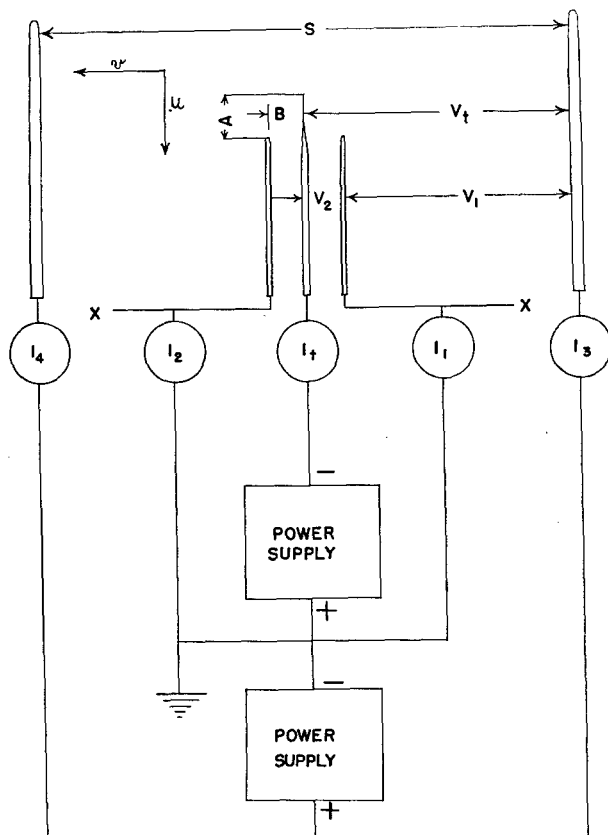


Figure 45. The electrical schematic diagram of the Model III probe for the measurement of transverse velocities. By using two power supplies, it was possible to operate the sensing needles at ground potential and have the sensing needle potential at any value with respect to plate needle and center needle potential.

needles were made of 3-mil wire and were completely insulated except for about 3 mils of the tip. This made the sensing needles approximately a point sensing device so that small changes in the ion beam passing over it could be detected. The sensing needle voltage was determined as follows: The sensing needles were connected to an electrostatic voltmeter. The center needle to the outside plate needle voltage was increased until the operating value of total corona current was obtained. The sensing needles then assumed the value of the electric field. In operation a voltage of 50 to 100 volts higher than this was used to obtain the desired sensing needle current. The value of sensing needle current was from about one-fifth to one-tenth the total corona current.

Calibrations of the probe were made to study the operation of the probe and its sensitivity. The probe was mounted in the 3-inch subsonic wind tunnel with a mount which permitted adjustment of the angle of attack. Initially, the probe was set at zero angle of attack, and the Mach number was increased until the sensing probes showed a maximum current. The Mach number was then decreased to a value below this so that the ion beam was then passing just in front of the sensing probes. This maximum was fairly broad and could not be

determined accurately. The angle of attack was changed and the corresponding changes in  $I_1$  and  $I_2$  were noted. This change in the angle of attack gave the approximate effect of a transverse velocity proportional to the angle of attack, placing one of the sensing needles in a region of higher ion density, and the other needle in a lower ion density. If the angle of attack is small, the change in the longitudinal velocity is small. The results of these experiments were inconclusive. As the angle of attack was changed from zero angle to about five degrees, the current in the sensing needle which was inserted into the ion beam decreased instead of increased. At higher angles of attack, i.e., approximately twenty degrees, the probe performed as expected with the sensing needle current increasing for the one which was inserted into the region of higher ion density. The results of these tests are shown in Figure 46. The lack of symmetry in the curves for positive and negative angles of attack is probably

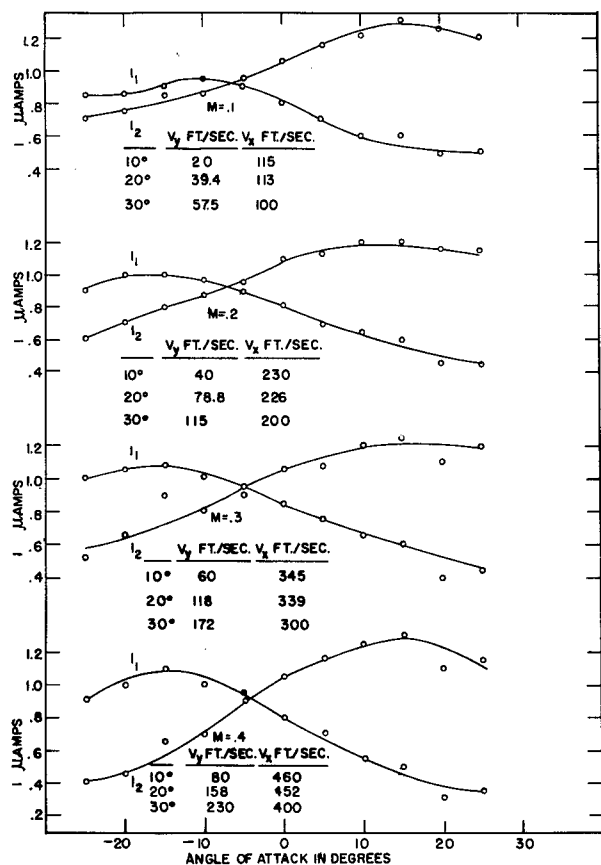


Figure 46. Plot of the two sensing needle currents vs. angle of attack at various Mach numbers.

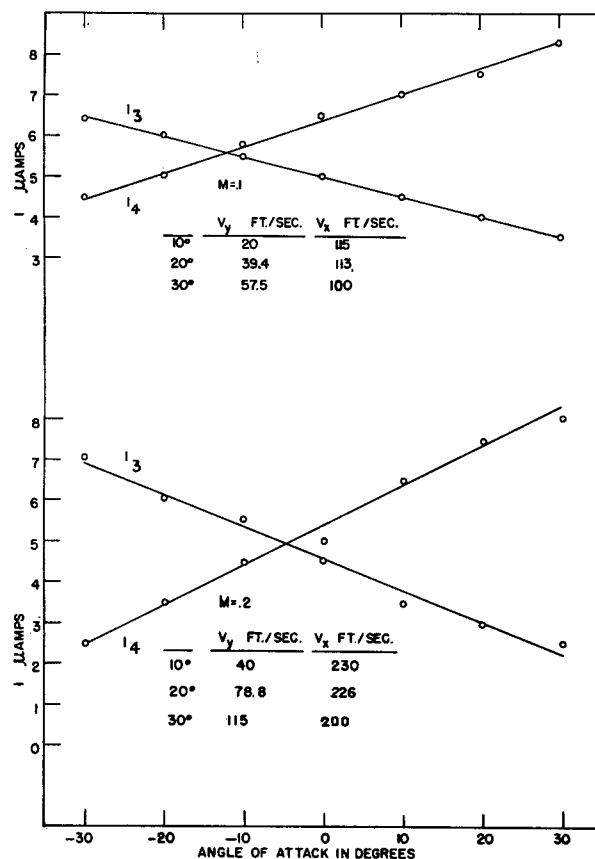


Figure 47. Plot of the two plate currents vs. angle of attack at various Mach numbers with sensing needles left floating.

because of lack of symmetry in construction of the probe. To study the probe further, meters  $I_3$  and  $I_4$  were then inserted into the plate needle circuits as shown in Figure 45. The sensing needles were left floating. The currents  $I_3$  and  $I_4$  vs. angle of attack were measured with constant Mach number. It was noted the two currents did not remain constant as the angle of attack was varied. In the design of the Model III probe, it had been assumed that these two currents would remain practically constant because these needles were extensive in the downstream direction. The current division, not remaining constant, had the effect on the Model III probe of causing the ion density of the beam which was bent closer to the sensing needle to become smaller, and the ion density of the beam which was bent away from the other sensing needle to become larger. These two effects apparently combined in a complex manner such that the division of current was the more important of the two phenomena. It was noted in the data that this effect was dependent only on the transverse components of velocity in the range of Mach numbers measured and not on the longitudinal component.  $I_3 - I_4$  was also linear to the transverse component of velocity in the range that was measured in contrast to  $I_1 - I_2$ . Figure 47 is a plot of  $I_3 - I_4$  vs. angle of attack.

#### C. Model IV Corona Probe for Turbulence Measurements

A new probe, the Model IV probe, was then constructed to make use of the observed division of current between the outer electrodes. The probe as shown in Figure 48 is essentially the Model III probe without the two, outside plate needles. The two plate needles, i.e., the sensing needles on the Model III probe, were made of 10-mil needles. The center needle to plate spacing was 35 mils. The schematic diagram of the experimental setup is shown in Figure 49. A calibration of  $I_1$  and  $I_2$  vs. angle of attack at various Mach numbers was made. The data are shown plotted in Figure 50. The results are very important because they show that  $I_1 - I_2$  is linear with respect to transverse components of velocity over the range measured. This was similar to the behavior of  $I_3$  and  $I_4$  for the Model III probe. Furthermore, these results show that  $I_1 - I_2$  is essentially independent of the longitudinal velocity in the range measured. On the other hand,  $I_1 + I_2$  is sensitive to longitudinal



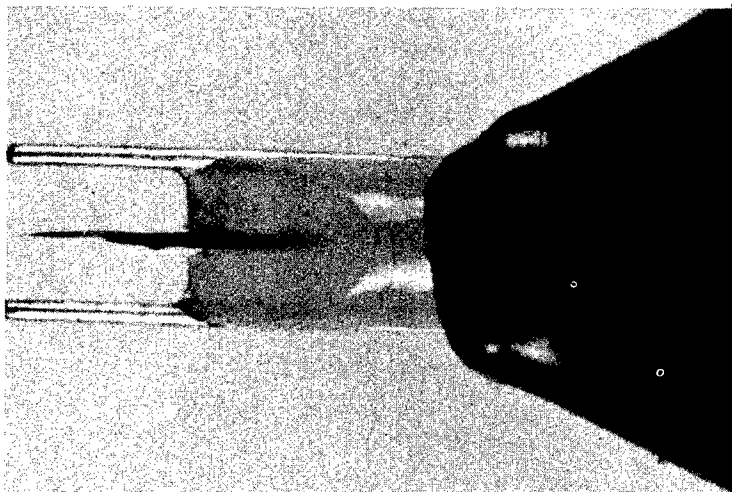


Figure 48. Model IV corona probe which was used in the subsonic turbulence tests. The center needle to plate spacing was 35 mils. The tip of the center needle was made of .3-mil platinum wire.

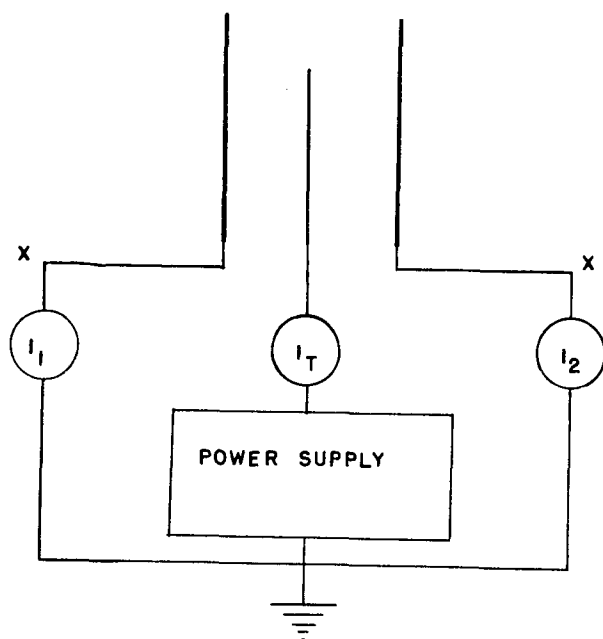


Figure 49. Electrical schematic diagram of the Model IV probe shown in Figure 48 for the measurement of transverse turbulence. In turbulence measurements, the meters  $I_1$  and  $I_2$  are replaced by resistors and the output is taken off from points x-x.

velocity. Thus, if resistors are placed in the two plate needles instead of the two meters, a transverse component of velocity increases the voltage across one resistor and decreases the voltage across the other. Thus if a differential output is taken off the probe at points x-x in Figure 49, the signal is sensitive only to the transverse component of velocity. A change in density either increases or decreases the total current and thus affects the signals in each plate needle circuit the same amount. Thus at zero angle of attack, there can be no sensitivity of the  $I_1 - I_2$  signal to density, so that density is, at worst, a second order effect for the signal.

It is important to note that the Model IV probe is capable of measuring the same information as the Model III probe. By providing another set of plate needles at right angles to the present set with currents  $I_3$  and  $I_4$ , one would be able to measure both components of transverse velocity. All the current passing from the center needle is not picked up by the plate needles. By properly insulating a part of the plate

needles, a significant percentage of the ions is blown away by the longitudinal velocity. This value fluctuates according to fluctuations in the longitudinal air flow. The total current is primarily a function of density so all three values of instantaneous velocity as well as the instantaneous density can be measured.

Separation of these four quantities may be fairly complicated in general. However, there are four independent measurements and four unknowns, and therefore, the problem can be solved for the four unknowns. In this case, measurements of  $I_1$ ,  $I_2$ ,  $I_3$ ,  $I_4$ , and  $I_t$  are possible and the unknowns are the three components of velocity and density. There is a relation among  $I_1$ ,  $I_2$ ,  $I_3$ , and  $I_4$  due to the symmetry of the probe, and therefore, of the five measurements, only four are independent.  $I_1 - I_2$  and  $I_3 - I_4$  measure the two transverse components with, at worst, second-order coupling effects. Separation of the longitudinal component and density, although possible, needs further study.

The complete probe described above was not constructed. It was more practical to experiment with the simpler probe, which has only three electrodes for measuring only one transverse component, and to compare this type with the hot-wire.

#### D. Failure of the Corona Wire Due to Air Loads

Another result important in the design of probes for air flow tests is the effect of air loads in bending over the small center needle (Reference 3).

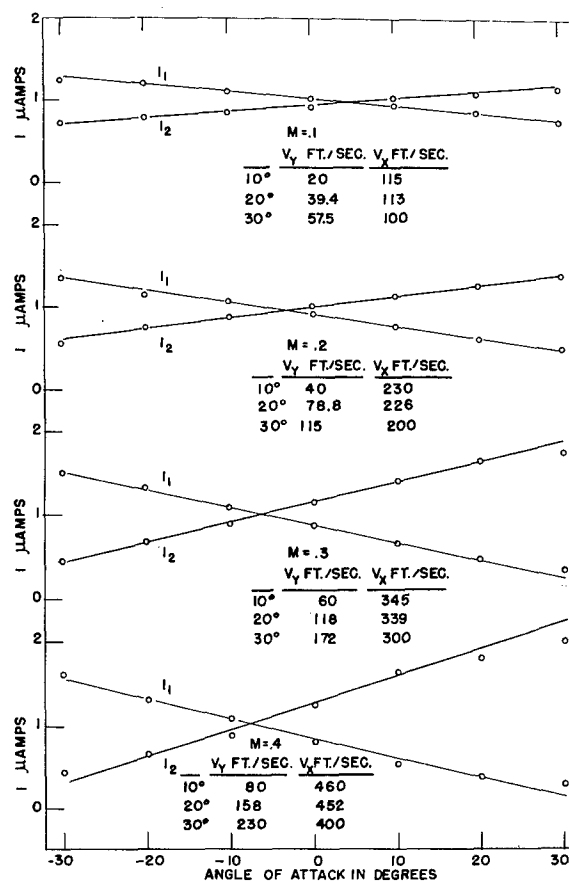


Figure 50. Plot of the two plate currents vs. angle of attack of the probe at various Mach numbers. This corresponds to a static calibration of the probe to transverse components of velocity.

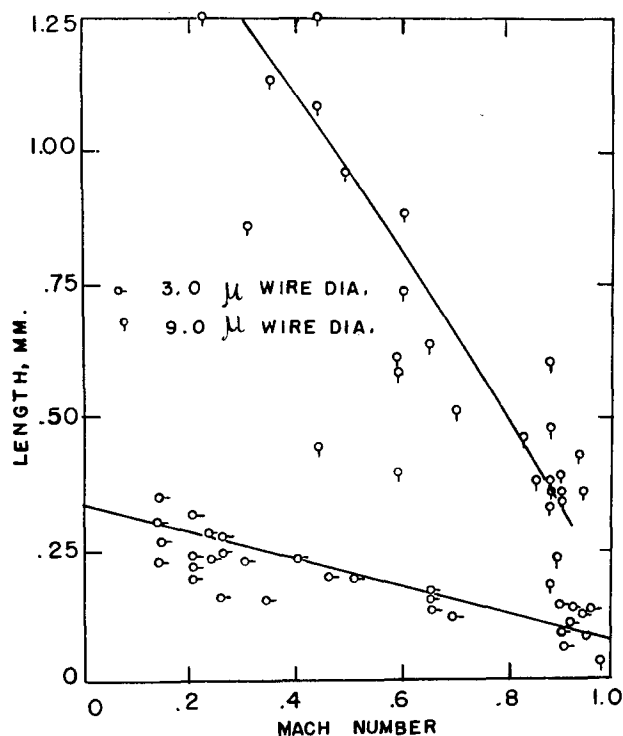


Figure 51. Length of wire at which the wire will bend over when pointing upstream. The wide scatter is probably largely due to slight inaccuracies in pointing the wire parallel to the airstream. For the air stream, the static pressure is one atm and  $T_0$  is  $23^\circ\text{C}$ . (Reference 3.)

In these tests a needle of a given length was pointed upstream. The Mach number for which the needle bent over was noted. The test was performed in a 1/2-inch free-jet wind tunnel which exhausted to the atmosphere. The data as shown in Figure 51 scatters badly and this probably results from the difficulty of mounting the wire parallel to the airstream. In normal operation, however, the length of the wire may be chosen much shorter than the maximum length predicted by Figure 51. For positive corona, such short lengths are satisfactory because the rate of disintegration is negligible. For negative corona, such short, permissible wire lengths necessitate relatively frequent wire renewal.

## SECTION VI

### TURBULENCE MEASUREMENTS

Some data on a preliminary study of the use of corona in measuring turbulence were discussed in our last previous report (Reference 4). Our recent studies of velocity sensitivity have thrown new light on the subject of the application of the corona to turbulence measurement. The present report gives similar data taken with a better understood type of probe. These new data compare favorably with hot-wire anemometer turbulence measurements.

The earlier experiment was set up in the following manner. A 1/16-inch Lucite cylinder was placed across the exit of a 1/2-inch free jet. A Model II corona probe was then traversed normal to the air flow through the turbulent

wake of the Lucite cylinder along a path 0.15 inch downstream of the center line of the cylinder. A load resistor was placed in the plate circuit of the corona probe and coupled into the input of an amplifier as shown in the schematic diagram of Figure 52. The amplifier had a gain of 900 and a rather sharp cutoff frequency response from 800 cycles to 50 kc. The output of the amplifier was observed with a Ballantine Model 300 Voltmeter. The probe was placed in the free stream to the side of the wake and the voltage resulting from the free stream turbulence was observed. The corona background noise was much lower than this free stream turbulence signal. As the probe passed behind the cylinder, the AC turbulence voltage increased. The ratio of the turbulence voltage behind the cylinder ( $E$ ) to the free stream voltage ( $E'$ ) was plotted in Figure 52. A hot-wire anemometer was then set in the air stream in place of the corona. The same procedure was used and the ratio of cylinder turbulence to the free stream turbulence for the hot-wire anemometer was found and plotted in the same figure.

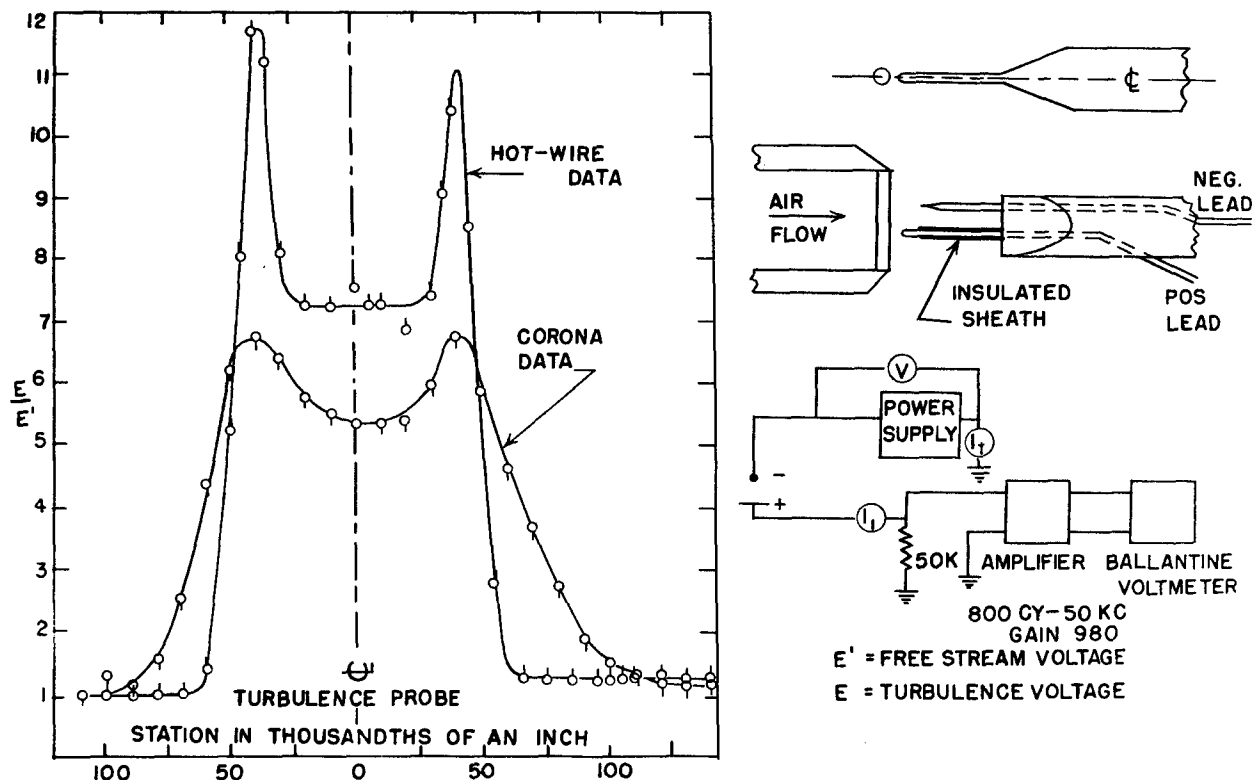


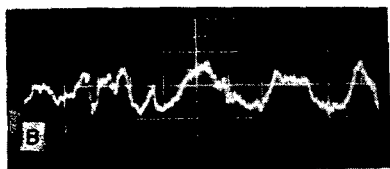
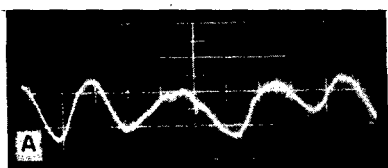
Figure 52. Preliminary measurements in turbulent air flow with a Model II corona probe. At the upper right is a sketch of the 1/2-inch diameter free jet with a 1/16-inch Lucite cylinder across its exit, and with the Model II corona probe in the wake of this cylinder. Below this is the electrical schematic diagram. At the left is a comparison between the wake survey with a hot-wire anemometer and with the corona probe, for a position 0.15 inch downstream of the centerline of the cylinder.

A better explanation for the apparent difference in the hot-wire anemometer and the corona curves of Figure 52 is now possible. A single hot-wire parallel to the Lucite cylinder and normal to the flow was used. Thus the hot-wire was measuring the longitudinal fluctuations of the turbulence. In the light of present experiments, the corona was primarily sensitive to the transverse fluctuations parallel to the cylinder while retaining considerable sensitivity to the longitudinal fluctuations. The transverse fluctuations parallel to cylinder are small. Thus the Model II probe was poorly adapted to these measurements. It is expected that if the experiment were repeated with a Model IV probe, much better corona results could be obtained. Further comment on the use of the Model II probe is difficult because it had only one plate needle. The 92-mil spacing was also important, as mentioned in the discussion. Present probe models have used a spacing of 35 mils which is still not considered a lower limit. Thus as the spacing used was comparable to the eddy size, the Model II probe was surely not measuring the finer detail of the turbulence. During the past year the measurement of turbulence with a corona discharge probe has been placed on much firmer ground, and the method of operation of the probe is now more clearly understood.

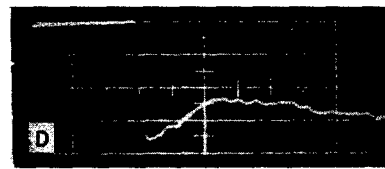
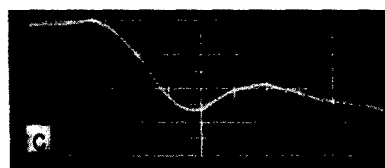
The experiments which are described below were made with Model IV probe as described in Figures 48 and 49. We concentrated on measurements of the transverse component since it is relatively well separated from density variations and the two other components of velocity. Since the setup for all of the turbulence measurements of the transverse component is basically the same, it will be explained here. The arrangement, shown in Figure 49, was used for the calibration of the probe for transverse components of velocity. The meters  $I_1$  and  $I_2$  are replaced by two resistors and a differential amplifier (measuring  $I_1 - I_2$ ) is connected to the points x-x. It should be noted that this type of hookup is sensitive to a transverse component of velocity and is insensitive to total current changes as discussed earlier. The plane of the three needles will be referred to in the future as the sensitive plane of this type of corona probe. When an amplifier is connected to measure  $I_1$  and  $I_2$ , the longitudinal component in this plane can be measured, at least for the case of constant-density turbulence.

For the first investigations with Model IV probes, two probes were constructed with different spacings to determine which region of the corona is

sensitive to velocity variations. One of the probes had a spacing of 35 mils from the center needle to each of the two outside plates. The second probe had a spacing of 7/8ths of an inch from the center needle to each of the two outside needles. The two probes were mounted in our 3-inch subsonic wind tunnel, six diameters behind the center line of a 1/2-inch cylinder placed normal to the flow. The Mach number was 0.2 and the corona current 4  $\mu$  amp. The oscillograms of Figure 53 show the probe response. It can be seen that the sensitive region involves most of the gap, because the probe with the wide spacing does not respond to the small variations, but does pick up very clearly the lower fundamental frequency of the Kármán vortex street that is generated behind the 1/2-inch cylindrical rod. On the other hand, it is quite clear that the small probe measures disturbances which have dimensions much smaller than the smallest disturbance sensed by the large probe, as expected.



Comparison of large Model IV probe (A) and small Model IV probe (B) mounted 6 diameters behind a 1/2-inch diameter cylinder, Mach number 0.2, total corona current 4  $\mu$  amp, and a sweep speed of 300  $\mu$  sec/div.



Comparison of large Model IV probe (C) and small Model IV probe (D) measuring the instantaneous change in velocity behind a shock wave, Mach number 0.1, total corona current 4  $\mu$  amp, and a sweep speed 30  $\mu$  sec/div. A shock tube breaking pressure of 4 psi was used, giving a transverse velocity of approximately 100 ft/sec.

Figure 53. The effect of center-needle to plate-needle spacing on the frequency response of the corona to turbulence fluctuations. The large, Model IV probe center-needle to plate-spacing was 0.875 inch while the small, Model IV probe spacing was 0.035 inch.

A second and more fundamental method was then carried out to find more information about the sensitive region. A shock tube was mounted in the side of the 3-inch subsonic wind tunnel so that the air behind the shock wave created

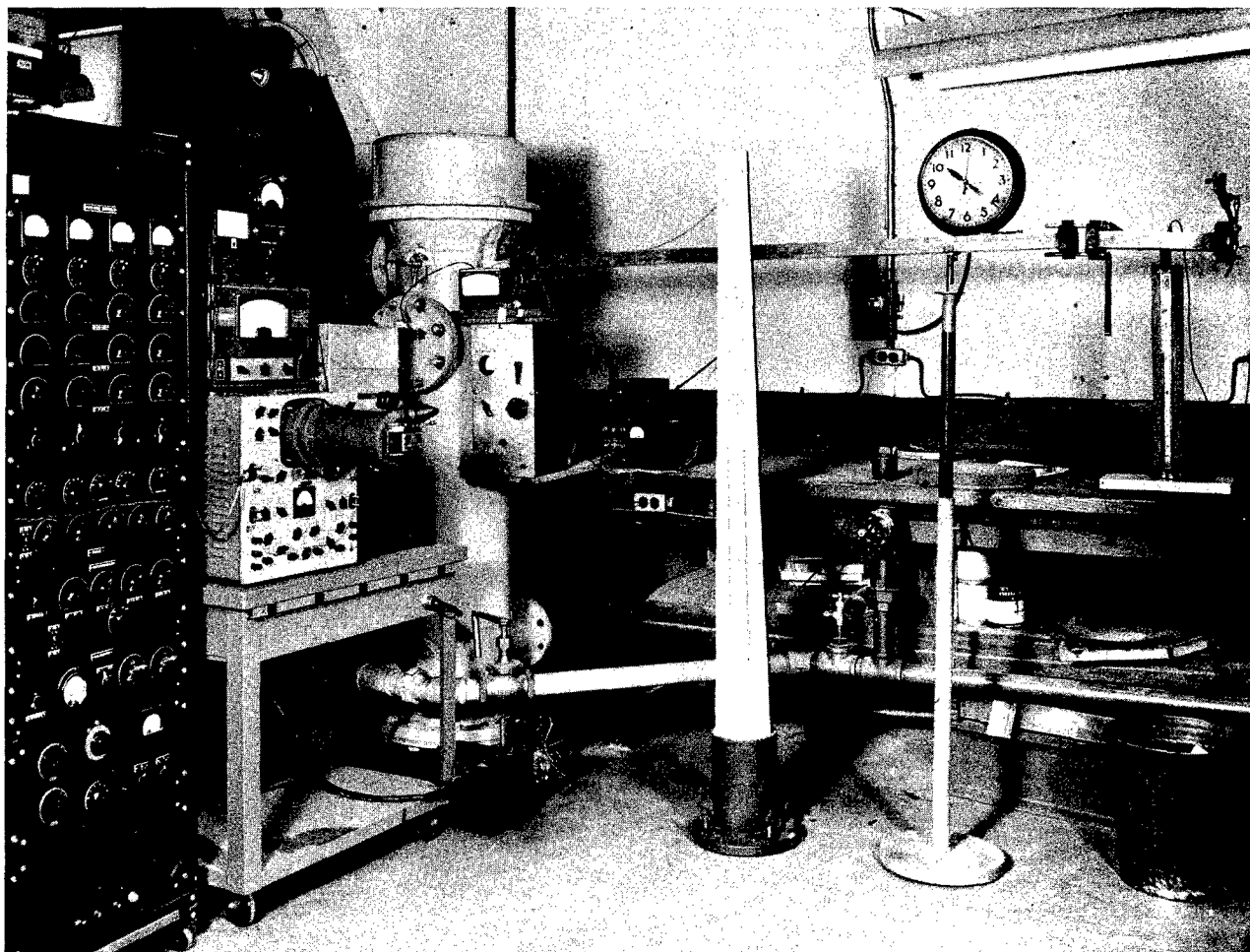


Figure 54. Photograph of equipment used in the hot-wire and corona correlation tests. The 3-inch enclosed free-jet wind tunnel with vertically-downward flow is at the left background, and the shock tube is the long projection to the right of the tunnel.

a transverse component of velocity. The wind tunnel may be seen in Figure 54, as the large vertical cylinder at the left background. The wooden entrance bellmouth is at the top and the flow is vertically downward. Power is supplied by suction from the ejector at the bottom. It is an enclosed, free-jet type of tunnel. The shock tube is the long, horizontal attachment just below and to the right of the entrance bellmouth. Thus we had an accurate device for study of the transient response of the probe for reproducible transverse velocity transients. It is possible to have a wide range of transverse velocities for any longitudinal velocity of the wind tunnel.

Behind the shock wave there is also a density change which was discussed before in Section IV. For the transverse velocity measurement, this density

variation was very simply separated from the measurements as previously described. As discussed in Section IV, the density sensitivity is localized in a very small region about the center needle. Thus a change in density only decreases the total current. The currents to the plate needles were originally equal, and are simultaneously decreased but remain equal to each other. It was found, by a simple calibration test, that the density could change over wide limits and the two currents would remain equal. For large total current reductions, however, it is possible that there is some loss in the sensitivity to the transverse velocity components, other factors remaining constant. This should be a second-order effect, however, and is demonstrated by oscillograms later in this section.

Two oscillograms, Figures 53-C and 53-D, were taken with the corona probe pointing upstream and the sensitive plane perpendicular to the shock front coming from the shock tube. For this test, the pressure in the high-pressure chamber of the shock tube was 6 psi above the pressure on the low-pressure side of the shock tube. The Mach number was 0.2 and the total corona current was 4  $\mu$  amp. The oscilloscope sweep speed was 30  $\mu$  sec/div. The response of the large probe was very similar to the small probe except that it has a much slower response time. The time required for the large corona probe to go to the new condition after the shock wave has passed over is about 110  $\mu$  sec, which is the time it takes the shock wave to cross the gap between the two plate needles. Thus the whole gap between the two plate needles is the sensitive region for velocity variations. However, the response is most steep near the center of the probe, showing that the velocity sensitivity is greatest here. The small probe gave a much more rapid response as the step function of velocity passed over it. The shock wave crossed the gap in approximately 8  $\mu$  sec, in agreement with the oscillogram, so that this is the limiting factor in this case also.

The hot-wire and the corona probe were then mounted six diameters behind the 1/2-inch cylinder in the wind tunnel. The probes were placed 1/2-inch apart and were positioned on a line parallel to the axis of the cylinder. The sensitive plane of the corona was normal to the axis of the cylinder. An "X" type of hot-wire, shown in Figure 55, was used so that it would measure the same component of velocity the corona probe was measuring. The wires were made of 0.3-mil platinum wire, 120-mils long. They were crossed at an angle of 60° to each other in the plane of the flow, and this plane was normal to



the cylinder. Each wire was at  $30^\circ$  to the flow direction. The probe was very similar to one described in Reference 44. Thus both probes measured the transverse component of velocity which is normal to the cylinder. The output from the hot-wire amplifier was fed into the horizontal amplifier of an oscilloscope while the output of the corona was fed into the vertical amplifier. A long-time exposure was then taken. The result is an ellipse, as shown in Figure 56A, the "correlation figure". The two amplifiers were checked so that there was little phase shift at frequencies below 25 kc. Above 25 kc, the shift resulted from the cutoff characteristic of the filters in the hot-wire amplifiers. Two identical corona probes were then mounted in place of the corona and hot-wire, and another correlation figure was taken.

This picture shown in Figure 56B, between corona and corona has about the same amount of correlation as the hot-wire and the corona in Figure 56A. Thus at these frequencies, the hot-wire and the corona appear to agree fairly well. The reason that the correlation patterns between

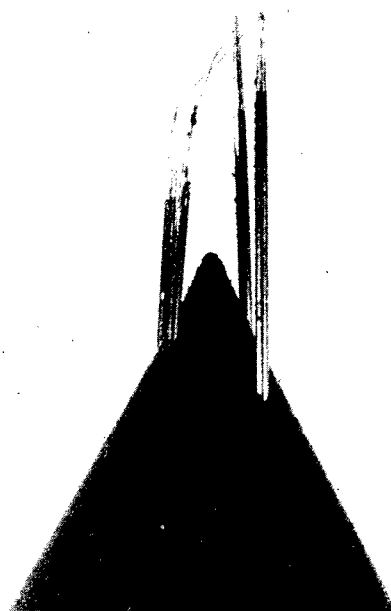


Figure 55. X-type hot-wire probe used in turbulence measurements. Wires are 120 mils long and made of 0.3-mil platinum wire. The probe was slightly damaged before the photo was taken.

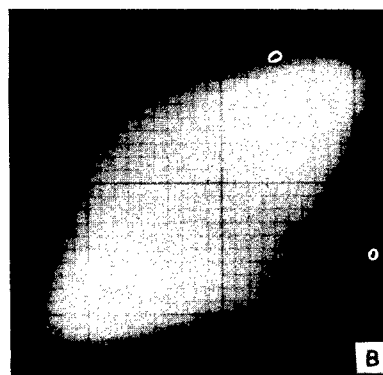
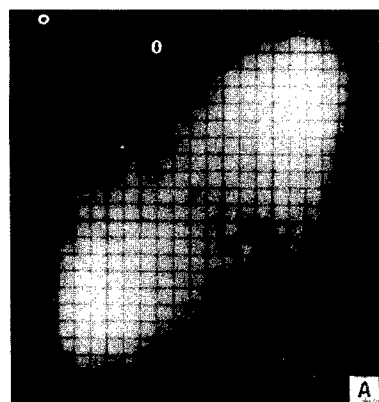


Figure 56. Long-time correlation tests. (A) The correlation pattern of the X-type hot-wire probe and the Model IV corona probe mounted 1/2-inch apart and six diameters downstream from a 1/2-inch diameter cylinder at Mach number 0.2. The hot-wire signal was connected to the horizontal input of the scope while the corona was connected to the vertical input. (B) The correlation pattern of two corona probes under the same conditions.

corona and corona are not better is characteristic of the turbulence which was generated. A Kármán vortex street is generated behind the cylinder; and if the Reynolds' number were approximately 250, the vortex pattern would be very stable and nearly two dimensional. The Reynolds' number was approximately 3000 so that the Kármán vortex street is no longer two dimensional. Thus the two probes were not seeing the same vortex pattern and could not be expected to correlate perfectly.

Because the vortex street was not strictly two dimensional, single trace pictures of hot-wire and corona were taken instead of simultaneous pictures. Figure 57-A, B, C, D, E, F, G, and H show a comparison of hot-wire and the corona. Figure 57-A and B show the hot-wire and the corona measuring the turbulence six diameters behind the 1/2-inch cylinder. Similarity in these traces is evident. The hot-wire has a higher noise level as can be observed in Figure 57-C and D. The sweep speed for these pictures was 300  $\mu$  sec/div. Figure 57-E, F, G, and H are the same pictures as above except that the oscilloscope sweep rate has been increased to 50  $\mu$  sec/div. This picture clearly shows that most of the high frequency signal variation on the hot-wire sweep results from the noise generated in the hot-wire amplifier. Furthermore, the hot-wire amplifier had a rather sharp cutoff at 25 kc and most of the high-frequency variations are in the vicinity of 100 kc, and therefore could not be response of the hot-wire to corresponding velocity fluctuations.

The hot-wire and the corona probes were then mounted in the 3-inch subsonic wind tunnel and at the exit of the shock tube, as discussed earlier. The lab setup is similar to that shown in Figure 54. Figure 58-A, B, C, D, E, and F show the corona and the hot-wire measuring the transverse velocity transient with varying values of longitudinal velocities. The sensitive planes of the corona and the hot-wire were oriented for maximum response to the transverse velocity transient caused by the shock wave. Figure 58-A and B show the case of a shock wave of 4-psi excess pressure with the Mach number of the tunnel set at 0.05. Figure 58-C and D show the case of a shock wave of the same strength with the Mach number of the tunnel set at 0.15. Figure 58-E and F show a similar case except that the Mach number of the tunnel has been increased to 0.25. The gain of both amplifiers was held a constant in all the pictures. The hot-wire was operated at constant hot-wire resistance. The figure shows that the corona response remains practically constant over this range of longitudinal velocity. The wavy line in Figure 58-B before the

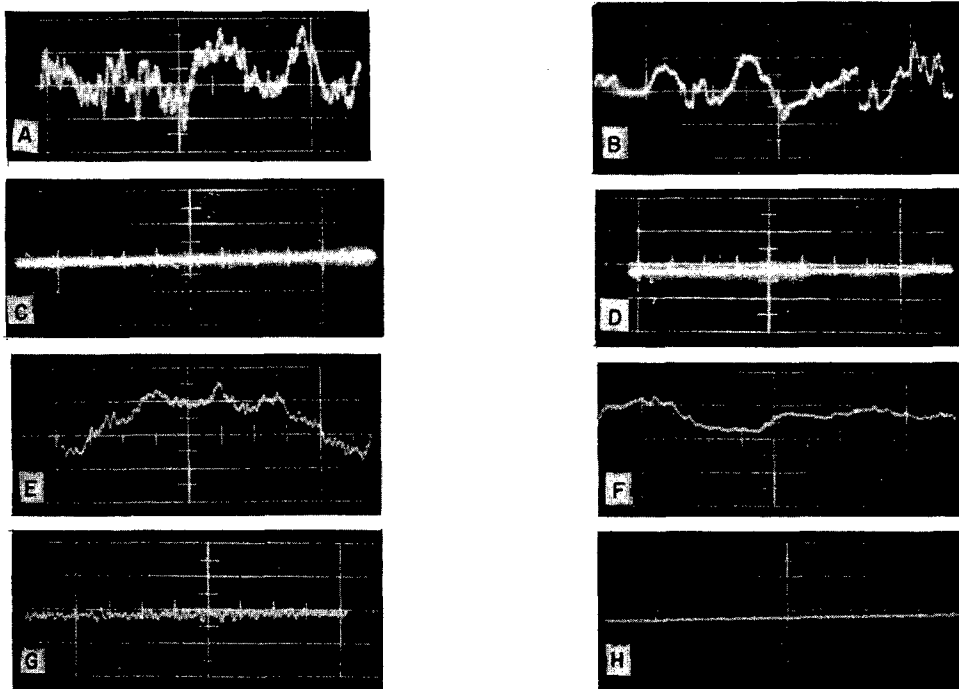


Figure 57. Oscillograms for comparison of a corona and a hot-wire mounted six diameters behind a 1/2-inch diameter cylinder. Both probes were measuring the transverse velocity components. The Mach number was 0.2, corona current was  $4 \mu$  amp, and hot-wire current was 100 milliamp. Pictures A, C, E, and G are hot-wire measurements. A is the turbulent signal with a sweep speed of  $300 \mu$  sec/div. C is the no-signal trace at this sweep speed. E and F are the traces for signal and no-signal with a sweep speed of  $50 \mu$  sec/div. B and D are the corona traces for signal and no-signal conditions with a sweep speed of  $300 \mu$  sec/div. F and H are similar to B and D except the sweep speed was expanded to  $50 \mu$  sec/div. The no-signal condition for the hot-wire was the same as the signal condition except there was no hot-wire current. The no-signal condition for the corona was the same as the signal condition except the corona voltage was turned down until there was no corona current.

shock results from an acoustic oscillation in the wind tunnel with a frequency of 15 to 20 kc. The hot-wire could not pick up this sound very well because it was barely above the noise level of the hot-wire amplifier. The rise time of the corona appears to be limited by the 350-kc frequency response of the amplifier. The rise time is so small on this picture that it is difficult to make an accurate calculation. On the hot-wire picture it is easier to calculate the frequency response, and here one obtains a value of about 40 kc which is about the limit (actually a little higher) for which the hot-wire was compensated. One notes that the corona and hot-wire wave forms are not the same after the shock wave has passed over the hot-wire and corona probes. From the hot-wire response, one is tempted to conclude that there exists a step function of transverse velocity to which the hot-wire signal is a

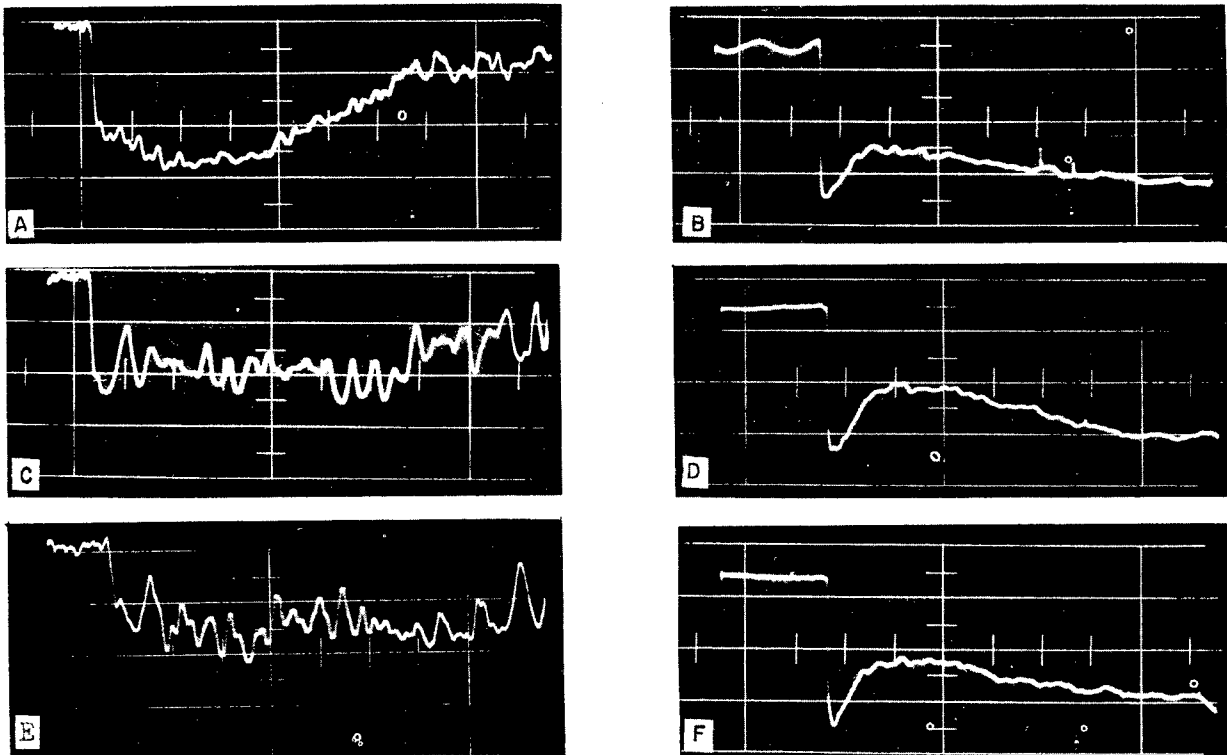


Figure 58. Oscillograms for comparison of the corona and hot-wire to the velocity transient associated with a shock wave. The shock-wave velocity was normal to the wind tunnel flow. The breaking pressure for the shock tube was 4 psi giving a transverse velocity of approximately 100 ft/sec. In this set of pictures, the variable was the Mach number of the tunnel. A and B are the hot-wire and corona measurements, respectively, of the transverse velocity at 0.05 Mach number. C and D are similar pictures for 0.15 Mach number. E and F are similar pictures for 0.25 Mach number. The gain was held constant for both the hot-wire and the corona.

reasonable approximation. As was pointed out to us by Dr. Fredrick Geiger, the actual velocity transient is certainly not a step function outside the end of the shock tube because of rarefaction initiated at the tube exit. It is noteworthy that qualitative reasoning predicts the approximate form shown by the corona probe trace. This type of experiment is well worth further study.

Figure 59 is an oscillogram of the shock wave passing over the corona probe after the probe had been rotated  $90^\circ$  about its axis. The probe placed in this manner should be insensitive to the density transient and to the velocity transient from the shock tube. Figure 59 shows that this is approximately so. The small sine wave type of disturbance following the shock wave is of undetermined origin. When the corona probe was rotated  $180^\circ$  about its

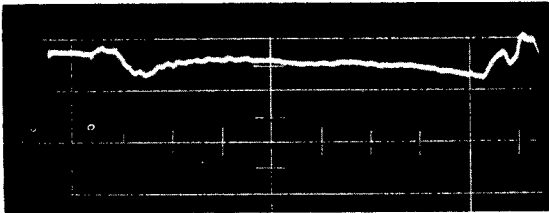


Figure 59. An oscillogram showing the ability of the corona to reject velocity transients normal to its sensitive plane. This figure had the same operating conditions as Figure 57-D except the probe was rotated  $90^\circ$  on its axis.

axis, it was found that the trace is inverted. Thus the disturbance is inherent in the tunnel and the disturbance is actually present as a transverse velocity component in the sensitive plane of the probe. The overall gain and sweep speed of this figure and the corona pictures shown in Figure 58 are the same, so that the sensitivity plane of the corona is well defined with very little interrelation among transverse components,

longitudinal components and density variations under the conditions of these experiments.

The final phase of experimentation with the corona probe was to operate the probe in supersonic turbulence. Experiments were made in a small tunnel with a test section 1.75 inches by 2 inches. The Mach number was 3.1. The stagnation pressure was 165 psi absolute, and the stagnation temperature varied from  $68^\circ$  to  $75^\circ\text{F}$ . The Model IV probe used is shown in Figure 60. The probe was mounted on a diamond shaped strut which fastened to a brass window in the test section of the tunnel. The center needle to plate spacing was 33 mils. The plate needles were constructed of 10-mil steel needles instead of 10-mil platinum wires used in the subsonic experiments.

This made the probe more rugged so that it would stand the heavier air loads. The center needle was made of 0.3-mil platinum wire. Approximately 1 mil of the 0.3-mil platinum wire was exposed. All the supersonic experiments were taken with this one wire. The experiments were performed with positive corona as usual because there is no burning-off of the needle and less dust collects on the needle. In all the air flow experiments, however, no trouble was encountered with dust.

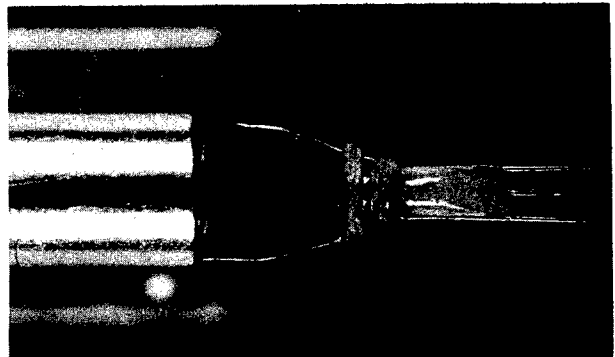


Figure 60. The Model IV corona probe used in the measurement of supersonic turbulence. Center needle to plate spacing was 33 mils. The center needle was made of 0.3-mil platinum wire.

Two types of data were taken. In one case the free-stream turbulence level of the tunnel was measured. Here again only the transverse components of turbulence were measured to the first approximation as discussed previously. It is expected that this probe would have had a relatively large sensitivity to longitudinal fluctuations because 40 percent of the total current was washed away from the plate needles at this high velocity. Measurement of longitudinal velocity was not attempted. In the second case, a 1/8-inch rod was placed normal to the air flow eight diameters in front of the corona probe. By placing the rod this far in front of the probe, the air stream regains supersonic velocity in the wake and probably approaches the free stream Mach number again.

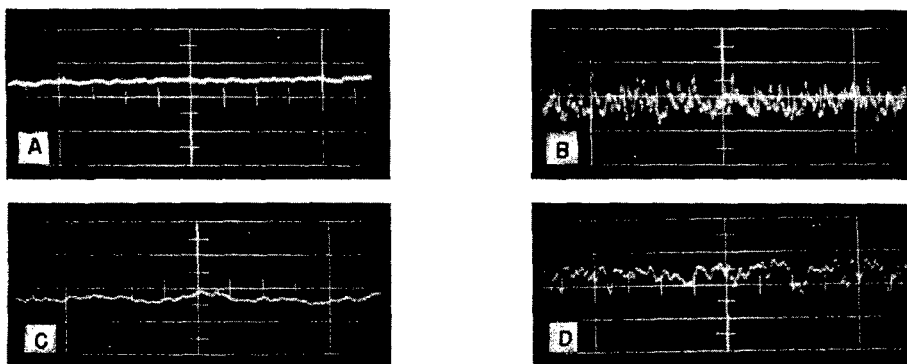


Figure 61. Oscillograms of corona measurements of turbulence in supersonic air flow of Mach number 3.1.  $p_o$  was 165 psi,  $T_o$  was approximately 73°F. A and C are the free-stream turbulence fluctuations at sweep speeds of 50  $\mu$  sec/div and 20  $\mu$  sec/div, respectively. B and D are similar to A and C except an 1/8-inch bar was placed eight diameters in front of the probe normal to the air flow.

The data are shown in Figure 61. Figure 61-A and C show the free stream turbulence without the bar in place. In all the pictures, the overall gain was held constant. In Figure 61-A the oscilloscope sweep speed was 50  $\mu$  sec/div, while in Figure 61-C the sweep speed was increased to 20  $\mu$  sec/div. Small variations were clearly visible. At times this level was approximately higher by a factor of two, but these pictures are representative of typical conditions. Figure 61-B is with the 1/8-inch cylinder in place and with an oscilloscope sweep speed of 50  $\mu$  sec/div; while in Figure 61-D the sweep speed was increased to 20  $\mu$  sec/div. By comparing the four pictures, one notes an increase in both the frequency and the amplitude of the turbulent level when the cylinder is in place. There also appears to be a tendency toward regular variation of the trace as can be seen in Figure 61-D. This variation has a frequency of

approximately 70 kc which is comparable to the vortex frequency which would be predicted by application of simple subsonic theory. The corona still resolves the very fine grain of the turbulence. By noting Figure 61-D, one can observe fluctuations as small as 0.1 of a division. This would give the corona a frequency response of approximately 500 kc. It was known that the half-power point of the input amplifier was 400 kc; but as this single stage amplifier fed into an amplifier whose half-power point is 20 megacycles, the gain at 500 kc was still quite good.

An interesting calculation can be made if one assumes the larger more regular variations in Figure 61-D to be eddies, then a value of the eddy size can be calculated. The assumed eddies pass the probe in times of 10 to 20  $\mu$  seconds. The velocity of the air under these conditions is approximately 2000 ft/sec. This gives a value of the eddy size of 0.2 inches. The smaller variations could be eddies of even small dimensions. This value appears reasonable since the cylinder which created the turbulence had a diameter of 1/8 inch. The fluctuations of 0.1 division in the trace correspond to eddies of about 0.04 inch which is the order of the probe size and would represent the minimum resolution of this probe.

Several experiments were performed to make certain that the signal picked up was not produced by mechanical vibrations or amplifier noise. When the wind tunnel was in operation, the corona voltage was raised to a point just below the corona onset potential. The amplifier was set at the gain used in taking the pictures shown in Figure 61. For these conditions the oscilloscope trace showed no signal. The background noise from the corona pulses do not show on these traces, because corona pulses for this sweep speed and amplifier frequency response would appear as very sharp spikes. Figure 21 shows some representative corona pulses at approximately the same sweep speed. In this case, however, the pulses were greatly spread out by reducing the frequency response in order to obtain better photographs of the pulses. Thus, we conclude that the signal can only be attributed to supersonic turbulence.

There are, however, many things which can and should be done to examine more completely the operation of the probe at supersonic velocities, and a systematic investigation is planned.

From the experiments in supersonic air flow, the corona appears to be measuring transverse fluctuations in the flow. Its frequency response appears to be in excess of 500 kc for this application.

The probe is mechanically strong and does not appear to be affected by vibrations. The probe is small, the size could be reduced still further for some applications. As the two outside needles are at approximately ground potential, the probe should perform successfully for boundary layer work. If the tunnel wall is made of insulated material, tests could be made within perhaps 0.01 inch of the wall. Even with metal walls, it appears that data can be obtained within 30 mils from the wall, however, this point requires further investigation.

## SECTION VII

### INSTRUMENTS

Some of the instruments used in making these measurements were designed by us to serve special needs and, in some cases, were not obtainable commercially.

To measure voltage in the corona investigations, two voltmeters were constructed. A circuit diagram is shown in Figure 62. The resistors used were either IRC type MVJ or Resistance Products Company type BBF. They have rather low temperature coefficients, especially low voltage coefficient, and are stable. The resistors vary a maximum of 3 percent under high humidity but return to the original value when the humidity is normal. We use silica gel in the instrument box to keep them dry. The resistors vary a maximum of 2 percent with aging. All the values were accurately determined by a 5-dial Leeds and Northrup Wheatstone Bridge. Twenty megohms was the largest individual value used so that all resistors would have voltages low enough to avoid excessive resistance changes caused by the voltage coefficient. Twice as many resistors as needed were obtained and combinations were chosen from this group of measured resistors, which were within 0.005 percent of the values given in Figure 62. A straight line was passed through zero and the calibration points for the upper half of the meter calibration. The slope of this line was adjusted to  $45^\circ$  by means of a shunting resistor as shown in Figure 62. This requires that the meter sensitivity be equal to or higher than the desired value. The current calibrations were made by means of a



precision potentiometer, an accurately known resistor, and a variable voltage supply. Series resistance of the meter is negligible even at the lowest voltage used so no adjustment of the series resistance was necessary. The meters used were Triplet #420, 0 to 50  $\mu$  amp with about a 4-inch scale length. The terminals were 2-inch, porcelain, feed-thru bushings mounted in a Lucite panel, and the resistors were suspended from these terminals. The accuracy of the meters is considered to be better than 2 percent on all ranges, since 40 percent of full scale is the lowest reading used.

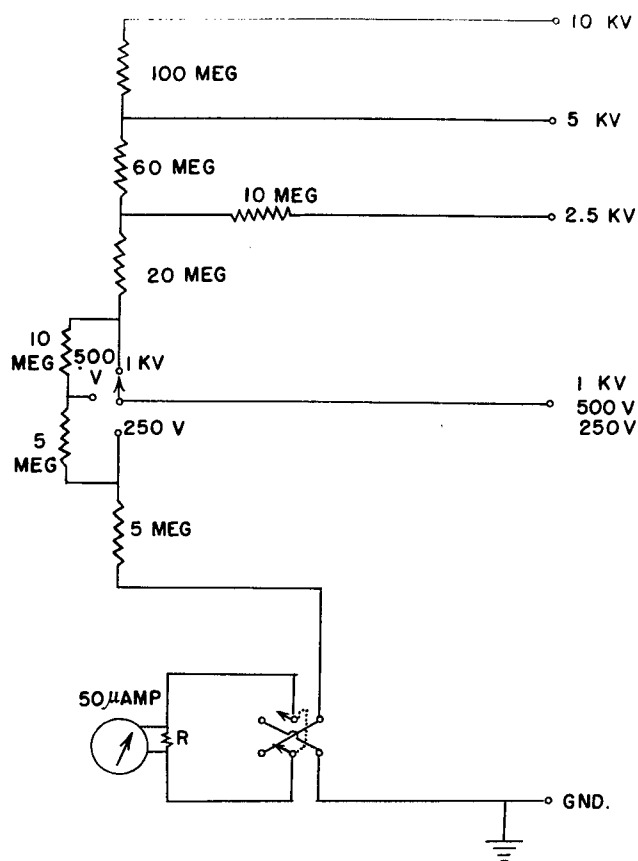


Figure 62. Schematic diagram of special multi-range, high-voltage voltmeter. (Reference 4.)

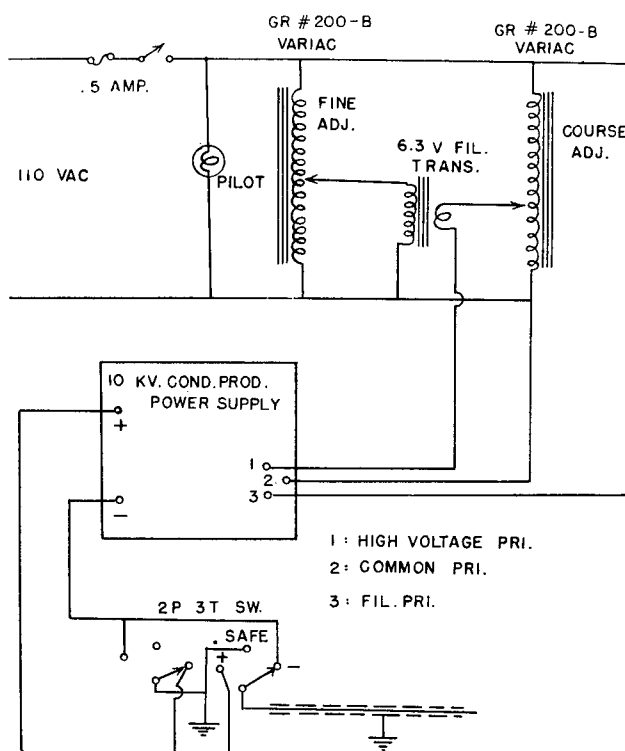


Figure 63. Schematic diagram of the 10-KV power supply. (Reference 4.)

The circuit diagram for our power supplies is shown in Figure 63. The supply has a Variac in the high voltage primary for coarse control, and another Variac with 6.3 volt transformer, as shown, for fine control. The power supplies are constructed so that either the plus or minus side of the supply can be grounded, making it simple to switch from positive to negative corona. There is also a third position on this switch which grounds both output

terminals to make it safe to work on the circuit without turning off the power supply. The power supplies principally used were supplied by Condenser Products Company, Chicago, Type PS-10.

For measuring small currents a portable reflecting type galvanometer was used (Rubicon Company, Philadelphia, Catalog No. 3401H). These galvanometers were provided with external shunts which were chosen to give 10  $\mu$  amp full scale. This also provided approximately critical damping. The Shallcross Company constructed an accurate Ayrton Shunt to our specifications for use with these galvanometers which provided full scale ranges of 10, 30, 100, 300, 1000, and 3000  $\mu$  amp.

In cases where higher sensitivity was required, i.e., in the range of  $10^{-6}$  to  $10^{-10}$  amp, a battery-operated Keithley Model 200 electrometer (Keithley Instruments, Cleveland) has proved valuable. The instrument has two ranges of 2 and 20 volts. The input impedance without a shunt is approximately  $10^{14}$  ohms, making it capable of measuring currents to  $10^{-14}$  amp. Shunts were made for it so that it covers the range of currents from  $5 \times 10^{-4}$  to  $4 \times 10^{-9}$  amp full scale. At the very small currents, the input impedance of the electronic microammeter is high. Therefore, care must be taken so that there are no leakage paths around it. It is possible to run both terminals above ground with this meter, which is advantageous at times. If the potential is too great, there is trouble with leakage to ground, etc. All our galvanometers and shunts were carefully checked and the errors are less than 2 percent for all ranges.

A small pulse amplifier was constructed for use as a pre-amplifier for our Tektronix 513-D oscilloscope to facilitate observation of the corona pulses. Its half-power points are at 100 cps. and 20 mc. The gain is about 35 for the midband range. The output is a cathode follower which has an output impedance of 100 ohms.

## REFERENCES

1. F. D. Werner. An Investigation of the Possible Use of the (Corona) Discharge as a Means for Measuring Air Flow Characteristics. Rev. Sci. Inst. Volume 21. (1950) pp. 61-8.
2. F. D. Werner. Physiological Effects of Ultrasound...Part C, Sound Measurements. (Research Report 54), Report submitted to ONR, Contract N8onr662, Task Order I, Project NR 172 628; University of Minnesota, Department of Aeronautical Engineering, Minneapolis, Minnesota. (1949).
3. F. D. Werner and J. R. Anderson. Investigation of a Corona Discharge for Measurements in Air Flow. Research Report 73, Report submitted to USAF, Office of Air Research, Contract AF 33(038)15833, University of Minnesota, Department of Aeronautical Engineering, Minneapolis, Minnesota. (1951).
4. F. D. Werner and R. L. Geronime. Investigation of a Corona Discharge for Measurements in Air Flow. Research Report 84, Report submitted to USAF, Contract AF 33(038)15833, University of Minnesota, Department of Aeronautical Engineering, Minneapolis, Minnesota. (1952).
5. L. B. Loeb. Fundamental Processes of Electrical Discharge in Gases. John Wiley and Sons, Inc., New York, 1939.
6. W. N. English. Corona From Fine Positive Points. Phys. Rev. Volume 71. (1947) pp. 638-9.
7. L. B. Loeb. The Mechanism of the Negative Point Corona at Atmospheric Pressure in Relation to the First Townsend Coefficient. Phys. Rev. Volume 71. (1947) pp. 712-14.
8. L. B. Loeb. The Threshold for the Positive Pre-Onset Burst Pulse Corona and the Production of Ionizing Photons in Air at Atmospheric Pressure. Phys. Rev. Volume 73. (1948) pp. 798-800.
9. W. N. English. Corona From a Water Drop. Phys. Rev. Volume 74. (1948) pp. 179-89.
10. W. N. English. Positive and Negative Point-to-Plane Corona in Air. Phys. Rev. Volume 74. (1948) pp. 170-8.
11. V. I. Popkov. Mobility of Ions under Conditions of Corona Discharge. (in Russian), C. R. Acad. Sci., USSR. Volume 58 (No. 6) (1947) pp. 1043-6.
12. L. B. Loeb. Recent Developments in Analysis of the Mechanisms of Positive and Negative Coronas in Air. J. Appl. Phys. Volume 19. (1948) pp. 882-97.
13. O. J. M. Smith. The Space Charge Due to Corona. Elect. Engg., New York. Volume 67. (1948) p. 979.
14. J. G. Hutton. Determination of Corona Starting Voltages for Non-Uniform Fields in Air. Trans. Amer. Inst. Elect. Engrs. Volume 66. (1947) pp. 1674-80.

15. W. N. English, and L. B. Loeb. Point-to-Plane Corona Onsets. J. Appl. Phys. Volume 20. (1949) pp. 707-11.
16. W. Fucks. Fluctuations of Discharge Parameters in Pre-Discharge Currents; and Measurements of Fluctuations. Z. Naturforsch., 5a, (1950) pp. 89-98.
17. L. B. Loeb, et al. The Choice of Suitable Gap Forms for the Study of Corona Breakdown and the Field Along the Axis of a Hemispherically Capped Cylindrical Point-to-Plane Gap. Rev. Sci. Inst. Volume 21. (1950) pp. 42-47.
18. W. N. English. Photon Pulses from Point-to-Plane Corona. Phys. Rev. Volume 77. (1950) p. 850.
19. A. Greenwood. Negative Point-to-Plane Corona--A New Model of the Discharge. Nature, London. Volume 168. (1951) pp. 41-42.
20. H. W. Bandel. Point-to-Plane Corona in Dry Air. Phys. Rev. Volume 84. (1951) pp. 92-99.
21. W. Fucks and W. Budde, Positive Sphere Corona: Oscillation Measurements. Z. Naturforsch., 6a (1951) pp. 494-504.
22. M. Menes and L. G. Fisher. Formative Time Lags of Positive Point Corona in Air. Phys. Rev. Volume 86. (1952) p. 134.
23. L. B. Loeb. The Mechanism of the Trichel Pulses of Short Time Duration in Air. Phys. Rev. Volume 86. (1952) p. 256.
24. L. B. Loeb. Fundamental Processes of Electrical Discharge in Gases. John Wiley and Sons, Inc., New York. (1939) p. 289.
25. ibid. p. 266.
26. ibid. p. 5.
27. ibid. p. 35.
28. ibid. p. 338.
29. ibid. p. 504.
30. ibid. p. 516.
31. ibid. p. 517.
32. ibid. p. 528.
33. ibid. p. 461.
34. ibid. p. 458.
35. ibid. p. 518.

36. J. D. Cobine. Gaseous Conductors. McGraw-Hill Book Co., New York. (1941) pp. 118-19.
37. H. L. Langhaar. Dimensional Analysis and Theory of Models. John Wiley and Sons, Inc., New York. (1951).
38. Anon. Reference Data for Radio Engineers. Federal Telephone and Radio Corp., New York. (1946) pp. 244-49.
39. Leslie S. G. Kovaszny. Development of Turbulence-Measuring Equipment. NACA TN 2839. (1953).
40. C. O. Griborn. Determination of Pressure-Time Curves of the Shock Wave By A New Method. Applied Scientific Research, Section A. Volume 3. pp. 225-36.
41. Memorandum from R. L. Geronime and F. D. Werner to Professor John D. Akerman, University of Minnesota, Department of Aeronautical Engineering. Status Report on the Investigation of the Application of Corona Discharge to Measurements in Air Flow. Contract AF 33(038)15833. Dated 17 October 1952 (Rev.).
42. Memorandum from R. L. Geronime and F. D. Werner to Professor John D. Akerman, University of Minnesota, Department of Aeronautical Engineering. Status Report on the Investigation of the Application of Corona Discharge to Measurements in Air Flow. Contract AF 33(038)15833. Dated 17 April 1953.
43. L. Bergmann. Ultrasonics. John Wiley and Sons, Inc., New York. (1946) p. 43.
44. G. B. Schubauer and P. S. Kelbanoff. Theory and Application of Hot-Wire Instruments in the Investigation of Turbulent Boundary Layers. Report No. ACR 5K27. March 1946.
45. D. Weimer. The Use of a Coronamicrophone in a Shock Tube. Rev. Sci. Inst. Volume 23. (1952) p. 377.

## BIBLIOGRAPHY

This is a brief bibliography of investigations directed at application of various types of gaseous conductivity to measurements in air flow. For the most part, the discharges considered are different in some essential features from our work, but these references will be of interest to anyone who chooses to consider the general field of possibilities.

1. P. Thomas. A Diaphragmless Microphone. J.A.I.E.E. Volume 42. (1923) p. 219.
2. F. C. Lindvall. A Glow Discharge Anemometer. Trans. A.E.E.E. Volume 53. (1934) pp. 1068-73.
3. W. Fucks. Extensive Investigations into the Glow Anemometer, the Dark Discharge, and the Corona Discharge, with principal emphasis on the Dark Discharges. These papers are obtainable from the Air Materiel Command and are identified as: ATI-37424, ATI-27009, ATI-19032, ATI-37077, ATI-32278, ATI-45549, ATI-36650, IP-4764 R-8243 F-4764, ZWB/THA/1944 R-8039 F-518; ZWB/THA/70 R-8037 F-831, ZWB/THA/54 R-3650 F-629. (1942----1944).
4. L. Agostini. A Corona Discharge Anemometer. Paper presented to Seventh International Congress of Applied Mechanics, London, 1948.
5. R. F. Mettler. The Anemometric Application of an Electrical Glow Discharge in Transverse Air Streams. Doctoral Thesis, California Institute of Technology, Pasadena, California. (1949).
6. A. J. A. Morgan and T. Vrebalovich. Investigation of Direct and Alternating Current Glow Anemometers. Report submitted to NACA under Contract NAW 5776, Guggenheim Aeronautical Laboratory, California Institute of Technology, Pasadena, California. (1950).
7. R. J. Koenig and R. S. Cesaro. Investigation of Spark-Over Voltage-Density Relation for Gas-Temperature Sensing. NACA TN 2090. (1950).
8. G. R. R. Fray, prepared by K. R. Eldredge, ONR, London Branch, Technical Report OANAR-13-48.